Determination of the Structural Allosteric Inhibitory Mechanism of Dihydrodipicolinate Synthase

A Thesis Submitted to the

College of Graduate Studies and Research

In Partial fulfillment of the Requirements for the Degree of

Masters of Science in the department of Chemistry

University of Saskatchewan, Saskatoon, SK

By

Cuylar Conly

© Copyright Cuylar Conly, October, 2015. All Rights Reserved.

PERMISSION TO USE

In presenting this thesis in partial fulfillment of the requirements for a postgraduate degree from the University of Saskatchewan, I agree that the Libraries of this University may make it freely available for inspection. I further agree that permission for copying of this thesis in any manner, in whole or in part, for scholarly purposes may be granted by the professors who supervised my thesis work or, in their absence, by the Head of Department or the Dean of the College in which my thesis work was done. It is understood that any copying or publication or use of this thesis or parts thereof for financial gain shall not be allowed without my written permission. It is also understood that due recognition shall be given to me and to the University of Saskatchewan in any scholarly use which may be made of any material in my thesis. Requests for permission to copy of to make other use of material in this thesis in whole or part should be addressed to:

Head of the department of Chemistry
University of Saskatchewan
Saskatoon, Saskatchewan (S7N 5C9)

ABSTRACT

Dihydrodipicolinate Synthase (EC 4.3.3.7; DHDPS), the product of the dapA gene, is an enzyme that catalyzes the condensation of pyruvate and S-aspartate-β-semialdehyde into dihydrodipicolinate via an unstable heterocyclic intermediate, (4S)-hydroxy-2,3,4,5-tetrahydro-(2S)-dipicolinic acid. DHDPS catalyzes the first committed step in the biosynthesis of L-lysine and *meso*-diaminopimelate; each of which is a necessary cross-linking component between peptidoglycan heteropolysacharide chains of bacterial cell walls. Therefore, strong inhibition of DHDPS would result in disruption of *meso*-diaminopimelate and L-lysine biosynthesis in bacteria leading to decreased bacterial growth and cell lysis. Much attention has been given to targeting the active site for inhibition; however DHDPS is subject to natural feedback inhibition by L-lysine at an allosteric site. L-Lysine is known to act as a partial uncompetitive inhibitor with respect to pyruvate and a partial mixed inhibitor with respect to ASA. Little is known about how the protein structure facilitates the natural inhibition mechanism and mode of allosteric signal transduction. This work presents ten high resolution crystal structures of DHDPS and the mutant Y110F-DHDPS with various substrates and inhibitors, including the first reported structure of DHDPS with ASA bound to the active site. As a body of work these structures reveal residues and conformational changes which contribute to the inhibition of the enzyme. Understanding these structure function relationships will be valuable for the design of future antibiotic lead compounds.

When an inhibitor binds to the allosteric site there is meaningful shrinkage in the solvent accessible volume between 33% and 49% proportional to the strength of inhibition. Meanwhile at the active site the solvent accessible volume increases between 5% and 35%

proportional to the strength of inhibition. Furthermore, inhibitor binding at the allosteric site consistently alters the distance between hydroxyls of the catalytic triad (Y137-T47-Y111') which is likely to affect local pKa's. Changes in active site volume and modification of the catalytic triad would inhibit the enzyme during the binding and condensation of ASA.

The residues H56, E88, R60 form a network of hydrogen bonds to close the allosteric site around the inhibitor and act as a lid. Comparison of L-lysine and bislysine bound to wild-type and Y110F DHDPS indicates that enhanced inhibition of bislysine is most likely due to increased binding strength rather than altering the mechanism of inhibition. When ASA binds to the active site the network of hydrogen bonds among H56, E88 and R60 is disrupted and the solvent accessible volume of the allosteric site expands by 46%. This observation provides some explanation for the reduced affinity of L-lysine in high ASA concentrations.

L-Lysine, but not other inhibitors, is found to induce dynamic domain movements in the wild-type DHDPS. These domain movements do not appear to be essential to the inhibition of the enzyme but may play a role in cooperativity between monomers or governing protein dynamics. The moving domain connects the allosteric site to the dimer-dimer interface. Several residues at the weak dimer interface have been identified as potentially involved in dimer-dimer communication including: I172, D173, V176, I 194, Y196, S200, N201, K234, D238, Y241, N242 and K245. These residues are not among any previously identified as important for formation of the quaternary structure.

ACKNOWLEDGEMENTS

I would like to acknowledge and thank my supervisors Dr. David A. R. Sanders and Dr. David R. J. Palmer for inviting me to work in their laboratories. I am grateful for their example and encouragement in the pursuit of the scientific method.

I especially appreciate the mentorship of Dr. Karen van Straaten and Dr. Sean Dalrymple. Their efforts were instrumental in the development of my own knowledge base.

I would like to thank all those who worked on DHDPS before me and contributed to the current foundation of knowledge. My thesis is one part of a greater whole, and none of this would have come so far without the enzymology and synthetic efforts of Dr. Yulia Skovpen and Shuo Li. I am blessed to work as part of such a qualified and motivated team.

Although I do not work with them; many people around the world have contributed to the current knowledge base. Their efforts foster a healthy competition that raises the level for all our efforts.

I would like to thank all the CMCF beam line staff at the Canadian Light Source for being so very helpful and accommodating: Pawel Grochulski, Michel Fodje, James Gorin, Kathryn Janzen, Shaun Labiuk.

I would like to thank the individuals who will inherit this project and continue to work with DHDPS when I am gone. Dr. David R. J. Palmer, Dr. David A. R. Sanders, Aarti Bhagwat, Mohadaseh Majdi Yazdi, Duncan Kirby, and those who have yet to arrive; Your efforts do me great honour.

Thank you to the former and present members of the Palmer Lab (Natasha Vetter, Julie Boisvert-Martel, Dr. Rajendra Jagdhane, Aarti Bhagwat, Bernardo Jung, Theerawat Prasertanan, Dr. Yulia Skovpen, Dr. Isaac Asiamah, Josseline Ramos-Figueroa, Mohadeseh Majdi Yazdi), and Sanders Labs (Dr. Karen van Straaten, Dr. Sean Dalrymple, Jijin Raj Ayanath Kuttiyatveetil, Dr. Drew Bertwistle, Nahedah Sahtout, Nataliya Zalatar and Siddarth Tiwari) for their support and companionship over the past few years.

I would also like to thank the members of my Advisory Committee, Dr. Ian Burgess, Dr. David A. R. Sanders, and Dr. David R. J. Palmer. I appreciate their time, knowledge and expertise to evaluate my work and performance as a student.

I am grateful to the Department of Chemistry, Dr. Palmer and Dr. Sanders, NSERC and the Provincial Government for the financial support to help complete this work.

DEDICATION

"I'll always remember the ones who were with me when things were tough, who never left my side, and made me smile when I didn't have anything to smile about."

— Unknown Author

TABLE OF CONTENTS

LIST OF TABLES

LIST OF FIGURES

LIST OF SCHEMES

LIST OF ABREVIATIONS

ASA;	(S)-aspartate-β-semialdehyde
apo	apo-protein
BH;	borohydride treatment of DHDPS
R,R-bislysine;	(2R,5R)-2,5-diamino-2,5-bis(4-aminobutyl)hexanedioate
CASTp;	Computed Atlas of Surface Topography of proteins
CCD	charge-coupled device
CLS;	Canadian Light Source
CMCF;	Canadian Macromolecular Crystallography Facility
COOT;	*Crystallographic Object-Oriented Toolkit* software
CSGID	Center for Structural Genomics of Infectious Disease
m-DAP;	meso-diaminopimalate
dap	diaminopimelate
DHDP;	2,3-dihydrodipicolinate
DHDPR;	dihydrodipicolinate reductase
DHDPS;	dihydrodipicolinate synthase
Dihydrodipicolinate;	(S)-2,3-dihydropyridine-2,6-dicarboxylate
DNA;	Deoxyribonucleic acid
DTT;	Dithiothreitol
DynDom;	Dynamic Protein Domain Motion Analysis
FEM;	Feature Enhanced Map
F form;	substituted enzyme form
GlcNAc;	N-Acetylglucosamine
HDX-MS;	Hydrogen Deuterium Exchange Mass Spectrometry
HEPES;	4-(2-hydroxyethyl)-1-piperazineethanesulfonic acid
HTPA;	(4S)-4-hydroxy-2,3,4,5-tetrahydro-(2S)-dipicolinic acid
$IC_{50;}$	the concentration of an inhibitor where the response (or binding) is reduced by half.
ITC;	Isothermal Titration Calorimetry
IPTG;	isopropyl-β-D-thiogalactopyranside
lac;	lactate; 2-Hydroxypropanoic acid
MAR	marresearch-detector
MolRep	Molecular Replacement
MS	molecular surface
MTZ	Compressed Metastream Scene File; 3D image file
MurNAc;	N-Acetylmuramic acid
$NaCNBH_3$	Sodium Cyanoborohydride
NADH;	Nicotinamide adenine dinucleotide
NMR	Nuclear Magnetic Resonance
PCR;	Polymerase Chain Reaction

PDB;	protein databank
PEG;	polyethylene glycol
PHENIX;	Python-based Hierarchical Environment for Integrated Xtallography software
pyr;	pyruvate
rmsd;	Root Mean Square Difference
SA;	solvent accessible surface
SAS;	succinate semi-aldehyde; 4-oxobutanoic acid
SDS-PAGE;	sodium dodecyl sulfate - polyacrylamide gel electrophoresis
TIM;	Triosephosphateisomerase
TRIS;	Tris(hydroxymethyl)aminomethane; 2-Amino-2-hydroxymethyl-propane-1,3-diol
VW;	van der Waals
wt;	wild type
XDS;	X-ray Spectrometer Detector System

Chapter 1 Introduction

1.1 Dihydrodipicolinate Synthase (DHDPS) as a herbicidal and antibiotic target

In the last 50 years, bacterial resistance to antibiotics has emerged as a significant medical challenge.[1] Therefore, one of the primary objectives of current medicinal chemistry is to identify new antibiotic targets for the development of new drugs.[2] Inhibitors of bacterial cell wall synthesis are proven to be very successful as antibiotics.[3] The bacterial cell wall requires *meso*-diaminopimelate (or L-lysine in some organisms) for cross-linking of peptidoglycan chains (figure 1.1). The *dap* pathway produces *Meso*-diaminopimelate which is then decarboxylated to form the final product L-lysine. Therefore enzymes of the *dap* pathway including dihydrodipicolinate synthase (DHDPS), encoded by *dapA*, are potential targets for drug development.[4-8] The *dapA* gene encodes DHDPS which regulates the biosynthetic pathway through feedback inhibition (figure 1.2). This is demonstrated in bacterial strains with a deleted *dapA* gene, which are not viable and lyse in the absence of *meso*-diamenopimelate in the growth medium.[9-11]

DHDPS (E.C. 4.2.1.52) is an allosterically regulated enzyme that catalyzes the first committed reaction of the L-lysine biosynthesis pathway in plants, bacteria, and some fungi. Specifically, DHDPS catalyzes the condensation of pyruvate and (S)-aspartate-β-semialdehyde (ASA) to form (4S)-hydroxy-2,3,4,5-tetrahydro-(2S)-dipicolinic acid, which then spontaneously dehydrates to (S)-2,3-dihydropyridine-2,6-dicarboxylate (dihydrodipicolinate). [12-15] There has been ongoing interest in DHDPS since the 1960s, with most of the attention focusing on plant, and some bacterial DHDPS. The plant enzyme allosterically regulates the production of L-lysine within the cell through feedback

inhibition. L-Lysine, the final product of the biosynthesis pathway, acts as the allosteric modulator. Plant DHDPS are very sensitive to L-lysine inhibition, and typically have low micromolar IC_{50} values, where IC_{50} is the concentration required to achieve half of the maximum inhibition.[16-18] Motivation for the study of plant DHDPS is removal of the mechanisms suppressing L-lysine production in crops, which would allow for agricultural products with higher L-lysine content and increased nutritional quality. Additionally, the highly conserved sequence of plant DHDPS provides the possibility of designing non-selective herbicides targeting DHDPS. Some progress has been achieved in modifying the allosteric site of the plant enzyme to engineer crops insensitive to L-lysine regulation, but there remain no compounds that are able to inactivate DHDPS and work as herbicides.

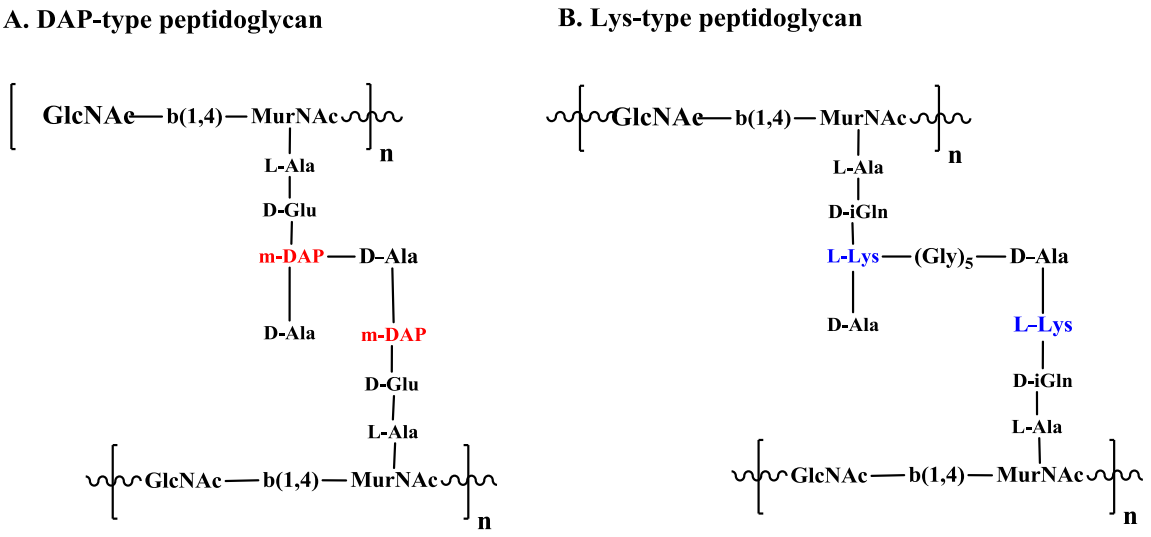

Figure 1.1 – **Two types of peptidoglycan found in bacterial species**; each dependent on the final products of the dapA biosynthetic pathway.

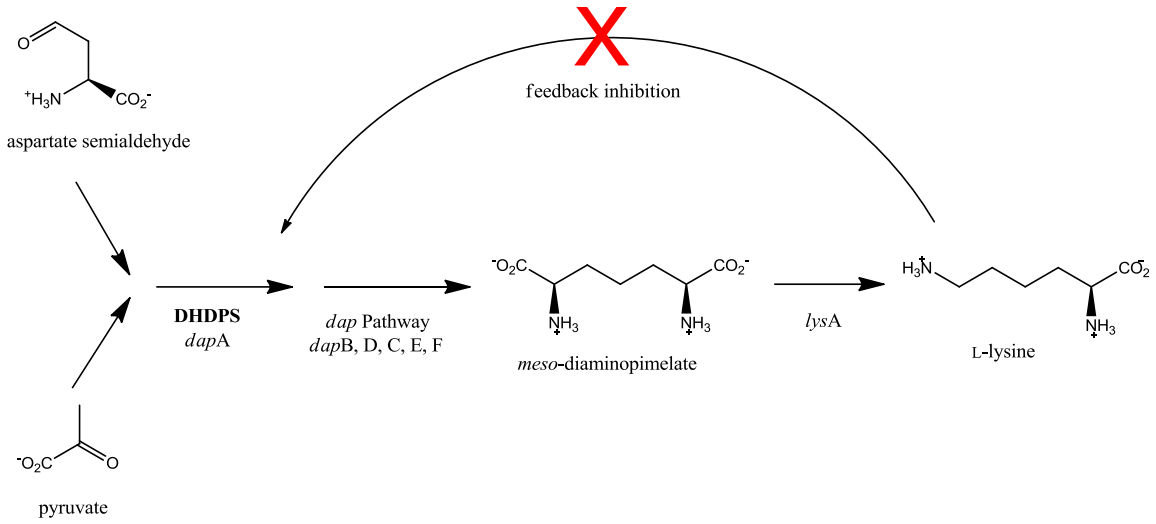

Figure 1.2 – **DHDPS is the first in a series of enzymes that make the unbranched dap biosynthetic pathway**. The products of this pathway are L-lysine and meso-diaminopimelate. The amount of L-lysine in the cell controls the dap pathway through feedback inhibition at DHDPS.

Bacterial DHDPS have less sequence identity between species than plant DHDPS's. Bacterial DHDPS are also less sensitive to L-lysine inhibition than DHDPS from plants. L-Lysine IC_{50} values of bacterial DHDPS range from micromolar and millimolar levels for DHDPS from Gram-negative bacteria to complete L-lysine insensitivity for DHDPS from Gram-positive bacteria.[19-23]

DHDPS is encoded by a *dapA* gene; studies have revealed that *dap*A$^-$ mutants are auxotrophic for diaminopimelate and undergo lysis in the absence of diaminopimelate in the medium.[10] *E. coli* AT997 (a Δ*dapA* mutant strain) can be maintained on nutrient medium only if the medium is supplemented with diaminopimelate.[9, 11] A systematic inactivation of the *Bacillus subtilis* genome lead to the classification of *dapA* as essential (i.e. bacteria lacking the *dapA* genes are not viable).[24] Genome analysis and mapping by *in vitro* transposition in *Haemophillus influenzae* putatively identified *dapA* as an essential

gene.[25] These results show that DHDPS is a potential target for drug development[7]; however, Schnell *et al.* has shown that *Pseudomonas aeruginosa* mutants with *dapA* deleted are viable, implying that *dapA* is not an optimal target for drug development against certain bacteria.[26]

DHDPS has additional significance for sporulating bacteria. The product of the reaction catalyzed by DHDPS, dihydrodipicolinate, is a precursor for dipicolinate which can comprise up to 15% of dry weight of bacterial spores.[27, 28] Mutants lacking DHDPS are not able to sporulate without supplementation of cultures with dipicolinate.[28] The absence of this L-lysine biosynthetic pathway in humans and its necessity in bacteria make DHDPS an attractive target for drug development.[7]

1.2 *Campylobacter jejuni*: A human and animal pathogen

C. jejuni is a Gram-negative helical bacterium, which readily engages in gene transfer contributing to the proliferation of antibiotic resistance.[29] *C. jejuni* are remarkably virulent with the ability to enter and survive within host epithelial cells.[30] Common strains of *C. jejuni* have developed resistance to most β-lactams, and the second generation of fluoroquinolone class of antibiotics including topoisomerase II and IV inhibitor Ciprofloxacin.[31] The rise of antibacterial resistance is prevalent among many bacterial species.[1]

Basic symptoms of campylobacteriosis include diarrhea, fever, and vomiting, however many complications can arise. An infection of *C. jejuni* can develop into serious autoimmune and neurological conditions such as Guillian-Barré syndrome and Miller-Fisher syndrome [30, 32-34] Campylobacteriosis is also associated with Reiter's syndrome, gall bladder inflammation, and irritable bowel syndrome.[35, 36] Recently, *C. jejuni* was found to

cause spondylodiscitis, a complication where the infection enters the intervertebral discs of the spinal cord.[37] As with other Gram-negative bacterial species, survival of *C. jejuni* depends on its ability to synthesize the components for the cell wall including the products of the *dap*A pathway controlled by DHDPS.

1.3 DHDPS Reaction Mechanism

DHDPS operates with a ping-pong, or "substituted-enzyme", catalytic mechanism (Scheme 1.1).[19, 38-40] The first substrate, pyruvate, condenses with the catalytic K166 of the native enzyme forming a Schiff base. The second substrate, ASA, binds and reacts with the enamine of the substituted DHDPS:pyr complex forming a new carbon-carbon bond via an aldol reaction. In solution ASA exists as an equilibrium of a number of species (figure 1.3). The current consensus, supported by NMR data, is that the hydrate form of ASA is involved in the DHDPS reaction mechanism.[12, 41, 42] However, due to the reactivity of ASA with DHDPS:pyr the actually binding conformation of ASA has never been confirmed crystallographically. The ligated intermediate then cyclizes, by trans-imination, into the unstable heterocyclic product (4S)-4-hydroxy-2,3,4,5-tetrahydro-(2S)-dipicolinic acid (HTPA).[38, 40] HTPA spontaneously dehydrates in solution forming dihydrodipicolinate, or enters the next step of the enzymatic pathway; reduction (with dehydration) catalyzed by dihydrodipicolinate reductase (DHDPR; Scheme 1.2).[13]

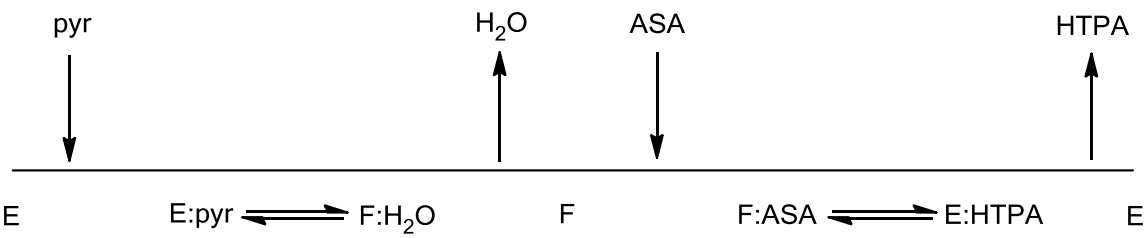

Scheme 1.1 – **The kinetic mechanism of DHDPS.** Within the Scheme E refers to the unligated enzyme and F to the covalently substituted form. Pyruvate is pyr, aspartate semialdehyde is ASA, and HTPA is (4S)-4-hydroxy-2,3,4,5-tetrahydro-(2S)-dipicolinic acid.[41]

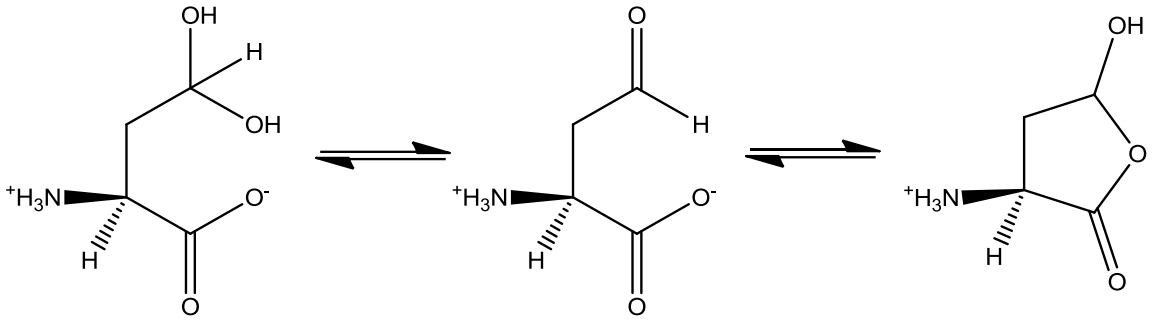

Hydrate Aldehyde Lactol

Figure 1.3 – **ASA has three resonance structures**. From left to right: hydrate, aldehyde, and lactol.

Involvement of specific residues has been inferred from protein crystallography and site directed mutagenesis of DHDPS from various species.[12, 21, 38, 43] In all species there is a conserved catalytic triad consisting of two tyrosine residues and one threonine; in addition to the key catalytic K166 residue.[38] This catalytic triad has been proposed to act as a proton relay by transferring protons to and from the active site.[38] DHDPS from most species exists as a tetramer in solution, [18, 40, 44-46] (figure 1.4) and one tyrosine in the catalytic triad belongs to the chain of an adjacent monomer (figure 1.5), and is believed to be involved in inter-monomer communication.[47] Furthermore, a highly conserved arginine residue plays a significant role in binding and reaction of the second substrate ASA.[43] The Michaelis constants have been published from a variety of sources and have a range between 0.19 – 11 mM for pyruvate and 0.11 – 5.1 mM for ASA (Table 1.1).

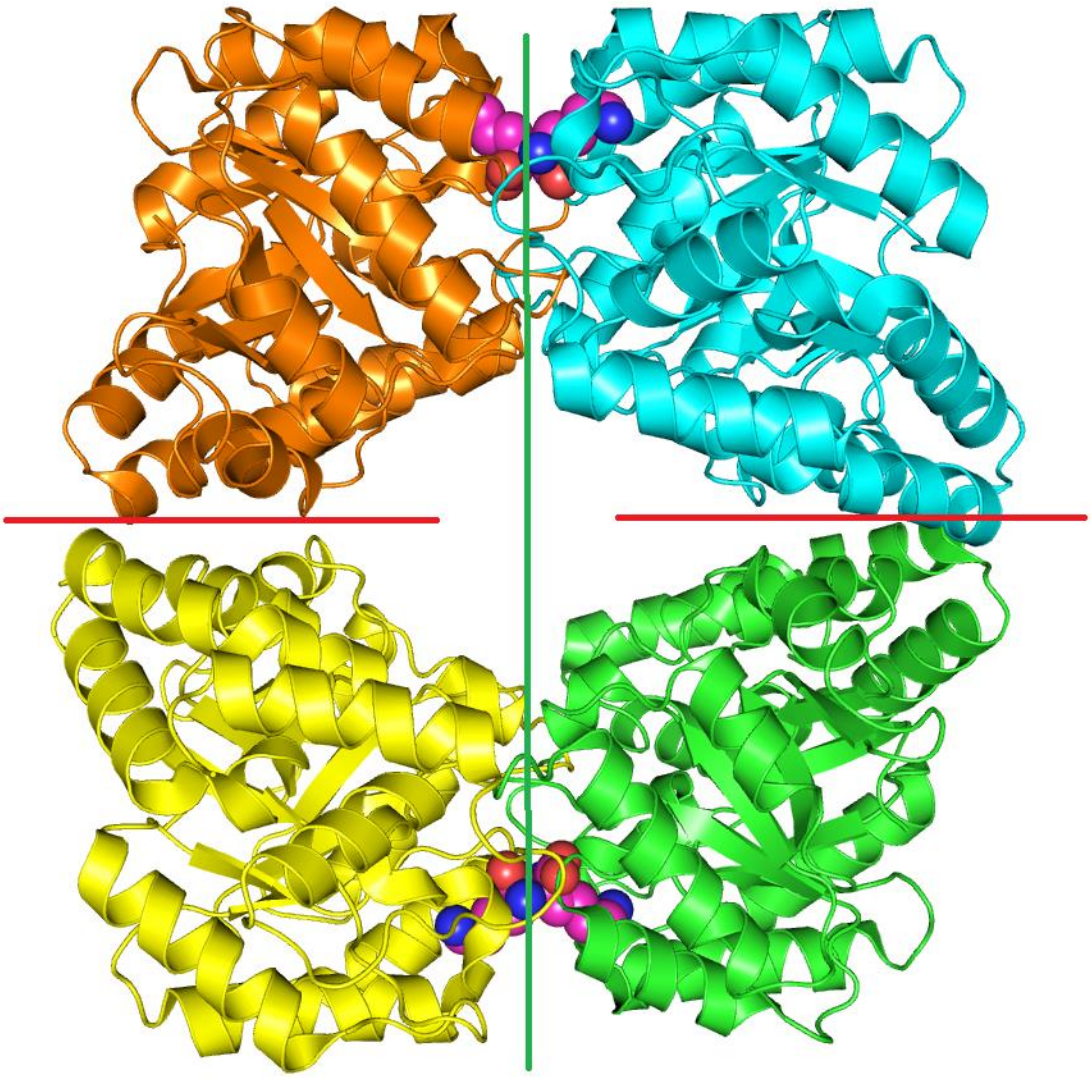

Figure 1.4 – ***E. coli* DHDPS with L-lysine bound at the active site.** (PDB: 2ATS) The green line demarcates the tight dimer interface, and the red line marks the weak dimer interface. The inhibitor lysine is shown as purple spheres, bound to the allosteric site.

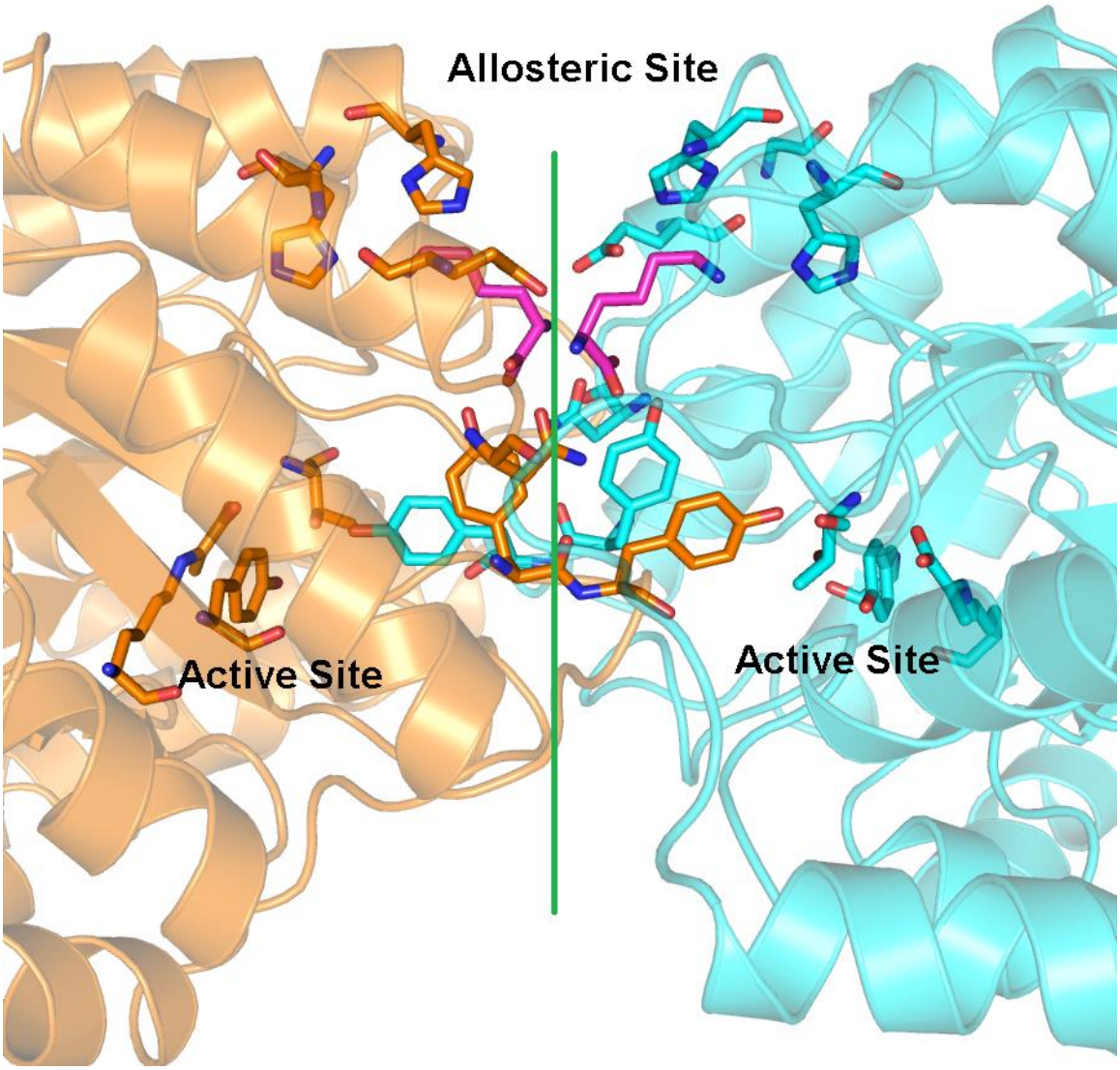

Figure 1.5 – **Interdigitation of Aromatic Residues at the Strong Dimer Interface** *Cj*-DHDPS:pyr:lys (PDB:4M19)[47] solved by Cuylar Conly prior to undertaking this thesis work. Tyrosine 111 crosses the strong dimer interface to complete the active site catalytic triad of the neighboring monomer. The tight dimer interface is indicated by the green line. The L-lysine inhibitor is shown in purple.

Table 1.1 – **Kinetic constants of DHDPS from various sources**

Organism	$K_{M\ Pyruvate}$ (mM)	$K_{M\ ASA}$ (mM)
Bacteria		
Campylobacter jejuni[19]	0.35	0.16
Escherichia coli[41]	0.19	0.12
Bacillus subtilis[48]	1.07	3.13
Bacillus licheniformis[49]	5.3	2.6
Bacillus sphericus[50]	9	5.1
Bacillus megaterium[51]	0.5	0.46
Plants		
Zea mays[18]	2.1	0.6
Pisum sativum[17]	1.7	0.4
Triticum aestivium[16, 52]	11.8	0.8

A. DHDPS Catalyzes condensation of pyruvate and ASA releasing the unstable product HTPA

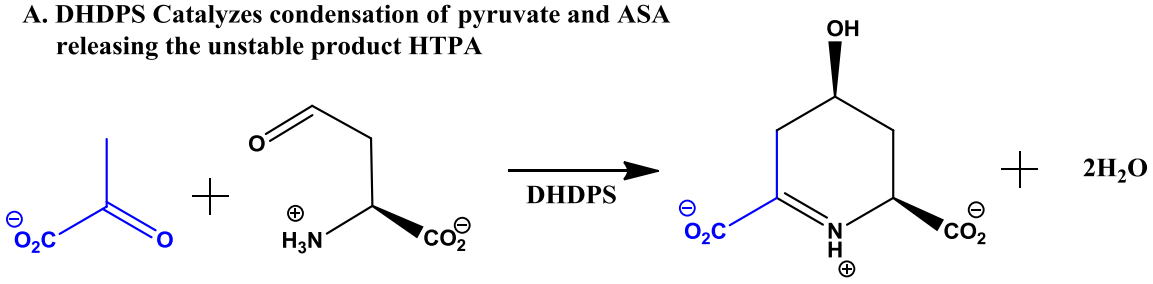

pyruvate ASA HTPA

B. HTPA is released from the enzyme active site and spontaneously dehydrates in solution

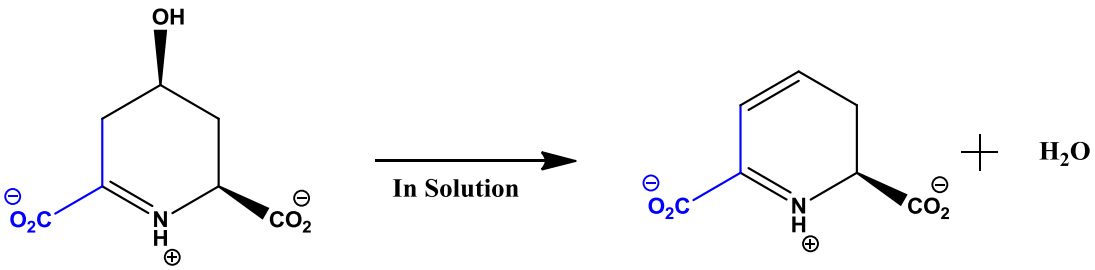

HTPA DHDP

Scheme 1.2 – **The reaction catalyzed by DHDPS.** Biosynthesis of DHDP occurs in two steps. First the DHDPS enzyme catalyzes condensation of pyruvate and ASA forming HTPA. HTPA is released into the solution where it spontaneously dehydrates to form DHDP.

1.3.1 *C. jejuni* DHDPS Reaction Mechanism

The active site of *Cj*-DHDPS centers on the catalytic Lys166, and includes the conserved catalytic triad of Tyr137, Thr37, Tyr111' (where the *primed* residue comes from the neighboring monomer of the tight-dimer). The active site is lined by a number of other residues believed to play minor roles in catalysis including: R142, I207, T48, G190, and N252. DHDPS from *C. jejuni* has received less attention than other species therefore many details of the proposed mechanism have been inferred from mutagenesis studies on closely related homologues including *E. coli* DHDPS; where sequence alignment reveals that *C. jejuni* DHDPS shares 37% sequence identity with *E. coli* DHDPS.[53-55] The details of the proposed catalytic mechanism of *Cj*-DHDPS are outlined in Scheme 1.3. The kinetic constants of *Cj*-DHDPS are shown in Table 1.2.[19] Substrate inhibition which is reported in some other species is not observed in DHDPS from *C. jejuni*.[19, 21]

Table 1.2 – **Kinetic Constants for *C. jejuni*[19]**

$K_{M(pyr)}$	$K_{M(ASA)}$	k_{cat}	$k_{cat}/K_{M(pyr)}$	$k_{cat}/K_{M(ASA)}$
0.35 ± 0.02 mM	0.16 ± 0.01 mM	76 ± 1 s^{-1}	(2.2 ± 0.1) x 10^5 $M^{-1}s^{-1}$	(4.8 ± 0.3) x 10^5 $M^{-1}s^{-1}$

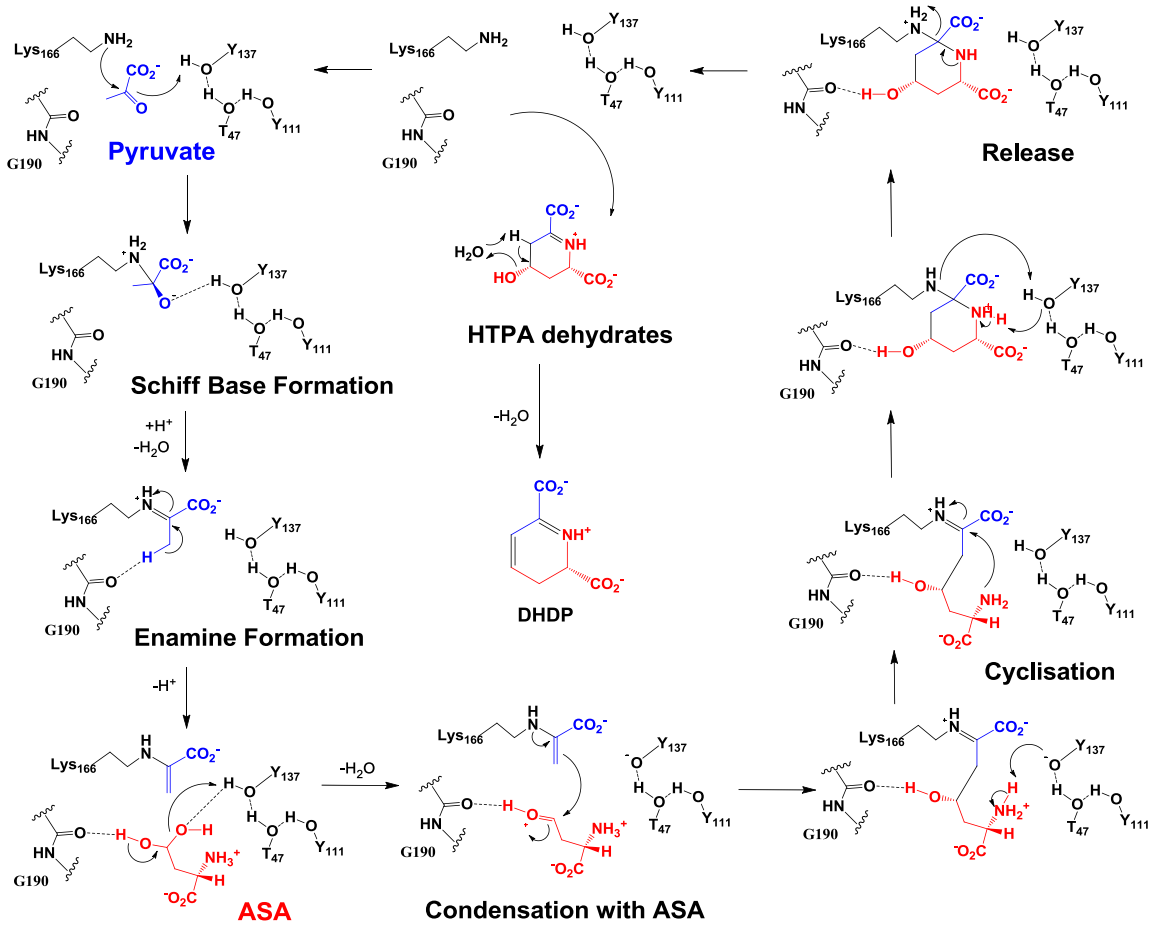

Scheme 1.3 – **Detailed catalytic mechanism of dihydrodipicolinate synthase.**[38, 40, 55]

1.4 Structure of Dihydrodipicolinate Synthase

DHDPS from many species exists as a homotetramer in solution, [18, 44-46] however dimeric forms also occur,[46, 56] and one DHDPS from *Pisum sativum* was reported as trimeric.[17] The tetramer is best described as a dimer of tight dimers, and any dimeric forms constitute only the tight-dimer which is considered to be the minimum biologically relevant form.[40] The monomer has a TIM barrel fold, a common versatile fold observed in many enzymes, consisting of eight α-helicis and eight β-strands.[57, 58] DHDPS contains two structural domains: the N-terminal domain of DHDPS forms an 8-strand β/α-barrel

structure connected to the α-helical C-terminal domain.[58] In tetrameric DHDPS there are four independent active sites and two dimeric allosteric sites, where L-lysine binds, located at the tight-dimer interface (Figure 1.4).

Many residues are conserved between species at the tight dimer interface.[12, 59] In particular the side chains of tyrosine 110 and 111 (*C. jejuni* numbers) of each monomer interdigitate, forming a hydrophobic stack of their aromatic rings.[58] This stacking forms a dense hydrophobic core and is considered to be responsible for the tight association between monomers. The backbone conformation of these tyrosines is within the forbidden region of the Ramachandran plot, suggesting an evolved purpose in catalysis and/or inhibition.[12, 47]

The tetramer is completed by a loose association of tight dimers. In bacterial DHDPS tetramerization leaves a large water-filled cavity in the center of the tetramer. In this so called head-to-head arrangement each monomer has contact with only two other monomers (figure 1.5).[45, 60] In contrast, plant DHDPS are known to form a back-to-back tetramer. In this back-to-back arrangement the weak dimer interface is on the opposite side of the tight dimer (relative to bacteria DHDPS), and the contact surface is entirely different.[45, 59] Each monomer has one independent active site, and one half of a dimeric allosteric site; which is completed by the neighboring monomer at the tight dimer interface. In bacterial DHDPS the active site opens into the center of the tetrameric arrangement, and the allosteric sites open away from the tetramer at opposite poles; while in plant DHDPS the active sites open away from the tetramer, and allosteric sites are open to the center of the tetramer (figure 1.6).[45, 60]

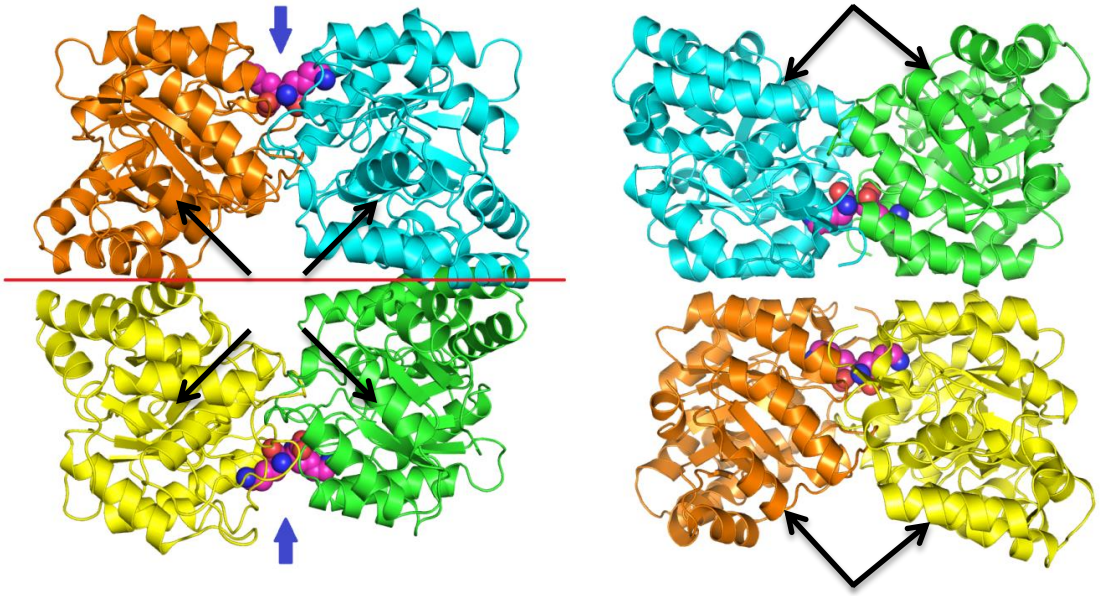

Figure 1.6 – ***Cj*-DHDPS:pyr:lys tetramer (PDB:4M19)[47] and Vitis vinifera (4HNN) Tetramer.[60]**
Panel A – The blue arrows indicate the allosteric binding site at the tight dimer interface. The red line denotes the weak dimer-dimer interface. Bound L-lysine is depicted as spheres. Black arrows indicate the location of each independent active site.
*Structure was solved by Cuylar Conly during an undergraduate research project prior to undertaking this thesis.
Panel B – DHDPS from plants such as V. vinifera form a "back-to-back" tetramer. L-Lysine (purple spheres) is shown bound to the allosteric site which opens to the center of the tetrameric arrangement. The black arrows denote the entrance to the active site which faces out from the tetramer.

In *E. coli*, Miriwaldt *et al.*(1995) mapped nine residues in 3 helices from each monomer that form interactions across the weak dimer interface.[58] Other species have been found to have many more weak dimer contacts;[39, 61, 62] as much as 20 residues from each monomer in *Thermotoga maritima*.[63] The structural role in tetramerization of these residues is suggested by the formation of a dimeric species, unable to form a tetramer.[38, 64] In *C. jejuni* it was found that L-lysine inhibition is cooperative across the weak dimer interface, as determined by Hill coefficients > 2.0.[19] The Hill coefficient indicates that when L-lysine binds at one dimeric allosteric site, it increases the affinity of L-lysine at the other dimeric allosteric site across the weak dimer interface. Therefore, interactions at the weak dimer interface must play a role in catalysis and inhibition, in addition to their structural role.

The active site of the enzyme is at the C-terminal ends of the β-strands, where one of the loops forms a short helix with a highly conserved arginine (Arg142 in *C. jeuni* numbering) whose side chain is situated over the β/α-barrel. The active site surrounds the key catalytic residue: lysine (166 in *C. jejuni* DHDPS). The absolute necessity of the catalytic lysine (K166) has been called into question in DHDPS from *E. coli* where the enzyme was demonstrated to function at 13% of the wild-type catalytic efficiency in the absence of the catalytic lysine (K166).[65] Three more residues comprising the 'catalytic triad' are also highly conserved; two tyrosine's and a threonine.[38, 66, 67] One tyrosine of the catalytic triad comes from the neighboring monomer crossing the tight dimer interface to do so.[38, 47]

The allosteric site of DHDPS is located at the interface of the monomers forming each tight dimer of the tetramer. L-Lysine binding pockets are situated side by side on each monomer, forming a large regulatory site, where residues of both adjacent monomers contribute to binding of each molecule of L-lysine. Crystal structures of L-lysine bound at the allosteric site of DHDPS have been obtained for several species (*Arabidopsis thaliana*, *C. jejuni*, *E. coli*, *Pseudomonas aruginosa*, *Vitis vinifera*), and residues responsible for coordination are known for these DHDPS.[19, 40, 45, 47, 68, 69]

The residues forming the allosteric site are reasonably conserved across DHDPS from species which are sensitive to L-lysine inhibition: gram negative bacteria, and plants (Figure A.1). However, the allosteric site of DHDPS from L-lysine-insensitive species is poorly conserved.[39, 59, 63] These insensitive DHDPS often have naturally substituted residues in the allosteric cleft which either add bulk, invert electrostatic charge, or both.[23, 56] Notably, the allosteric site of DHDPS from *Staphylococcus aureus,*[56] *Corynebacterium*

glutamicum,[23] and *T. maritima*,[63] are incompatible with L-lysine binding. In *S. aureus* for example, two of the eight residues making direct hydrogen bonds to L-lysine in *C. jejuni* have been replaced by lysine residues. These are His59 and Glu88 in *C. jejuni*, which are Lys58 and Lys86 in *S. aureus* respectively.[56] The result of these mutations is that the allosteric site of *Sa*-DHDPS is shallower, more like a saucer than a cup, with a substantially different charge profile (figure 1.7). The significance of these residues is confirmed in maize DHDPS, where a point variant of Glu162 to Lys (equivalent to Glu88 in *C. jejuni* DHDPS) resulted in insensitivity to L-lysine inhibition.[12, 70] It is worth noting that although these enzymes are not inhibited by L-lysine, there remains an opportunity to design non-lysine allosteric inhibitors for those enzymes insensitive to L-lysine if we can better understand the mechanism of signal transduction.[56]

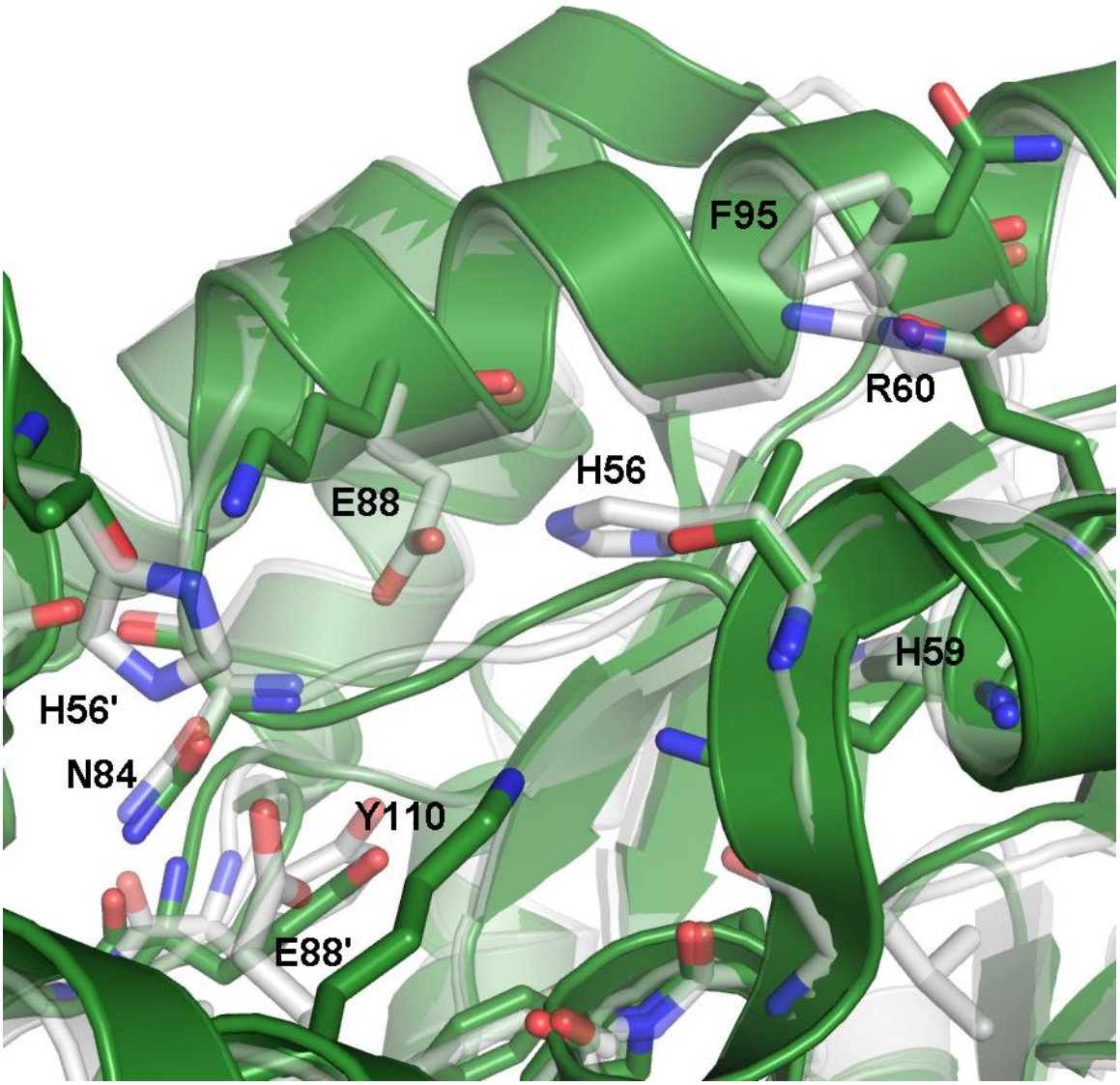

Figure 1.7 – **Allosteric Site of S. aureus DHDPS superimposed on *C. jejuni* DHDPS.** *Sa*-DHDPS (3DI1) is shown in green superimposed on *Cj*-DHDPS shown in ghost white. Key residues in the allosteric site of *Cj*-DHDPS (4LY8) are labeled for reference. The conserved residues are Y110 and N84. Other key residues have been substantially substituted.

1.4.1 Structure of *C. jejuni* DHDPS

Two crystal structures of *C. jejuni* DHDPS have been deposited in the PDB by the Center for Structural Genomics of Infectious Disease (CSGID): one in the apo-form (PDB: 3M5V) and one with pyruvate at the active site (PDB: 3LER). DHDPS from *C. jejuni* is a tetramer in solution and when crystallized. There is a high degree of conservation in

secondary and tertiary structures relative to DHDPS from other species. DHDPS from *C. jejuni* is closely related to DHDPS from *E. coli* which shares a 37% sequence identity, and all major structural features are conserved.[53, 54] The tetramer forms in the head-to-head fashion typical of bacterial DHDPS. The four active sites are open to a large cavity at the center of the tetramer. The allosteric site of DHDPS is located at the interface of the monomers that make each tight dimer in the tetramer. L-Lysine binding pockets are situated side by side on each monomer, forming a large double binding site, where amino acid residues of both adjacent monomers are involved in binding each molecule of L-lysine.[47]

The crystal structures of DHDPS with L-lysine bound at the allosteric site have been obtained for several species including *Cj*-DHDPS, which was solved by Conly *et al.* shortly before undertaking this thesis.[47] The residues of importance at the allosteric site are readily predicted from comparison to DHDPS from homologous species (*Arabidopsis thaliana, E. coli, Pseudomonas aeruginosa, Vitis vinifera*).[19, 40, 45, 68, 69]

The allosteric site of *C. jejuni* DHDPS is shown in Figure 1.8. Each molecule of L-lysine will make hydrogen bonds with Ser51, Ala52, Leu54, His59, Tyr110, Asn84', and Glu88', while His56 can form a cation π-interaction with the ε-amino group of L-lysine (the amino acid residues indicated with a prime belong to the adjacent monomer (Figure 1.8).[47] The most conserved residue in the allosteric site of all DHDPS are Tyr110 and Asn84' (Figure A.1). Despite the sequence divergence among bacterial DHDPS, including allosteric site residues, the architecture of allosteric sites of DHDPS from different species is very similar.

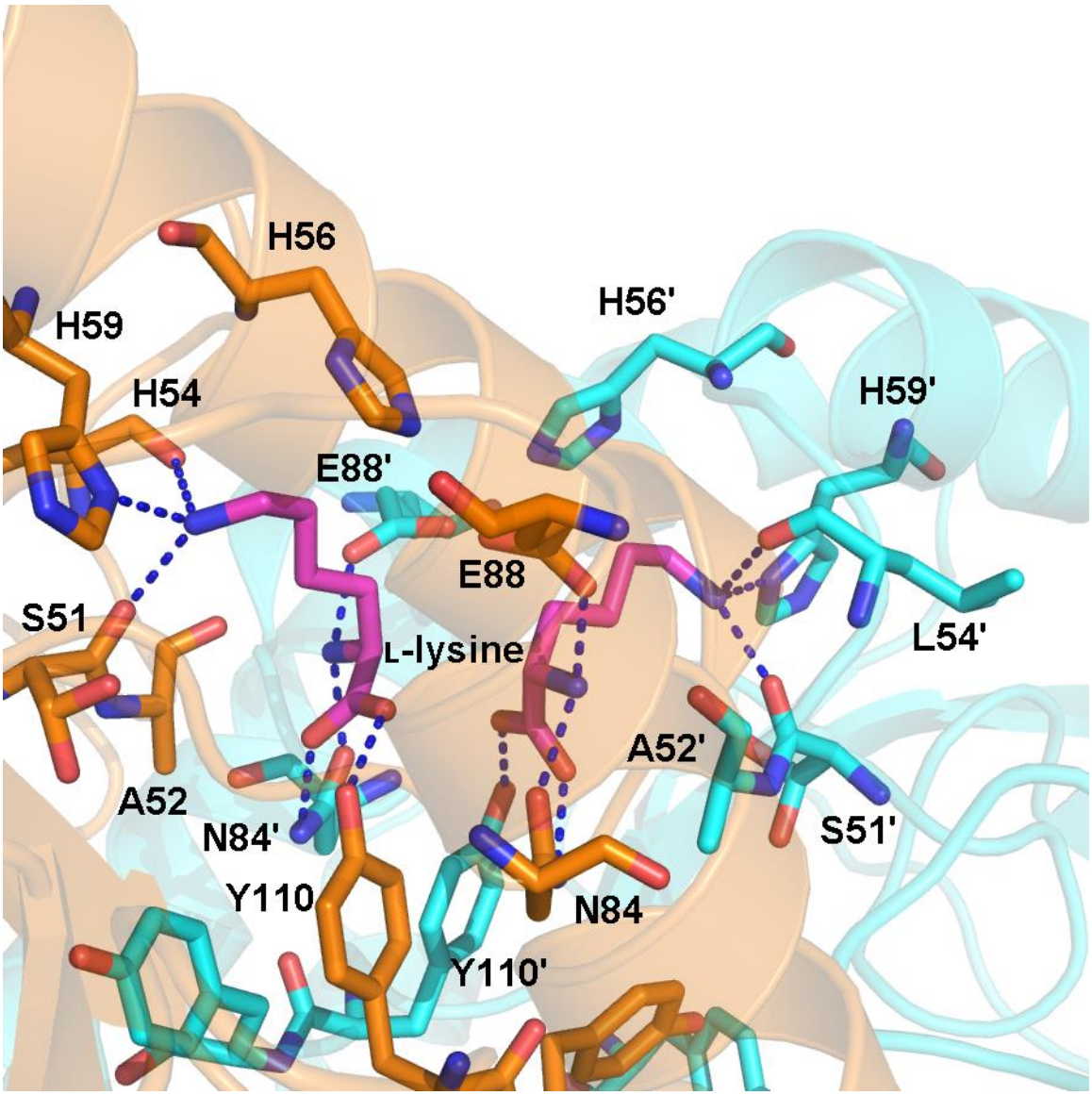

Figure 1.8 – **Hydrogen bonding of L-Lysine in the Allosteric Site of *Cj*-DHDPS.** Monomer A is depicted in orange, monomer B is shown in blue, and L-lysine is shown as purple. Each hydrogen bond is denoted by a blue dashed line.

1.5 Inhibition of Dihydrodipicolinate synthase

Dihydrodipicolinate synthase is the key regulation point in the biosynthesis of L-lysine in plants and bacteria. The activity of DHDPS is regulated by allosteric feedback inhibition from the pathway's end product, L-lysine.[12, 14, 19, 52, 59, 71] Despite variations in L-lysine sensitivity it is believed that the mechanism of inhibition will be the same across all species

of DHDPS. To date, variable sensitivities to L-lysine across species have been explained by alterations in the L-lysine-binding site. As discussed in section 1.4, DHDPS can be divided into three groups based on their sensitivity to L-lysine inhibition.[72] Plant enzymes are strongly inhibited by L-lysine with IC_{50}'s between 0.01 – 0.05 mM.[17, 18, 52, 73] Gram negative bacteria such as *C. jejuni*, produce DHDPS which is weakly inhibited by L-lysine with IC_{50}'s between 0.25 – 1.0 mM.[14, 19, 50, 74] In Gram positive bacteria DHDPS appears not to be inhibited by L-lysine at all (IC_{50} > 10 mM).[27, 48, 51, 75-77]

1.5.1 Kinetic Models of L-Lysine Inhibition

Most DHDPS display partial L-lysine inhibition, meaning some residual activity remains at saturating concentrations of L-lysine, although there are a few examples of plant DHDPS where full L-lysine inhibition is observed.[71, 78] DHDPS from Gram-negative bacteria can be weakly, moderately or strongly inhibited by L-lysine showing IC_{50} values from micromolar to millimolar range: 53 μM for *N. meningitis*,[20] 0.2 mM for *E. coli*,[79] and 0.7 mM for *Sinorhizobium meliloti*.[80] Various research groups have reported different mechanisms of L-lysine inhibition. For instance: in *Triticum aestivum* (wheat) L-lysine is a competitive inhibitor with respect to ASA and a noncompetitive inhibitor with respect to pyruvate;[16] in DHDPS from *Zea mays* (corn) L-lysine is a competitive inhibitor against pyruvate and a mixed inhibitor with respect to ASA.[18] From *E. coli* and *Bacillus subtilis* L-lysine is a non-competitive partial inhibitor with respect to ASA.[21, 45] Due to the contradictory nature of reported inhibition models, the mechanism of L-lysine inhibition remains controversial. Binding of L-lysine to DHDPS has been shown to be cooperative for DHDPS from several sources including *E. coli*, *S. meliloti*, and *V. vinifera*.[41, 45, 81, 82] Only recently in the reports of Atkinson *et al.* and Skovpen *et al*. have cooperativity

coefficients been included while fitting kinetic models to experimental data.[16, 17, 19, 41, 45, 81, 82]

1.5.2 Plant DHDPS are highly sensitive to L-Lysine Inhibition

All known plant DHDPS are sensitive to L-lysine inhibition, and this is one of the reasons why unmodified crops do not accumulate L-lysine. A number of research groups are working to increase L-lysine content in crops to improve nutritional value. Expressing bacterial DHDPS (L-lysine-insensitive or reduced L-lysine sensitivity) in several plants has achieved higher levels of L-lysine in some crops, while other transgenic plants do not accumulate L-lysine in high concentrations. This is likely due to the existence some other down-regulation mechanism, or increased utilization of excess L-lysine.[45, 83-85]

1.5.3 DHDPS lacking L-Lysine Inhibition

DHDPS from gram-positive and select gram negative bacteria are known to be insensitive to L-lysine inhibition.[27, 48, 51, 56, 75-77] Among the L-lysine sensitive DHDPS (from plants and gram-negative bacteria) specific mutations at the allosteric site will reduce or eliminate L-lysine inhibition. For example, *A. thaliana* becomes totally insensitive to L-lysine feedback inhibition upon substitution of Trp53 (His53 in *E. coli*, His56 in *C. jejuni*) for Arg.[78] Mutations in *Zea mays* DHDPS including S157N, E162K, A166T, and A166V (A79, E84 and L88, respectively, in *E. coli* and S83, E88, L92 in *C. jejuni*) also results in an enzyme insensitive to L-lysine.[70] Increased L-lysine accumulation was observed in maize cells transformed with a plasmid bearing the A166V mutated DHDPS maize gene.[86]

Among the DHDPS of gram-positive bacteria, weak L-lysine inhibition is most likely caused by variations in the amino acid composition of the allosteric site which are

unfavorable for L-lysine binding.[22, 56, 63] For instance, binding is prevented by a clash of positive charges with the side chain of the allosteric L-lysine when His56 is replaced by either lysine or arginine. DHDPS from Gram-positive *Corynebacterium glutamicum* has Lysine in position 56, and is insensitive to L-lysine feedback inhibition, making this organism useful for industrial production of L-lysine.[87] *Staphylococcus aureus*, known for its resistant strains to front-line antibiotics, contains dimeric DHDPS.[56] This enzyme has Lys in positions 56 and 84, making the allosteric site shallow and changing the charge distribution in the binding pockets, with the end result of this enzyme being insensitive to L-lysine inhibition.[56] Currently there is no natural inhibitor known for L-lysine-insensitive gram-positive DHDPS; making the design of inhibitors for the allosteric site an especially challenging task. A deeper understanding of the mechanism for allostery in DHDPS would aid in *de-novo* inhibitor design.

1.5.4 Inhibition of DHDPS from *C. jejuni*

Skovpen and Palmer have recently characterized the inhibition of DHDPS from *C. jejuni* with its natural allosteric inhibitor, L-lysine.[19] *C. jejuni* DHDPS is strongly inhibited by L-lysine with an apparent IC_{50} of 65 µM.[19, 55] Substrate inhibition by ASA, which has been reported for DHDPS from some sources and/or with some ASA preparations, is not observed in DHDPS from *C. jejuni.*[21] There is no evidence of significant cooperativity of substrates, but Hill coefficients indicate that there is cooperativity between allosteric sites across the weak dimer interface.[19]

As with DHDPS from other species, *Cj*-DHDPS exhibits partial inhibition with approximately 10% residual activity at saturating concentrations of L-lysine.[19-21, 71] Skovpen and Palmer find that L-lysine binds highly cooperatively, and primarily to the

pyruvate substituted 'F form' of the enzyme during the ping-pong mechanism (Scheme 1.1).[19] L-Lysine is an uncompetitive partial inhibitor with respect to pyruvate while L-lysine acts as a mixed partial inhibitor with respect to its second substrate, (S)-aspartate-β-semialdehyde (ASA). This differs from the kinetic models for inhibition reported for DHDPS from other sources.[19]

Skovpen and Palmerdemonstrated in *Cj*-DHDPS that pyruvate promotes L-lysine binding at the allosteric site, while ASA hinders the binding of L-lysine.[19,55] In *Cj*-DHDPS, the IC_{50} value of L-lysine decreases with increasing concentration of pyruvate up to a saturating value. Conversely, IC_{50} values of L-lysine increase with increasing concentration of ASA (Figure 1.9). Simply stated, the presence of pyruvate increases the affinity of the allosteric site for L-lysine, while the presence of ASA decreases the affinity of the allosteric site for L-lysine. In each case, the properties of the allosteric site have changed subtly, yet no structural link from allosteric site to active site has been clearly identified.

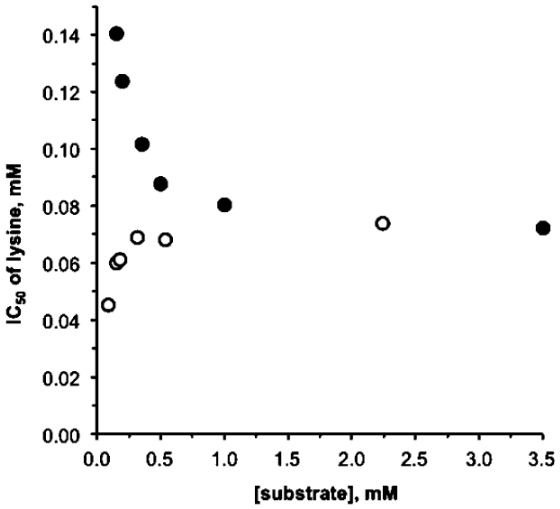

Figure 1.9 – [19,55] **Relationship between IC_{50} of L-lysine and concentration of substrates.** (●) Pyruvate is the variable substrate; concentration of ASA is 2.24 mM; (○) ASA is the variable substrate; concentration of pyruvate is 3.50 mM.

It was reported that Hill coefficients vary from 2.0 to 3.2 depending on substrate concentrations. That the degree of cooperativity exceeds 2.0 indicates that the two allosteric sites are not entirely independent and binding of L-lysine at one allosteric site will affect the binding of L-lysine at the diametrically opposed binding site. Therefore, the enzyme functions as a tetrameric catalyst, rather than as a dimer of independent dimers.[19, 55]

Further to the complexity of the observed inhibition is that L-lysine at high concentrations induces antagonistic cooperativity in the second substrate, ASA. The presence of ASA drives up the apparent inhibition constant of L-lysine, and the presence of L-lysine drives up the apparent K_M of ASA; when ASA binds the active site L-lysine may be rejected at the allosteric site, and vice versa. It is possible that the observed cooperativity between ASA at each active site may be enhanced due to a rejection of L-lysine at the allosteric site, which induces rejection of L-lysine at other allosteric sites therefore removing inhibition at other active sites. Notwithstanding the empirical evidence, specifics of the signal transduction between active site and allosteric site, and between antipodal allosteric sites, remain unclear.

1.5.5 DHDPS from *C. jejuni* made insensitive to L-lysine inhibition

The residues forming the aromatic core at the tight dimer interface are obvious candidates for involvement in the allosteric mechanism. Tyrosine 111 crosses the tight dimer interface to complete the catalytic triad of the neighboring monomer while its neighbor tyrosine 110 makes a direct hydrogen bond to the inhibitor L-lysine in the allosteric site. Recently Skovpen and Palmer successfully mutated Tyr110 to phenylalanine in *Cj*-DHDPS.[47, 55] The Y110F mutation in *Cj*-DHDPS dramatically affects

the ability of the enzyme to be inhibited by L-lysine. Kinetic data obtained for the mutant Y110F indicates that the mutant apparently operates by the same kinetic mechanism as wt-*Cj*-DHDPS, and shows only minor differences in the values of the Michaelis constants, as shown in Table 1.3.[19, 47, 55] The value of k_{cat}, however, is reduced about two-fold relative to wild-type *Cj*-DHDPS. The importance of the side chain of Y110 to catalysis is not obvious, but likely derives from some effect on the adjacent Y111 which completes the catalytic triad, or on the nearby secondary and tertiary structure elements at the tight-dimer interface. The removal of the hydroxyl group results in an estimated L-lysine IC_{50} of about 40 mM, an increase of three orders of magnitude (Figure 1.10).[47, 55] This makes the enzyme insensitive to L-lysine regulation at its physiological concentrations, however, when sufficiently saturated (> 80 mM) the Y110F enzyme displays partial L-lysine inhibition (Figure 1.10).[47, 55] The effect on inhibition is surprisingly large, suggesting that this particular hydrogen bond is a key contributor to inhibitory signal transduction.

Table 1.3 – **Kinetic constants for Y110F and wt-DHDPS.**[19, 47, 55]

	$K_{M(pyr)}$, mM	$K_{M(ASA)}$, mM	k_{cat}, s^{-1}	$k_{cat}/K_{M(pyr)}$, $M^{-1}s^{-1}$	$k_{cat}/K_{M(ASA)}$, $M^{-1}s^{-1}$
Wt[19, 55]	0.35 ± 0.02	0.16 ± 0.01	76 ± 1	(2.2 ± 0.1) x 10^5	(4.8 ± 0.3) x 10^5
Y110F[47, 55]	0.19 ± 0.01	0.12 ± 0.01	33 ± 1	(1.8 ± 0.1) x 10^5	(2.7 ± 0.1) x 10^5

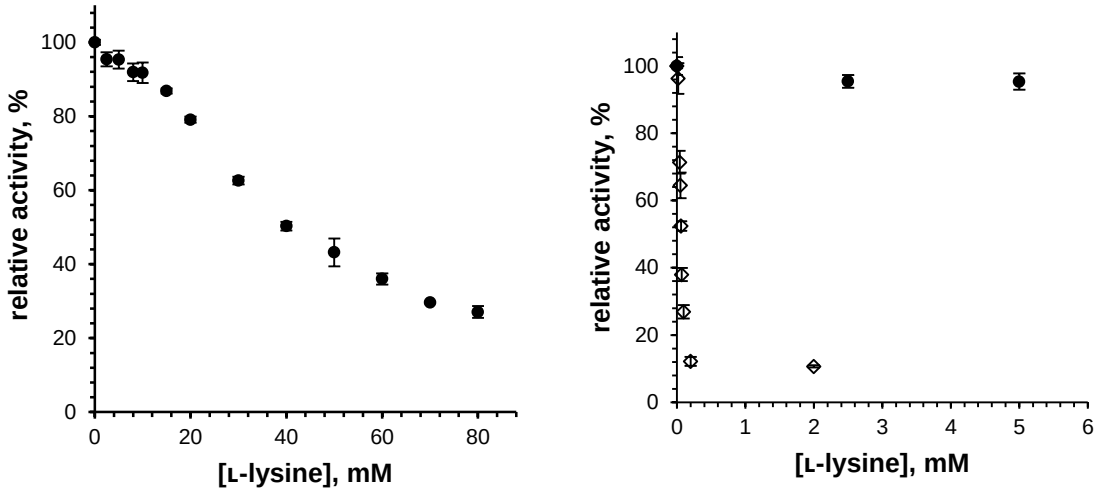

Figure 1.10 – [47,55] **L-Lysine inhibition curves for wt-DHDPS and Y110F-DHDPS.** Left: L-lysine inhibition curve for Y110F, (ASA 0.12 mM, pyruvate 3.70 mM). Right: Comparison of L-lysine inhibition for Y110F (●) and wild-type (○), (ASA 0.16 mM, pyruvate 3.50 mM).

1.5.6 Allosteric Site Inhibitors

A number of millimolar inhibitors targeting the allosteric site of the enzyme have been reported. [41, 55, 88] Among them are homoserine lactone, 2-aminocyclopentanone, (S)-glutamic acid, (S)-aspartic acid, and S-(2-aminoethyl)-L-cysteine (L-thialysine): a L-lysine mimic containing a sulfur atom.[88] Despite a high structural similarity to L-lysine, L-thialysine binds ten times more weakly in *E. coli* DHDPS than L-lysine.[41]

L-Thialysine (Figure 1.11) is a very close mimic of L-lysine, having just one replacement of the methylene group for sulfur in the side chain. Yet L-thialysine is a much weaker inhibitor. In experiments with *E. coli* DHDPS, L-thialysine has an inhibition constant about one order of magnitude (IC_{50} is approximately 30x higher) higher than that of L-lysine.[41] *C. jejuni* DHDPS is even less sensitive to L-thialysine inhibition than the *E. coli* enzyme, showing an apparent IC_{50} of 2 mM.[55]

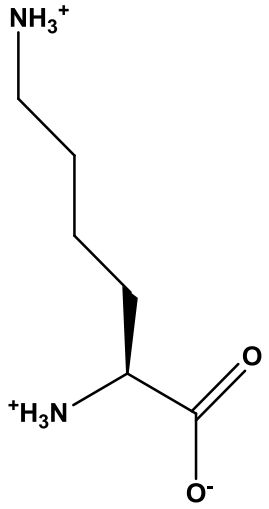

L-lysine

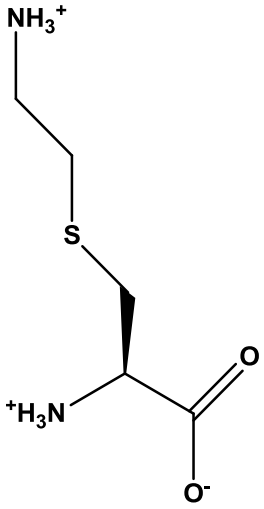

L-thialysine

Figure 1.11 – **L-lysine and L-thialysine**

Until recently, there have been no attempts at rational design of allosteric inhibitors for DHDPS. Based on results from isothermal titration calorimetry, Phenix and Palmer suggested an effective inhibitor design should mimic a pair of bound L-lysine molecules.[82] Later, Skovpen and Palmer successfully synthesized (2R,5R)-2,5-diamino-2,5-bis(4-aminobutyl)hexanedioate colloquially known as "R,R-bislysine", which mimics two L-lysine molecules by joining the α-carbons with a two-carbon linker (Figure 1.12).[55] This bis-inhibitor analog is over two orders of magnitude more effective than L-lysine itself, likely because the entropic barrier to binding of the second inhibitor molecule has been eliminated.[82]

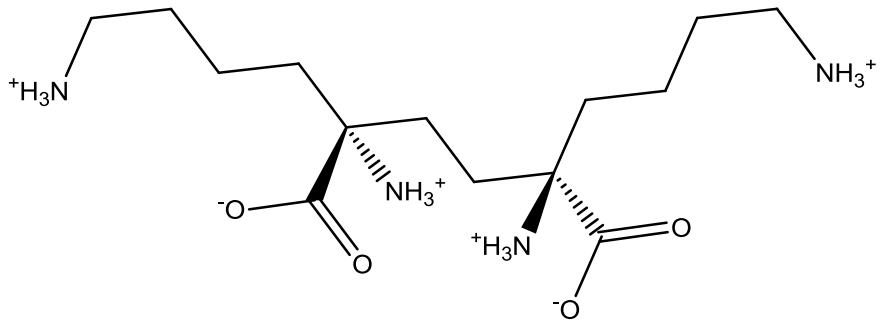

R,R-bislysine

Figure 1.12 – **(2R,5R)-2,5-diamino-2,5-bis(4-aminobutyl)hexanedioate;** better known as R,R-bislysine

1.5.6.1 R,R-bislysine is a potent Allosteric Inhibitor

Similar to L-lysine, R,R-bislysine is a partial inhibitor of *Cj*-DHDPS.[19] At saturating concentrations of R,R-bislysine (>1.7 μM) the enzyme still demonstrates 7 – 10% of the maximal activity (Figure 1.13).[55] Binding of R,R-bislysine is cooperative and the values of Hill coefficients (1.6 and 1.7) indicate that binding of a second molecule of R,R-bislysine at one pair of adjacent allosteric sites in the dimer promotes binding of one molecule of R,R-bislysine at the polar opposite allosteric site of the other dimer. In other words, *Cj*-DHDPS demonstrates inter-dimer cooperativity upon binding of R,R-bislysine. The inhibitor does not form any covalent bonds with the enzyme, and is therefore reversible. Unlike L-lysine, R,R-bislysine binds (and demonstrates inhibitory properties) to both the free enzyme (E form) and the enzyme-pyruvate complex (E:pyr) with different affinities, indicating a mixed partial model of inhibition.[55] R,R-bislysine binds with similar affinity to all enzyme forms, with an average inhibition constant of 200 nM. The inhibitory activity of R,R-bislysine is approximately 310 times higher than that of L-lysine.

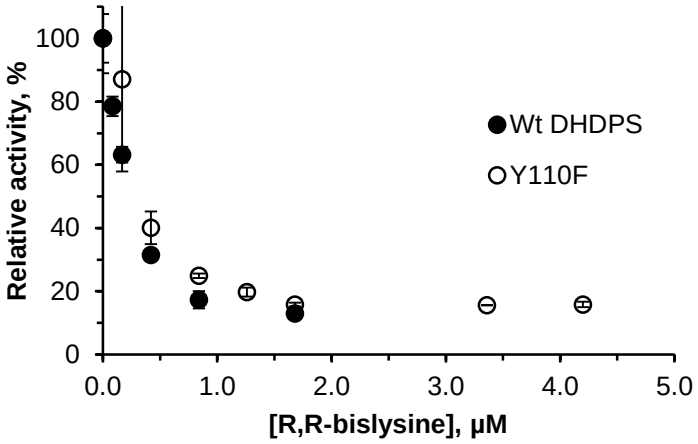

** Figure adapted with permission from the Thesis of YuliaSkovpen.[55]

Figure 1.13 – ***R,R*-bislysine inhibition curves for wild type DHDPS and Y110F.** Concentrations of substrates: ASA 0.10 mM, pyruvate 3.7 mM.

Prior to attempting the synthesis of R,R-bislysine, the inhibitory properties of another L-lysine mimic, α-methyl-DL-lysine (Figure 1.14) was tested. These results indicate that the methyl group at the α-position dramatically decreases inhibitory properties of the molecule (IC_{50}^{app} > 10 mM), possibly by preventing proper binding of molecules of the inhibitor in the proximal allosteric sites.[55]

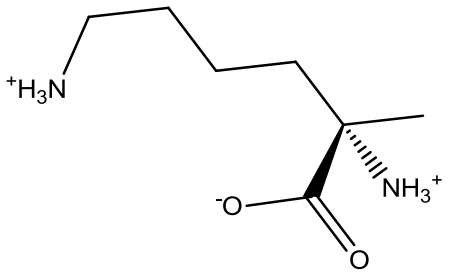

α-methyl-DL-lysine

Figure 1.14 – **α-methyl-DL-lysine**

1.5.6.2 R,R-bislysine Inhibits the L-Lysine insensitive Y110F-DHDPS

The Y110F mutation dramatically affects the ability of the enzyme to be inhibited by L-lysine. The removal of the hydroxyl group results in an estimated L-lysine IC_{50} of about

40 mM; an increase of three orders of magnitude (Figure 1.10).[47, 55] Despite the loss of sensitivity to the natural inhibitor, the synthetic inhibitor bislysine is capable of strongly inhibiting the Y110F mutant DHDPS. The inhibitory efficiency of R,R-bislysine toward Y110F is almost as high as for wt-DHDPS (Figure 1.13).[55] R,R-bislysine binds to Y110F approximately 100,000 times stronger than L-lysine. These recent inhibition results demonstrate that Tyr 110 is important for binding and inhibition of the natural inhibitor L-lysine, but they are not crucial for R,R-bislysine. The high inhibitory effectiveness of R,R-bislysine against Y110F indicates that Tyr110 is not the only essential component of the signal transduction system in *C. jejeuni* DHDPS. Stronger inhibition may be attributable to tighter binding, or enhanced activation of allosteric mechanisms. It is anticipated that crystallization of the synthetic inhibitor bislysine, with each of wild-type and Y110F-DHDPS would provide insight into the mechanism for enhanced inhibition, and therefore natural inhibition of L-lysine.

1.6 Proposed Mechanism for Signal Transduction

The exact mechanism of signal transduction from allosteric site to active site is not yet completely understood, although available crystal structures and molecular dynamics simulations allow us to propose a mechanism of allosteric regulation. The carboxylic group of the allosteric L-lysine creates a hydrogen bond with the phenolic OH of Tyr110, which may be altering its position. This Tyr110 movement promotes a shift of Tyr111, which is a residue of the catalytic triad, and therefore its displacement causes a reduction in catalytic effectiveness within the active site. Tyr110 participates in L-lysine binding by donating a hydrogen bond to the carboxyl group of L-lysine, while Tyr111 is a part of the catalytic triad. It is likely that signal transduction occurs via Tyr110 movement upon L-

lysine binding, where a shift of Tyr110 affects the position of the catalytic Tyr111, and alters the catalytic activity of the enzyme (Figure 1.15).[47] Mutation of Tyr110 to Phe110 has been found to significantly reduce the effectiveness of L-lysine as an allosteric inhibitor. It is unclear if reduced the lack of inhibition is due to reduced binding affinity or disruption of signal transduction to the active site.[47]

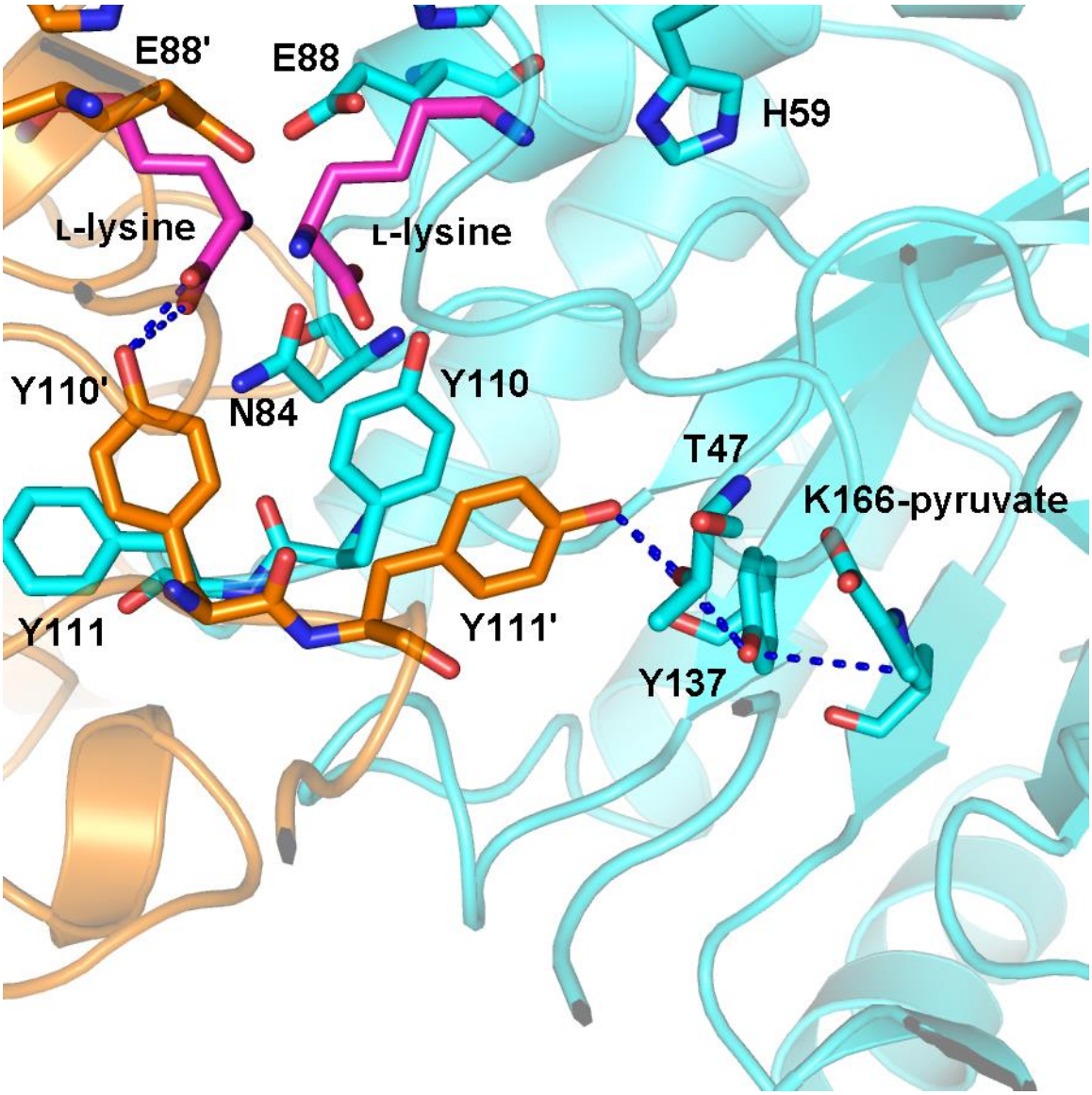

Figure 1.15 – **Y110/111 links the allosteric site to the catalytic triad (*Cj*-DHDPS; PDB: 4M19).** A series of hydrogen bonds links L-lysine in the allosteric site via Y110/111 to the catalytic triad in the active site. Monomer A is shown in orange, monomer B is shown in blue and L-lysine is shown in purple. The applicable hydrogen bonds are denoted with dark blue dashed lines.

Furthermore, according to Atkinson *et al*. (who studied *V. vinifera* DHDPS), Tyr131 (equivalent of Tyr110 in *C. jejuni*) forms a hydrophobic stack with the catalytic triad residue Tyr132' (Tyr111' in *C. jejuni*).[45] Disruption of this stack upon L-lysine binding displaces the hydroxyl group of Tyr132' (Tyr111' in *C. jejuni*) and slows down or disrupts the function of the catalytic triad. Previous inhibition studies of DHDPS consistently show that the presence of pyruvate somehow affects the sensitivity of the allosteric site for binding L-lysine. This is consistent with the proposed mechanism in which pyruvate binds before L-lysine.

The role of the aromatic residues Tyr110/111 is decidedly crucial for inhibition of DHDPS with its natural inhibitor, L-lysine. However, recent evidence for strong inhibition of Y110F-DHDPS by the R,R-bislysine indicates that Tyr110/111 is not the sole conduit for allosteric communication. It is far more likely that allosteric inhibition is the result of a combination of structural effects which vary in the magnitude of their importance within the complete mechanism of allosteric inhibition. To understand the various ways an allosteric inhibitor can have a negative effect on activity at the active site will aid in designing inhibitors across the diversity of homologous DHDPS.

To understand inhibition as a sum of parts process we must also consider several other theories that have been proposed to explain mechanism of allosteric inhibition. In *Ec*-DHDPS, it was identified that inhibition may be linked to perturbation of the proton relay of the catalytic triad, resulting from a small change in the position of Tyr107' (Tyr111 in *C. jejuni*).[40] Additionally, it has been proposed that Schiff base formation may be prevented by occlusion of a conserved water channel connecting the active site and allosteric sites.[40] Furthermore, L-lysine may stabilize a less catalytically competent

conformer to prevent the binding or reaction of ASA.[82] The observed modes of inhibition suggest that L-lysine and pyruvate can be bound at the same time, and kinetic studies of cooperativity show that pyruvate actually improves L-lysine binding.[19, 21, 65] More recently, the importance of the quarternary structure has been demonstrated.[89] Dimeric variants of DHDPS exhibit reduced catalytic activity, suggesting that the tetrameric structure optimizes enzyme dynamics for catalysis. Griffin *et al.* probed the sensitivity of the dimer−dimer interface with a series of point mutations[90] and showed that single-point mutations have an effect on both catalysis and tetramerization. In general the dimer−dimer interface is small and not well conserved across species; however, between DHDPS from *E. coli* and *C. jejuni* there is more agreement in this region than between DHDPS from other species.[40, 53, 55, 90] It is not yet clear how L-lysine binding affects the tetrameric structure or dynamics. With more evidence we may begin to understand which mechanisms contribute the greatest, or most cohesive, effect to inhibition in any one, or all, DHDPS homologues.

1.7 Competitive Active Site Inhibition and ASA

Most research groups focus their attention on active site inhibitors of DHDPS. There are a few weak inhibitors reported to be competitive with respect to ASA, such as succinate β-semialdehyde, and with respect to pyruvate, such as 2-ketobutyrate, 2-ketovalerate, 3-fluoropyruvate and glyoxalate.[12, 41] Several inhibitors of DHDPS are shown in Figure 1.16 and given in Table 1.4. Product mimics such as dipicolinic (**1.1**) and chelidamic (**1.3**) acids are weak millimolar inhibitors.[41, 91] Interestingly, inhibition of growth of the late blight fungus *Phytophthora infestans* by millimolar concentrations of dipicolinic and chelidonic acids (**1.1** and **1.2** respectively) was observed *in vivo* using infected potato leaf discs.[92]

Moderate inhibition of *E. coli* growth was observed for the piperidine diester (**1.4**) and chelidamic (**1.3**) acid at 20 mM.[93] 2-Ketopimelic acid was found to be a weak irreversible inhibitor, and based on this observation, several compounds mimicking the acyclic enzyme-bound condensation product of ASA and pyruvate have been proposed.[12, 94] The continuation of that work was synthesis of phenolic ketoacid derivatives (**1.7** and **1.8**), which condense with the enzyme in a time-dependent manner.[95] Analogues of 4-oxo-heptanoic acid (**1.5** and **1.6**) proved to be irreversible inhibitors of DHDPS.[96] The disadvantage of an active site inhibitor is the potential for non-specific aldolase interactions, and for the inhibitor to be overwhelmed by increased amounts of substrate. Furthermore current efforts proceed without a crystallographic model for binding of ASA in the active site, or what effect this may have on the allosteric inhibition.

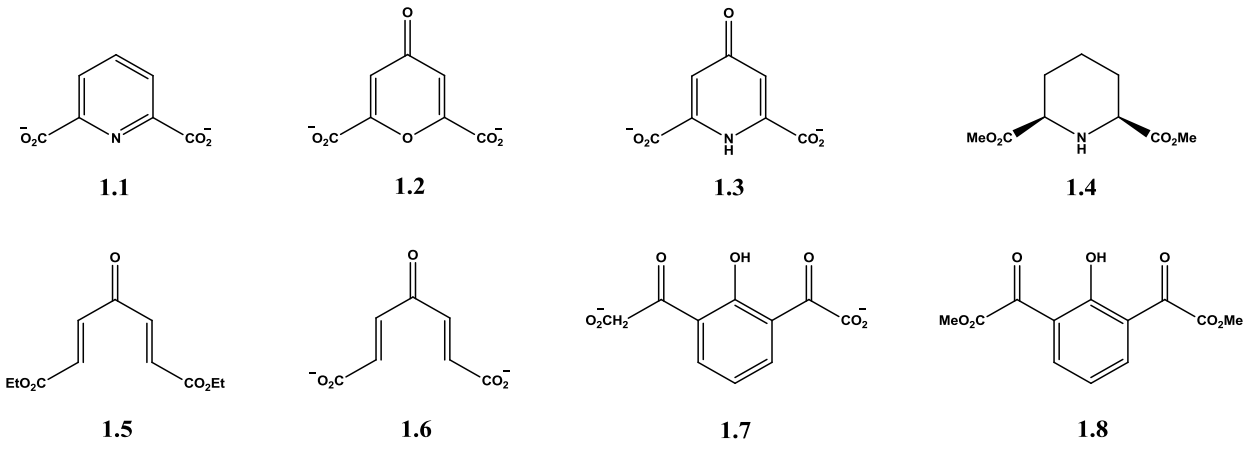

Figure 1.16 – **Inhibitors targeting the active site of DHDPS**

Table 1.4 – **Inhibitors targeting the active site of DHDPS.**

Compound	Inhibition parameter	Organism	Reference
1.1	K_i 11 mM wrt pyr; 18 mM wrt ASA 1 mM decrease activity by 75%	*E. coli* *P. infestans*	*41, 91* *92*
1.2	1 mM decrease activity by 54%	*P. infestans*	*92*
1.3	IC_{50} 22 mM	*E. coli*	*91*
1.4	IC_{50} 20 mM	*E. coli*	*91*
1.5	K_i^{app} 4.95 mM	*E. coli*	*96*
1.6	K_i^{app} 1.63 mM	*E. coli*	*96*
1.7	K_i^{app} 11.8 mM	*E. coli*	*95*
1.8	K_i^{app} 12.0 mM	*E. coli*	*95*

1.7.1 The bound conformation of ASA is unknown

The second step in the reaction mechanism of DHDPS is the binding of ASA followed by aldol condensation (Scheme 1.1, Scheme 1.3). In solution, ASA exists as an equilibrium of a number of species (Figure 1.3): however, the specific configuration which binds and reacts within the active site of DHDPS is unknown.[12, 41, 42] At physiological pH the proportion of ASA in the hydrated form is estimated to be as high as 85%.[97] Under physiological conditions the ASA lactol is not observed by ^{1}H NMR.[42] Blickling *et al.* have noted that G190 and R142 (*Cj*. numbering) are well placed in the active site to coordinate the hydroxyl groups of the hydrate.[12] For these reasons it is widely believed that the aldehyde or hydrate form of ASA must be the catalytically relevant species. However, no crystal structure of DHDPS from any species has ever been determined with

ASA bound to the active site. The absence of a suitable model for the binding of the natural substrate may be retarding efforts to design an active site inhibitor.

The principle challenge of obtaining a crystal structure lies in the reactivity of the ASA. ASA may only bind once the enzyme has been activated by formation of the K166-pyr Schiff base. Unfortunately, the activated enzyme will react with ASA preventing any stable complexation suitable for X-ray diffraction, and ASA will not bind in the absence of pyruvate. One potential strategy is to create a DHDPS dead end complex which will approximate the active site of the catalytically competent DHDPS:pyr enzyme.

If the double bond associated with the K166-pyruvate can be reduced the result would be a non-reactive tetrahedral adduct (Figure 1.17). This strategy has been employed by others for various investigations; most often to demonstrate the formation of the Schiff base.[15, 44, 71] Incubation of DHDPS with borohydride and either pyruvate or ASA is used as evidence that pyruvate is the first substrate. DHDPS activity was eliminated when incubated with pyruvate and sodium borohydride, but not ASA and sodium borohydride. If the DHDPS:pyr complex is first inactivated by reduction, it may be possible to crystallize the dead end complex with ASA bound in the unreactive catalytic site. No attempts at this have ever been reported.

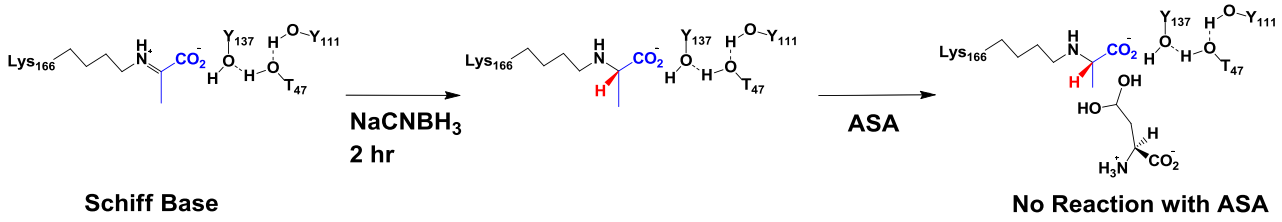

Figure 1.17 – **Reaction Scheme for the reduction of the K166-pyruvate Schiff Base** Using sodium cyanoborohydride the DHDPS:pyr Schiff base is reduced to an sp^3 hybridized dead-end complex.

1.8 Proposal and Research Objectives

The main goal of this research is to provide crystallographic data and structural analysis of DHDPS yielding insights about the natural allosteric inhibition mechanism that will be valuable for the design of synthetic inhibitors. The attention of most research groups studying DHDPS is focused on inhibitors binding at the active site, and aside from random inhibitor screening, no attempts have been made to develop an inhibitor to specifically target the allosteric site. The allosteric site was chosen as a target because noncompetitive inhibitors cannot be overwhelmed by an excessive amount of substrate, therefore pyruvate and ASA inside the cell would not interfere with allosteric inhibitors. Until recently there has been no known noncompetitive inhibitor stronger than the natural inhibitor L-lysine. Regardless of the strength of any reported noncompetitive inhibitors, the mechanism of allosteric signal transduction remains open to debate.

This study aims to determine the subtleties of the allosteric mechanism of inhibition. This will be accomplished by obtaining crystal structures of wild type and Y110F DHDPS with different inhibitors of varying efficacy. The structural effect that inhibitors have on the enzyme will be investigated and correlated to the known strength of each inhibitor. Ideally the crystal structures of wild type and Y110F DHDPS with different inhibitors will

allow us to identify those structural features which are most critical to signal transduction from the allosteric site to the active site. Structural information gleaned throughout this study will contribute to the existing body of knowledge to rationally design synthetic inhibitors which will lead to the development of new clinical antibiotics.

The secondary objective of this study will endeavor to obtain diffraction quality crystals of DHDPS with ASA bound to the active site and to solve the structure at a sufficient resolution to properly model ASA within the active site. Such attempts have not been reported for DHDPS from any source. The strategy employed will first attempt to create a non-reactive dead-end complex of DHDPS and pyruvate. If this dead-end DHDPS will be stable in solution then crystallization with ASA is theoretically possible.

1.9 Contributions of the Author to the Work Presented in this Thesis

All experimental work was performed by the candidate except:

- Cloning and transformation of the *dapA* gene from *C. jejuni* into *E. coli* XL1-Blue strain was performed by Yulia Skovpen;
- DHDPS mutant Y110F was generated by Shuo Li;
- Full kinetic characterization and inhibition studies of wt- and Y110F DHDPS was conducted by Yulia Skopvpen;
- Synthesis of ASA was performed by Yulia Skovpen;
- Design and synthesis of bislysine was undertaken by Yulia Skovpen.
- The crystal structure of wt-DHDPS:pyr:lys (PDB: 4M19) determined by Cuylar Conly prior to initiation of this Thesis as part of an undergraduate Honours Project.

Inclusion of work done by Shuo Li and Yulia Skovpen is done so with their permission, and with that of their supervisor Dr. David Palmer.

1.10 References

[1] Stanton, T. B. (2013) A call for antibiotic alternatives research, *Trends in Microbiology 21*, 111-113.

[2] Lewis, K. (2013) Platforms for antibiotic discovery, *Nature Reviews Drug Discovery 12*, 371-387.

[3] Tipper, D. J. (1985) Mode of action of beta-lactam antibiotics, *Pharmacology & Therapeutics 27*, 1-35.

[4] Bugg, T. D. H., and Walsh, C. T. (1992) Intracellular steps of bacterial cell wall peptidoglycan biosynthesis: enzymology, antibiotics, and antibiotic resistance, *Natural Product Reports 9*, 199-215.

[5] Cummins, C. S., and Harris, H. (1956) The chemical composition of the cell wall in some gram-positive bacteria and its possible value as a taxonomic character, *Journal of General Microbiology 14*, 583-600.

[6] Cox, R. J., Sutherland, A., and Vederas, J. C. (2000) Bacterial diaminopimelate metabolism as a target for antibiotic design, *Bioorganic & Medicinal Chemistry 8*, 843-871.

[7] Hutton, C. A., Southwood, T. J., and Turner, J. J. (2003) Inhibitors of lysine biosynthesis as antibacterial agents, *Mini-Reviews in Medicinal Chemistry 3*, 115-127.

[8] Hutton, C. A., Perugini, M. A., and Gerrard, J. A. (2007) Inhibition of lysine biosynthesis: an evolving antibiotic strategy, *Molecular Biosystems 3*, 458-465.

[9] Yeh, P., Sicard, A. M., and Sinskey, A. J. (1988) General organization of the genes specifically involved in the diaminopimelate-lysine biosynthetic pathway of *Corynebacterium glutamicum*, *Molecular & General Genetics 212*, 105-111.

[10] Frederick Carl, N., and Roy, I. I. I. C. (1996) *Escherichia coli and Salmonella : Cellular and Molecular Biology*.

[11] Bukhari, A. I., and Taylor, A. L. (1971) Genetic analysis of diaminopimelic acid- and lysine-requiring mutants of *Escherichia coli*, *Journal of Bacteriology 105*, 844-854.

[12] Blickling, S., Renner, C., Laber, B., Pohlenz, H. D., Holak, T. A., and Huber, R. (1997) Reaction mechanism of *Escherichia coli* dihydrodipicolinate synthase investigated by X-ray crystallography and NMR spectroscopy, *Biochemistry 36*, 24-33.

[13] Devenish, S. R. A., Blunt, J. W., and Gerrard, J. A. (2010) NMR studies uncover alternate substrates for dihydrodipicolinate synthase and suggest that dihydrodipicolinate reductase is also a dehydratase, *Journal of Medicinal Chemistry 53*, 4808-4812.

[14] Yugari, Y., and Gilvarg, C. (1965) The condensation step in diaminopimelate synthesis, *Journal of Biological Chemistry 240*, 4710-4716.

[15] Borthwick, E. B., Connell, S. J., Tudor, D. W., Robins, D. J., Shneier, A., Abell, C., and Coggins, J. R. (1995) *Escherichia coli* dihydrodipicolinate synthase - characterization of the imine intermediate and the product of bromopyruvate treatment by electrospray mass-spectrometry, *Biochemical Journal 305*, 521-524.
[16] Kumpaisal, R., Hashimoto, T., and Yamada, Y. (1987) Purification and characterization of dihydrodipicolinate synthase from wheat suspension cultures, *Plant Physiology 85*, 145-151.
[17] Dereppe, C., Bold, G., Ghisalba, O., Ebert, E., and Schär, H.-P. (1992) Purification and characterization of dihydrodipicolinate synthase from pea, *Plant Physiology 98*, 813-821.
[18] Frisch, D. A., Gengenbach, B. G., Tommey, A. M., Sellner, J. M., Somers, D. A., and Myers, D. E. (1991) Isolation and characterization of dihydrodipicolinate synthase from maize, *Plant Physiology 96*, 444-452.
[19] Skovpen, Y. V., and Palmer, D. R. J. (2013) Dihydrodipicolinate synthase from *Campylobacter jejuni*: kinetic mechanism of cooperative allosteric inhibition and inhibitor-induced substrate cooperativity, *Biochemistry*, 5454-5462.
[20] Devenish, S. R. A., Huisman, F. H. A., Parker, E. J., Hadfield, A. T., and Gerrard, J. A. (2009) Cloning and characterisation of dihydrodipicolinate synthase from the pathogen *Neisseria meningitidis*, *Biochimica Et Biophysica Acta-Proteins and Proteomics 1794*, 1168-1174.
[21] Dobson, R. C. J., Griffin, M. D. W., Roberts, S. J., and Gerrard, J. A. (2004) Dihydrodipicolinate synthase (DHDPS) from *Escherichia coli* displays partial mixed inhibition with respect to its first substrate, pyruvate, *Biochimie 86*, 311-315.
[22] Domigan, L. J., Scally, S. W., Fogg, M. J., Hutton, C. A., Perugini, M. A., Dobson, R. C. J., Muscroft-Taylor, A. C., Gerrard, J. A., and Devenish, S. R. A. (2009) Characterisation of dihydrodipicolinate synthase (DHDPS) from *Bacillus anthracis*, *Biochimica et Biophysica Acta - Proteins and Proteomics 1794*, 1510-1516.
[23] Rice, E. A., Bannon, G. A., Glenn, K. C., Jeong, S. S., Sturman, E. J., and Rydel, T. J. (2008) Characterization and crystal structure of lysine insensitive *Corynebacterium glutamicum* dihydrodipicolinate synthase (cDHDPS) protein, *Archives of Biochemistry and Biophysics 480*, 111-121.
[24] Kobayashi, K., Ehrlich, S. D., Albertini, A., Amati, G., Andersen, K. K., Arnaud, M., Asai, K., Ashikaga, S., Aymerich, S., Bessieres, P., Boland, F., Brignell, S. C., Bron, S., Bunai, K., Chapuis, J., Christiansen, L. C., Danchin, A., Débarbouillé, M., Dervyn, E., Deuerling, E., Devine, K., Devine, S. K., Dreesen, O., Errington, J., Fillinger, S., Foster, S. J., Fujita, Y., Galizzi, A., Gardan, R., Eschevins, C., Fukushima, T., Haga, K., Harwood, C. R., Hecker, M., Hosoya, D., Hullo, M. F., Kakeshita, H., Karamata, D., Kasahara, Y., Kawamura, F., Koga, K., Koski, P., Kuwana, R., Imamura, D., Ishimaru, M., Ishikawa, S., Ishio, I., Le Coq, D., Masson, A., Mauël, C., Meima, R., Mellado, R. P., Moir, A., Moriya, S., Nagakawa, E., Nanamiya, H., Nakai, S., Nygaard, P., Ogura, M., Ohanan, T., O'Reilly, M., O'Rourke, M., Pragai, Z., Pooley, H. M., Rapoport, G., Rawlins, J. P., Rivas, L. A., Rivolta, C., Sadaie, A., Sadaie, Y., Sarvas, M., Sato, T., Saxild, H. H., Scanlan, E., Schumann, W., Seegers, J. F. M. L., Sekiguchi, J., Sekowska,

A., Séror, S. J., Simon, M., Stragier, P., Studer, R., Takamatsu, H., Tanaka, T., Takeuchi, M., Thomaides, H. B., Vagner, V., van Dijl, J. M., Watabe, K., Wipat, A., Yamamoto, H., Yamamoto, M., Yamamoto, Y., Yamane, K., Yata, K., Yoshida, K., Yoshikawa, H., Zuber, U., and Ogasawara, N. (2003) Essential *Bacillus subtilis* genes, *Proceedings of the National Academy of Sciences 100*, 4678-4683.

[25] Akerley, B. J., Rubin, E. J., Novick, V. L., Amaya, K., Judson, N., and Mekalanos, J. J. (2002) A genome-scale analysis for identification of genes required for growth or survival of Haemophilus influenzae, *Proceedings of the National Academy of Sciences of the United States of America 99*, 966-971.

[26] Schnell, R., Oehlmann, W., Sandalova, T., Braun, Y., Huck, C., Maringer, M., Singh, M., and Schneider, G. (2012) Tetrahydrodipicolinate N-succinyltransferase and dihydrodipicolinate synthase from *Pseudomonas aeruginosa*: structure analysis and gene deletion, *PLoS One 7*, e31133.

[27] Hoganson, D. A., and Stahly, D. P. (1975) Regulation of dihydrodipicolinate synthase during growth and sporulation of *Bacillus cereus*, *Journal of Bacteriology 124*, 1344-1350.

[28] Fukuda, A., and Gilvarg, C. (1968) The relationship of dipicolinate and lysine biosynthesis in *Bacillus megaterium*, *Journal of Biological Chemistry 243*, 3871-3876.

[29] Parker, C. T., Miller, W. G., Horn, S. T., and Lastovica, A. J. (2007) Common genomic features of *Campylobacter jejuni* subsp. doylei strains distinguish them from *C. jejuni* subsp. *jejuni*, *BioM Central Microbiology 7*, 50.

[30] Young, K. T., Davis, L. M., and DiRita, V. J. (2007) *Campylobacter jejuni*: molecular biology and pathogenesis, *Nature Reviews Microbiology 5*, 665-679.

[31] Allos, B. M., and Blaser, M.J. (2009) *Campylobacter jejuni* and related species, In *In Principles and Practice of Infectious Disease* (Mandell, G. L., Bennett, J.E., and Dolin, R., Ed.) 7th ed., pp 2793-2802, Elsevier, Philidelphia.

[32] Kaldor, J., and Speed, B. (1984) Guillain-Barre syndrome and *Campylobacter jejuni*: a serological study, *British Medical Journal 288*, 1867-1870.

[33] Jacobs, B. C., Endtz, H. P., van der Meché, F. G., Hazenberg, M. P., Achtereekte, H. A., and van Doorn, P. A. (1995) Serum anti-GQ1b IgG antibodies recognize surface epitopes on *Campylobacter jejuni* from patients with Miller Fisher syndrome, *Annals of neurology 37*, 260-264.

[34] Hughes, R. (2004) *Campylobacter jejuni* in Guillain-Barré syndrome, *The Lancet Neurology 3*, 644.

[35] Molbak, K., and Havelaar, A. (2008) *Burden of illness of campylobacteriosis and sequelae*, 3rd ed., ASM Press, Washington, DC.

[36] Vaughan-Shaw, P. G., Rees, J. R., White, D., and Burgess, P. (2010) *Campylobacter jejuni* cholecystitis: a rare but significant clinical entity, *British Medical Journal Case Reports 2010*.

[37] Tappe, D., Schulze, M. H., Oesterlein, A., Abele-Horn, M., Baron, S., Durchholz, D., Langen, H.-J., Jany, B., and Schoen, C. (2012) Molecular detection of *Campylobacter jejuni* as a cause of culture-negative spondylodiscitis, *Journal of Clinical Microbiology 50*, 1499-1500.

[38] Dobson, R. C. J., Valegard, K., and Gerrard, J. A. (2004) The crystal structure of three site-directed mutants of *Escherichia coli* dihydrodipicolinate synthase: Further evidence for a catalytic triad, *Journal of Molecular Biology 338*, 329-339.
[39] Kefala, G., Evans, G. L., Griffin, M. D. W., Devenish, S. R. A., Pearce, F. G., Perugini, M. A., Gerrard, J. A., Weiss, M. S., and Dobson, R. C. J. (2008) Crystal structure and kinetic study of dihydrodipicolinate synthase from *Mycobacterium tuberculosis*, *Biochemical Journal 411*, 351-360.
[40] Renwick C. J. Dobson, Michael D. W. Griffin, and, G. B. J., and Gerrard, J. A. (2005) The crystal structures of native and (S)-lysine-bound dihydrodipicolinate synthase from *Escherichia coli* with improved resolution show new features of biological significance, *Acta Crystallographica D D61*, 1116–1124.
[41] Karsten, W. E. (1997) Dihydrodipicolinate synthase from *Escherichia coli*: pH dependent changes in the kinetic mechanism and kinetic mechanism of allosteric inhibition by L-lysine, *Biochemistry 36*, 1730-1739.
[42] Coulter, C. V., Gerrard, J. A., Kraunsoe, J. A. E., Moore, D. J., and Pratt, A. J. (1996) (S)-Aspartate semi-aldehyde: Synthetic and structural studies, *Tetrahedron 52*, 7127-7136.
[43] Dobson, R. C. J., Devenish, S. R. A., Turner, L. A., Clifford, V. R., Pearce, F. G., Jameson, G. B., and Gerrard, J. A. (2005) Role of arginine 138 in the catalysis and regulation of *Escherichia coli* dihydrodipicolinate synthase, *Biochemistry 44*, 13007-13013.
[44] Shedlarski, J. G., and Gilvarg, C. (1970) The pyruvate-aspartic semialdehyde condensing enzyme of *Escherichia coli*, *Journal of Biological Chemistry 245*, 1362-1373.
[45] Atkinson, S., Dogovski, C., Downton, M., Czabotar, P., Dobson, R. J., Gerrard, J., Wagner, J., and Perugini, M. (2013) Structural, kinetic and computational investigation of *Vitis vinifera* DHDPS reveals new insight into the mechanism of lysine-mediated allosteric inhibition, *Plant Molecular Biology 81*, 431-446.
[46] Burgess, B. R., Dobson, R. C. J., Bailey, M. F., Atkinson, S. C., Griffin, M. D. W., Jameson, G. B., Parker, M. W., Gerrard, J. A., and Perugini, M. A. (2008) Structure and evolution of a novel dimeric enzyme from a clinically important bacterial pathogen, *Journal of Biological Chemistry 283*, 27598-27603.
[47] Conly, C. J. T., Skovpen, Y. V., Li, S., Palmer, D. R. J., and Sanders, D. A. R. (2014) Tyrosine 110 plays a critical role in regulating the allosteric inhibition of *Campylobacter jejuni* dihydrodipicolinate synthase by lysine, *Biochemistry 53*, 7396-7406.
[48] Yamakura, F., Ikeda, Y., Kimura, K., and Sasakawa, T. (1974) Partial purification and some properties of pyruvate-aspartic semialdehyde condensing enzyme from sporulating *Bacillus subtilis*, *Journal of Biochemistry 76*, 611-621.
[49] Halling, S. M., and Stahly, D. P. (1976) Dihydrodipicolinic acid synthase of *Bacillus licheniformis*. Quaternary structure, kinetics, and stability in the presence of sodium chloride and substrates, *Biochimica et Biophysica Acta 452*, 580-596.
[50] Bartlett, A. W., P. (1986) Regulation of the enzymes of lysine biosynthesis in *Brevibacterium lactofermentum* NCTC 9602 during vegetative growth., *Journal of General Microbiology 132*, 3169-3177.

[51] Webster, F. H., and Lechowich, R. V. (1970) Partial purification and characterization of dihydrodipicolinic acid synthetase from sporulating *Bacillus megaterium*, *Journal of Bacteriology 101*, 118-126.
[52] Kumpaisal, R., Hashimoto, T., and Yamada, Y. (1989) Inactivation of wheat dihydrodipicolinate synthase by 3-bromopyruvate, *Agricultural and Biological Chemistry 53*, 355-359.
[53] Larkin, M. A., Blackshields, G., Brown, N. P., Chenna, R., McGettigan, P. A., McWilliam, H., Valentin, F., Wallace, I. M., Wilm, A., Lopez, R., Thompson, J. D., Gibson, T. J., and Higgins, D. G. (2007) Clustal W and Clustal X version 2.0, *Bioinformatics 23*, 2947-2948.
[54] Goujon, M., McWilliam, H., Li, W., Valentin, F., Squizzato, S., Paern, J., and Lopez, R. (2010) A new bioinformatics analysis tools framework at EMBL-EBI, *Nucleic Acids Research 38*, W695-699.
[55] Skovpen, Y. (2014) *Novel inhibitors of dihydrodipicolinate synthase*, (Doctor of Philosphy). Retrieved from Department of Chemistry, University of Saskatchewan
[56] Girish, T. S., Sharma, E., and Gopal, B. (2008) Structural and functional characterization of *Staphylococcus aureus* dihydrodipicolinate synthase, *Federation of European Biochemical Societies Letters 582*, 2923-2930.
[57] Wierenga, R. K. (2001) The TIM-barrel fold: a versatile framework for efficient enzymes, *Federation of European Biochemical Societies Letters 492*, 193-198.
[58] Mirwaldt, C., Korndorfer, I., and Huber, R. (1995) The crystal structure of dihydrodipicolinate synthase from *Escherichia coli* at 2.5 Å resolution, *Journal of Molecular Biology 246*, 227-239.
[59] Blickling, S., Beisel, H. G., Bozic, D., Knablein, J., Laber, B., and Huber, R. (1997) Structure of dihydrodipicolinate synthase of *Nicotiana sylvestris* reveals novel quaternary structure, *Journal of Molecular Biology 274*, 608-621.
[60] Atkinson, S. C., Dogovski, C., Newman, J., Dobson, R. C. J., and Perugini, M. A. (2011) Cloning, expression, purification and crystallization of dihydrodipicolinate synthase from the grapevine *Vitis vinifera*, *Acta Crystallographica F 67*, 1537-1541.
[61] Voss, J. E., Scally, S. W., Taylor, N. L., Atkinson, S. C., Griffin, M. D. W., Hutton, C. A., Parker, M. W., Alderton, M. R., Gerrard, J. A., Dobson, R. C. J., Dogovski, C., and Perugini, M. A. (2010) Substrate-mediated stabilization of a tetrameric drug target reveals achilles heel in anthrax, *Journal of Biological Chemistry 285*, 5188-5195.
[62] Blagova, E., Levdikov, V., Milioti, N., Fogg, M. J., Kalliomaa, A. K., Brannigan, J. A., Wilson, K. S., and Wilkinson, A. J. (2006) Crystal structure of dihydrodipicolinate synthase (BA3935) from *Bacillus anthracis* at 1.94 Å resolution, *Proteins: Structure, Function, and Bioinformatics 62*, 297-301.
[63] Pearce, F. G., Perugini, M. A., McKerchar, H. J., and Gerrard, J. A. (2006) Dihydrodipicolinate synthase from *Thermotoga maritima*, *Biochemical Journal 400*, 359-366.
[64] Pearce, F. G., Dobson, R. C. J., Weber, A., Lane, L. A., McCammon, M. G., Squire, M. A., Perugini, M. A., Jameson, G. B., Robinson, C. V., and Gerrard, J. A. (2008) Mutating the tight-dimer interface of dihydrodipicolinate synthase disrupts

the enzyme quaternary structure: toward a monomeric enzyme, *Biochemistry 47*, 12108-12117.
[65] da Costa, T. P. S., Muscroft-Taylor, A. C., Dobson, R. C. J., Devenish, S. R. A., Jameson, G. B., and Gerrard, J. A. (2010) How essential is the 'essential' active-site lysine in dihydrodipicolinate synthase?, *Biochimie 92*, 837-845.
[66] Devenish, S. R. A., Gerrard, J. A., Jameson, G. B., and Dobson, R. C. J. (2008) The high-resolution structure of dihydrodipicolinate synthase from *Escherichia coli* bound to its first substrate, pyruvate, *Acta Crystallographica F 64*, 1092-1095.
[67] Dobson, R. C. J., Perugini, M. A., Jameson, G. B., and Gerrard, J. A. (2009) Specificity versus catalytic potency: The role of threonine 44 in *Escherichia coli* dihydrodipicolinate synthase mediated catalysis, *Biochimie 91*, 1036-1044.
[68] Kaur, N., Gautam, A., Kumar, S., Singh, A., Singh, N., Sharma, S., Sharma, R., Tewari, R., and Singh, T. P. (2011) Biochemical studies and crystal structure determination of dihydrodipicolinate synthase from *Pseudomonas aeruginosa*, *International Journal of Biological Macromolecules 48*, 779-787.
[69] Griffin, M. D. W., Billakanti, J. M., Wason, A., Keller, S., Mertens, H. D. T., Atkinson, S. C., Dobson, R. C. J., Perugini, M. A., Gerrard, J. A., and Pearce, F. G. (2012) Characterisation of the first enzymes committed to lysine biosynthesis in *Arabidopsis thaliana*, *PLoS ONE 7*, e40318.
[70] Shaver, J. M., Bittel, D. C., Sellner, J. M., Frisch, D. A., Somers, D. A., and Gengenbach, B. G. (1996) Single-amino acid substitutions eliminate lysine inhibition of maize dihydrodipicolinate synthase, *Proceedings of the National Academy of Sciences 93*, 1962-1966.
[71] Laber, B., Gomisruth, F. X., Romao, M. J., and Huber, R. (1992) *Escherichia coli* dihydrodipicolinate synthase - identification of the active-site and crystallization, *Biochemical Journal 288*, 691-695.
[72] Blickling, S., and Knablein, J. (1997) Feedback inhibition of dihydrodipicolinate synthase enzymes by L-lysine, *Biological Chemistry 378*, 207-210.
[73] Ghislain, M., Frankard, V., and Jacobs, M. (1995) A dinucleotide mutation in dihydrodipicolinate synthase of *Nicotiana sylvestris* leads to lysine overproduction, *Plant Journal 8*, 733-743.
[74] Bakhiet, N., Forney, F., Stahly, D., and Daniels, L. (1984) Lysine biosynthesis in *Methanobacterium thermoautotrophicum* is by the diaminopimelic acid pathway, *Current Microbiology 10*, 195-198.
[75] Stahly, D. P. (1969) Dihydrodipicolinic acid synthase of *Bacillus licheniformis*, *Biochimica et Biophysica Acta - Enzymology 191*, 439-451.
[76] Cremer, J., Eggeling, L., and Sahm, H. (1990) Cloning the dapA dapB cluster of the lysine-secreting bacterium *Corynebacterium glutamicum*, *Molecular and General Genetics 220*, 478-480.
[77] Tosaka, O., and Takinami, K. (1978) Pathway and regulation of lysine biosynthesis in *Brevibacterium lactofermentum*, *Agricultural and Biological Chemistry 42*, 95-100.
[78] Vauterin, M., Frankard, V., and Jacobs, M. (2000) Functional rescue of a bacterial dapA auxotroph with a plant cDNA library selects for mutant clones encoding a feedback-insensitive dihydrodipicolinate synthase, *Plant Journal 21*, 239-248.

[79] Joerger, A. C., Mayer, S., and Fersht, A. R. (2003) Mimicking natural evolution in vitro: An N-acetylneuraminate lyase mutant with an increased dihydrodipicolinate synthase activity, *Proceedings of the National Academy of Sciences of the United States of America 100*, 5694-5699.

[80] Tam, P. H., Phenix, C. P., and Palmer, D. R. J. (2004) MosA, a protein implicated in rhizopine biosynthesis in *Sinorhizobium meliloti* L5-30, is a dihydrodipicolinate synthase, *Journal of Molecular Biology 335*, 393-397.

[81] Muscroft-Taylor, A. C., Soares da Costa, T. P., and Gerrard, J. A. (2010) New insights into the mechanism of dihydrodipicolinate synthase using isothermal titration calorimetry, *Biochimie 92*, 254-262.

[82] Phenix, C. P., and Palmer, D. R. J. (2008) Isothermal titration microcalorimetry reveals the cooperative and noncompetitive nature of inhibition of *Sinorhizobium meliloti* L5-30 dihydrodipicolinate synthase by (S)-lysine, *Biochemistry 47*, 7779-7781.

[83] Falco, S. C., Guida, T., Locke, M., Mauvais, J., Sanders, C., Ward, R. T., and Webber, P. (1995) Transgenic canola and soybean seeds with increased lysine, *Biotechnology 13*, 577-582.

[84] Ohnoutkova, L., Zitka, O., Mrizova, K., Vaskova, J., Galuszka, P., Cernei, N., Smedley, M. A., Harwood, W. A., Adam, V., and Kizek, R. (2012) Electrophoretic and chromatographic evaluation of transgenic barley expressing a bacterial dihydrodipicolinate synthase, *Electrophoresis 33*, 2365-2373.

[85] Long, X., Liu, Q., Chan, M., Wang, Q., and Sun, S. S. M. (2013) Metabolic engineering and profiling of rice with increased lysine, *Plant Biotechnology Journal 11*, 490-501.

[86] Bittel, D. C., Shaver, J. M., Somers, D. A., and Gengenbach, B. G. (1996) Lysine accumulation in maize cell cultures transformed with a lysine-insensitive form of maize dihydrodipicolinate synthase, *Theoretical and Applied Genetics 92*, 70-77.

[87] Sahm, H., Eggeling, L., Eikmanns, B., and Krämer, R. (1995) Metabolic design in amino acid producing bacterium *Corynebacterium glutamicum*, *Federation of European Microbiological Societies Microbiology Reviews 16*, 243-252.

[88] Coulter, C. V., Gerrard, J. A., Kraunsoe, J. A. E., and Pratt, A. J. (1999) *Escherichia coli* dihydrodipicolinate synthase and dihydrodipicolinate reductase: kinetic and inhibition studies of two putative herbicide targets, *Pesticide Science 55*, 887-895.

[89] Griffin, M. D. W., Dobson, R. C. J., Pearce, F. G., Antonio, L., Whitten, A. E., Liew, C. K., Mackay, J. P., Trewhella, J., Jameson, G. B., Perugini, M. A., and Gerrard, J. A. (2008) Evolution of quaternary structure in a homotetrameric enzyme, *Journal of Molecular Biology 380*, 691-703.

[90] Griffin, M. D. W., Dobson, R. C. J., Gerrard, J. A., and Perugini, M. A. (2010) Exploring the dihydrodipicolinate synthase tetramer: How resilient is the dimer-dimer interface?, *Archives of Biochemistry & Biophysics 494*, 58-63.

[91] Turner, J. J., Gerrard, J. A., and Hutton, C. A. (2005) Heterocyclic inhibitors of dihydrodipicolinate synthase are not competitive, *Bioorganic & Medicinal Chemistry 13*, 2133-2140.

[92] Walters, D. R., McPherson, A., and Robins, D. J. (1997) Inhibition of lysine biosynthesis in *Phytophthora infestans*, *Mycological Research 101*, 329-333.

[93] Mitsakos, V., Dobson, R. C. J., Pearce, F. G., Devenish, S. R., Evans, G. L., Burgess, B. R., Perugini, M. A., Gerrard, J. A., and Hutton, C. A. (2008) Inhibiting dihydrodipicolinate synthase across species: Towards specificity for pathogens?, *Bioorganic & Medicinal Chemistry Letters 18*, 842-844.
[94] Boughton, B. A., Dobson, R. C. J., Gerrardc, J. A., and Hutton, C. A. (2008) Conformationally constrained diketopimelic acid analogues as inhibitors of dihydrodipicolinate synthase, *Bioorganic & Medicinal Chemistry Letters 18*, 460-463.
[95] Boughton, B. A., Hor, L., Gerrard, J. A., and Hutton, C. A. (2012) 1,3-Phenylene bis(ketoacid) derivatives as inhibitors of *Escherichia coli* dihydrodipicolinate synthase, *Bioorganic & Medicinal Chemistry 20*, 2419-2426.
[96] Boughton, B. A., Griffin, M. D. W., O'Donnell, P. A., Dobson, R. C. J., Perugini, M. A., Gerrard, J. A., and Hutton, C. A. (2008) Irreversible inhibition of dihydrodipicolinate synthase by 4-oxo-heptenedioic acid analogues, *Bioorganic & Medicinal Chemistry 16*, 9975-9983.
[97] Shames, S. L., and Wedler, F. C. (1984) Homoserine kinase of *Escherichia coli*: kinetic mechanism and inhibition by L-aspartate semialdehyde, *Archives of Biochemistry and Biophysics 235*, 359-370.

Chapter 2 EXPERIMENTAL METHODS

2.1 Chemical Reagents

2.1.1 ASA Synthesis

ASA was synthesized according to the reported procedure.[1] Due to the hydroscopic properties of ASA, the concentration of each newly prepared solution of ASA was determined using the DHDPS-DHDPR coupled kinetic assay as previously described, in the presence of excess NADH.[2] ASA was synthesized by Yulia Skovpen who generously shared her secret stash.

2.1.2 Bislysine Synthesis

Bislysine was synthesized by Yulia Skovpen according to the procedures of Skovpen and Palmer,[3] and generously provided on demand.

2.2 Crystallographic Studies of DHDPS

2.2.1 Protein Preparation

2.2.1.1 Cloning and overexpression

C.jejuni genomic DNA was prepared by Dr. Bonnie Chaban, Western College of Veterinary Medicine, University of Saskatchewan. The *dapA* genes (encoding DHDPS) were PCR-amplified from genomic DNA using Kapa HiFi DNA polymerase (Kapa Biosystems) with the following forward and reverse primer pairs:

5'-GAAAGGGGATCCATGGATAAAAATATTATCATTGGGGC-3',

5'-ATTCTGCTGCAGTTAAAATCCTTTGATCTTATATTTTTTCATCACTTC-3'.

The *dapA* gene was ligated into a pQE-80L vector (Qiagen) as a *Bam*HI/*Pst*I restriction fragment using T4 DNA ligase (New England BioLabs). *E. coli* XL1-Blue competent cells were then transformed with these plasmids. Colonies containing the correct recombinant plasmids were

identified by analysis of restriction enzyme products, with positive candidates sequenced by the DNA Technologies Unit of the National Research Council, Saskatoon SK, Canada.

A plasmid containing the *dapA* gene (encoding DHDPS or its mutant, and bearing an N-terminal hexahistidine tag) was transformed into *E. coli* as previously described[4]. The cells were cultured at 310 K with shaking in Terrific Broth media, containing 50 mg/L ampicillin until cultures reached an OD_{600} of 0.5 – 0.6. Over-expression of DHDPS was induced with the addition of IPTG (isopropyl-β-D-thiogalactopyranoside) to a concentration of 0.5 mM and incubated for a further 15 hours at 288 K. Cells were pelleted in 500 mL batches at 277 K by centrifugation at 4400 x g for 30 minutes, and stored at 190 K. The sample was chilled in an ice bath during all manipulations.

2.2.1.2 Purification

Frozen cell pellets (from 500 mL batches) were resuspended in 25 mL of lysis buffer (50 mM HEPES, 500 mM NaCl, 5% glycerol, 5 mM imidazole, pH 7.9) with 0.2 mg DNAse and 0.4 mg lysozyme. Cells were disrupted by sonication (15 seconds on, 15 seconds off for 3 minutes, level 6) using a Virisonic 600 Ultrasonic Cell Disrupter. The supernatant was separated from the cell debris by centrifugation at 27000 × *g* for 10 minutes at 277 K. The supernatant was passed through a 0.45 µm filter and loaded onto a 1 mL GE Health Care Gravis His Trap Column (GE Healthcare)**.** The column was operated according to the manufacturers recommended procedure with the following modifications: the concentration of imidazole in the binding buffer was changed from 20 mM to 50 mM; an additional wash step using 100 mM imidazole was added prior to enzyme elution to enhance the purity of the final eluent; DHDPS was eluted using the elution buffer described by the manufacturer; prior to storage, the column was washed with 15 mL rather than 10 mL of ethanol to ensure maximum cleanliness and improve the life of the column. The purity

of collected fractions was assessed by SDS-PAGE. Pure fractions of DHDPS were pooled and dialyzed overnight (20 mM HEPES, 250 mM NaCl, 2 mM DTT, 10% v/v glycerol), then concentrated using Sartorius Stedim Vivaspin 20 centrifuge filters. The protein was aliquoted into 50 µL fractions at ~10 mg/mL and flash frozen in liquid nitrogen before being stored at 193 K. Enzyme concentrations were determined by NanoDrop® ND-1000 using calculated parameters (protParam)[5] (molecular weight and extinction coefficient) for DHDPS (MW 34069 Da, ε_{280} =18068 M^{-1} cm^{-1}).[3, 5]

2.2.2 Crystallization Screening

The commercially available screening kit PEGII Suite (Hampton Research, USA) was selected for its broad overlap of crystallization conditions reported for DHDPS from *C. jejuni* and other species[6-9]. Crystallization trials were carried out at 287 K using 96 well sitting drop plates from Hampton Research, USA. Sitting drops were mixed with 1.0 µL wild type protein solution (~10 mg/mL) and 1.0 µL precipitant solution with a 100 µL well of the same precipitant solution. Several positive hits were identified and selected for further optimization using the hanging drop method with 3 µL drops mixed 1:1 over a 500 µL well.

2.2.3 Crystal Optimization

For each of the wild type and mutant DHDPS, in combination with various substrates and inhibitors, hanging drop vapor diffusion trials were conducted to systematically optimize positive hits identified from the PEGII Suite (Hampton Research, USA). Modifications were made to precipitant and protein concentrations, temperature, drop volume, and pH. The best diffracting crystallization conditions for each obtained crystal structure is listed in Table A.1.

2.2.4 Ligand Soaking Experiments

2.2.4.1 Soaking with L-lysine

The inhibitor L-lysine was introduced to crystallized DHDPS as a component of the cryoprotectant solution (10% ethylene glycol, 30% PEG 400, 60% precipitant solution with 10 mM lysine and 30 mM lysine in Y110F). In the absence of lysine, crystals were stable in the cryoprotectant solution. With lysine present in the cryoprotectant, crystal quality degraded if soaked for an extended period. Crystals which maintained diffraction quality were soaked in the aforementioned cryoprotectant solution for 5 minutes before being flash-cooled in liquid nitrogen.

2.2.4.1 Soaking with Thialysine

The inhibitor thialysine was introduced to crystallized DHDPS as a component of the cryoprotectant solution (10% ethelyne glycol, 30% PEG 400, 60% precipitant solution with 30 mM Thialysine). In contrast with L-lysine soaking, DHDPS was stable for extended periods of time in the presence of thialysine.

2.2.5 Co-crystallization Experiments

2.2.5.1 Co-crystallization with Bislysine

Diffraction quality crystals were grown in a solution of 0.2 M sodium acetate, 16% PEG4000, 0.1 mM Tris pH 8.5 using the hanging drop vapour diffusion method. Protein and precipitant solutions were mixed in a 1:1 3 µL drop over 500 µL well. DHDPS was pre-incubated with 20 mM bislysine prior to setting up crystallization trials. Crystals were transferred to a cryoprotectant solution consisting of 10% ethylene glycol, 30% PEG 400, 60% precipitant solution with 10 mM bislysine and then flash frozen in liquid nitrogen.

Co-crystallization of Y110F:bislysine was accomplished in a solution of 0.28 M Sodium Acetate, 13% P4000, 0.1 M Tris pH 8.5 using the hanging drop vapour diffusion method. Protein and precipitant where mixed in a 1:1 3 µL drop over 500 µL well. Y110F-DHDPS was pre-incubated with 25 mM bislysine prior to setting up crystallization trials. Crystals were transferred to a cryoprotectant solution consisting of 10% ethylene glycol, 30% P400, 60% precipitant solution with 20 mM bislysine and then flash frozen in liquid nitrogen.

2.2.5.2 Dead end complexation with ASA

2.2.5.2.1 Active Site Clearing with ASA

Since the *Cj*-DHDPS enzyme co-purifies with pyruvate bound in the active site it was necessary to incubate with ASA in order to obtain the apoenzyme form of DHDPS. apo-DHDPS crystals were cyoprotected in a solution of 10% ethylene glycol, 30% PEG 400, 60% precipitant solution. Prior to crystallization, purified DHDPS was incubated with 10 mM ASA for 30 min. This was followed by dialysis (20 mM HEPES, 250 mM NaCl, 2 mM DTT) to remove excess ASA and dihydrodipicolinic acid.

2.2.5.2.2 Crystallization with ASA

To obtain DHDPS crystals with ASA it is necessary to ensure that no reaction will occur. A strategy was developed to create a dead-end complex by reducing the Schiff base; therefore trapping pyruvate in the active site. DHDPS samples were removed from storage (353.15 ˚K) and incubated with 3 mM pyruvate for 30 min to ensure full occupancy. This is followed by 2 hour incubation with 6 mM sodium cyanoborohydride ($NaCNBH_3$). The modified DHDPS is then dialyzed (20 mM HEPES, 250 mM NaCl, 2 mM DTT) to remove excess pyruvate and $NaCNBH_3$ (BH). Samples were then centrifuged to the desired concentration using Sartorius Stedim Vivaspin 20 centrifuge filters.

2.2.5.2.3 Verification of dead-end complexation

Dead-end complexation of BH-DHDPS:lac was verified using the DHDPS-DHDPR coupled assay, as described previously.[2] A binary assessment of activity was made for the DHDPS enzymatic reaction by monitoring the decrease in absorbance at 340 nm due to oxidation of NADH (ε_{340} = 6220 $M^{-1}cm^{-1}$). All kinetic measurements where performed on a Beckman DU640 spectrophotometer at 25 ˚C maintained by a circulating water bath. Only freshly prepared substrates were used in the assay. All measurements where made using 100 mM HEPES buffer at pH 8.0. A typical assay contained 0.16 mM NADH, 1.0 µg of DHDPS, 7.15 µg DHDPR and 0.124 mM of ASA and 0.37 mM of pyruvate. The excess amount of DHDPR was determined experimentally, to ensure that the DHDPS-catalyzed reaction would be rate-limiting. Cuvettes containing the assay mixture were incubated for three minutes to equilibrate at 25 ˚C before the reaction was triggered by the addition of DHDPS.

Modified DHDPS (without ASA) was crystallized using the hanging drop vapour diffusion method in a solution of 0.2 M sodium acetate, 15% PEG 4000, and 0.1 mM Tris buffer at pH 8.5. Crystals containing ASA were co-crystallized in the presence of 100 mM ASA using the hanging drop vapor diffusion method and a solution of 0.16 M Di-Ammonium tartarate, 12% PEG 3350, pH 8.5, with a protein concentration of 5.13 mg/mL. Protein and precipitant solutions where mixed in a 1:1 with 3 µL drop over 500 µL well. Crystals of reduced-DHDPS in the absence of ASA were cryoprotected in a solution of 10% ethylene glycol, 30% PEG 400, 60% precipitant and then flash frozen in liquid nitrogen. Crystals of reduced-DHDPS co-crystallized with 100 mM ASA were flash frozen directly from the mother liquor without additional cryoprotection.

2.2.6 Diffraction, Data Collection, and Data Processing

Diffraction experiments were conducted using synchrotron radiation at the Canadian Macromolecular Crystallography Facility (CMCF-1) beamlines (08ID-1 and 08B1-01) at the Canadian Light Source (CLS), Saskatoon, Saskatchewan, Canada. The crystal was kept at a temperature of 100 K in a stream of nitrogen gas during data collection. Diffracted x-rays were detected using a MAR 300CCD detector. Intensity data was indexed, integrated and scaled using either auto-XDS/XSCALE, or d*Trek[10, 11]. Pertinent data-collection statistics and refinement parameters are given in Table A.1 in the appendix.

2.2.7 Structure Solution and Refinement

MolRep was used to find a molecular replacement solution for each DHDPS structure using the atomic coordinates of the solvent-stripped wild type structure (PDB: 3M5V) as the search model.[12] The solution found four monomers organized as a tetramer in the asymmetric unit, with the exception of the Y110F:pyr:lys (PDB: 4MLR) structure, and the wt-DHPS:thialysine structure which each contain two tetramers in the asymmetric unit. Solvent content determined from Matthews coefficients were consistently between 40% and 50%.[13] Further refinements were made using PHENIX[14], with manual model correction in COOT.[15] Final refinement statistics are given in Table A.2 in the appendix.

2.2.8 Validation of Structures

When the DHDPS structures could no longer be improved using refinement and modeling, the final model was validated using Molprobity[14] in Phenix[14] and validation tools in COOT.[15]

2.3 Determination of Dynamic Domains

2.3.1 Use of DynDom

DynDom web server and the associated domain movement database can be freely accessed at http://fizz.cmp.uea.ac.uk/dyndom/. The web server accepts either direct upload of PDB files, or queries to the Protein Data Bank. DynDom can be used as a web application or downloaded for offline use. For a brief introduction to the function of dynDom see Appendix B; for an in depth review see the original work of Hayward and Poornam *et al.* (1994-1996).[16-19]

DynDom was used extensively to examine each structure in Table A.1 against each other structure in Table A.1. The dynDom program allows the user to designate which of two structures will be the reference, and which will be the moving structure. Each structure from Table A.1 was assigned the role of reference structure in turn. The program allows, per run, the comparison of one monomer from the moving structure against one monomer of the reference structure. Thus each of four monomers of the designated moving structure was compared to each of four monomers of the designated reference structure. The roles of reference and moving structure were reversed and comparisons were made again. This process was repeated for all possible structure pairings from Table A.1. Results of each pairing are discussed in the applicable sections to follow.

2.4 Calculation of Cavity Volumes

2.4.1 Use of CASTp

CASTp is made freely available at the website http://cast.engr.uic.edu. The web server accepts direct upload of PDB files, and delivers outputs by e-mail. For a brief introduction to the function of CASTp see Appendix B; for an in depth review see the origional work of Edelsbruner *et al.* (1994-1996).[20-23]

All solvent molecules are explicitly removed from the input model. Ligands and hetero atoms were excluded for each calculation. A probe of radius of 1.2 Å was used for water during the calculations.[24] The outputs of all computations give two sets of parameters, one based on molecular surface (MS) and one based on solvent accessible surface (SA).[25, 26] Molecular visualization of pockets and cavities are generated using RasMol.[27]

Each DHDPS structure was submitted in turn. All solvent molecules and inhibitors were excluded from the analysis. In order to properly define the active site it was necessary to submit only the tight-dimer half of DHDPS, rather than the complete structure. This was due to a computational anomaly where the location of active sites ("within the DHDPS doughnut hole"; Figure 2.1) allowed the algorithm to encompass all 4 active sites within a single defined cavity. Visualizations and structural superposition was carried out in pymol using the CASTp extension.

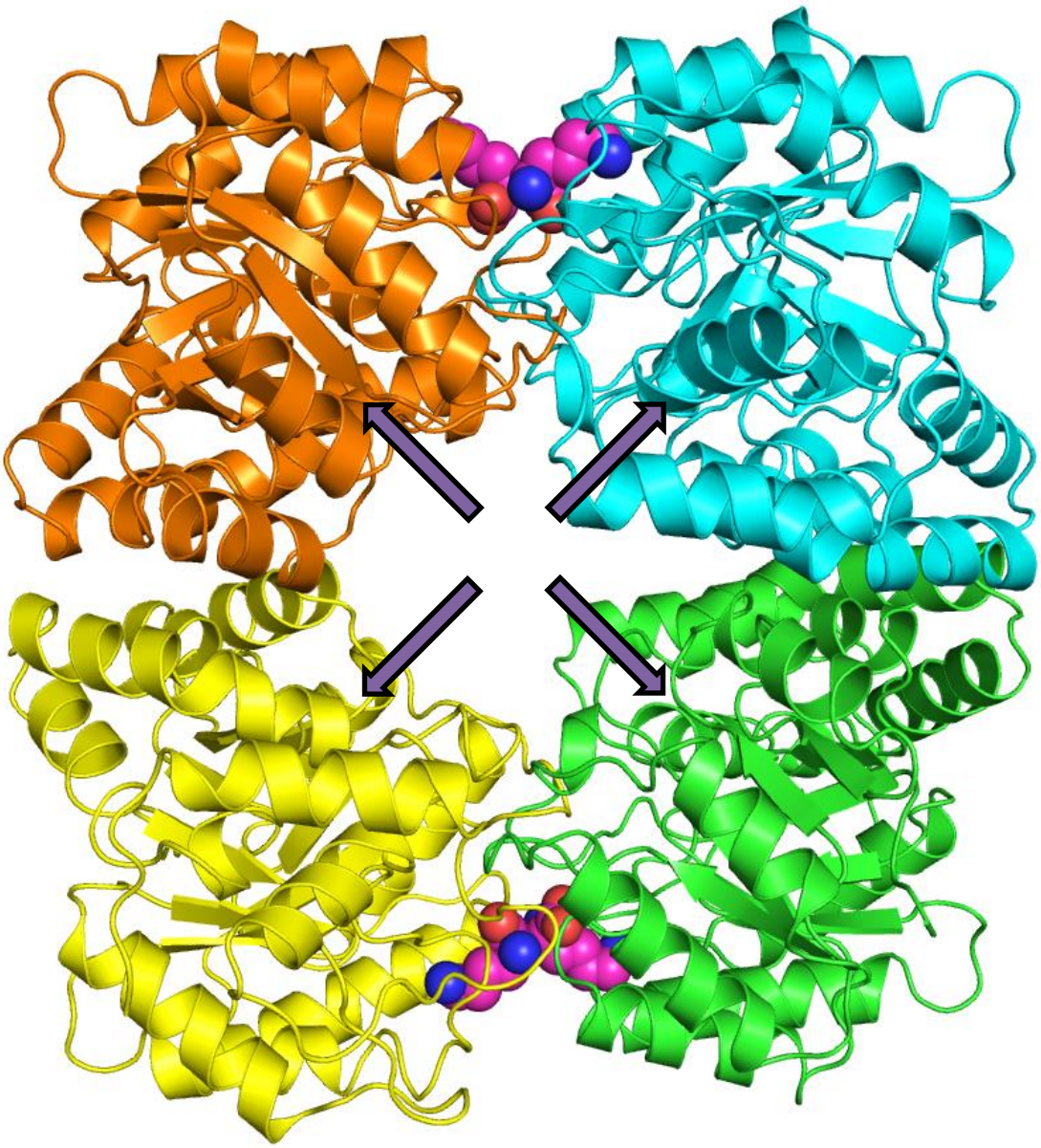

Figure 2.1 – **The DHDPS Tetramer.** Each monomer has one active site which is accessible through the large solvent void formed by the tetrameric formation. Purple arrows indicate access to each of the active sites. (PDB: 4M19)

2.5 Acknowledgements

I would like to thank Dr. Janet Hill and Dr. Bonnie Chaban (Department of Veterinary Microbiology, Western College of Veterinary Medicine, University of Saskatchewan) for providing *C. jejuni* genomic DNA.

Dr. Yulia Skovpen conducted the work to prepare transgenic *E. coli* and the production of mutant *Cj*-DHDPS.

Total kinetic characterization of *Cj*-DHDPS, and its mutants, was directed and carried out by Dr. Yulia Skovpen. Shou Li worked specifically to characterize the Y110F-DHDPS mutant.

I would like to thank Dr. Yulia Skovpen for her generous supply of substrates and inhibitors. Many hours went into the synthesis of such limited resources which were so rapidly consumed in crystallization experiments.

2.6 References

[1] Roberts, S. J., Morris, J. C., Dobson, R. C. J., Baxter, C. L., and Gerrard, J. A. (2004) Two complete syntheses of (S)-aspartate semi-aldehyde and demonstration that Δ^2-(2)-tetrahydroisophthalic acid is a non-competitive inhibitor of dihydrodipicolinate synthase, *Archives for Organic Chemistry*, 166-177.

[2] Yugari, Y., and Gilvarg, C. (1965) The condensation step in diaminopimelate synthesis, *Journal of Biological Chemistry 240*, 4710-4716.

[3] Skovpen, Y. (2014) *Novel inhibitors of dihydrodipicolinate synthase*, (Doctor of Philosphy). Retrieved from Department of Chemistry, University of Saskatchewan

[4] Skovpen, Y. V., and Palmer, D. R. J. (2013) Dihydrodipicolinate synthase from *Campylobacter jejuni*: kinetic mechanism of cooperative allosteric inhibition and inhibitor-induced substrate cooperativity, *Biochemistry*, 5454-5462.

[5] Walker, J. M. (2005) *The Proteomics Protocols Handbook*, Humana Press, Totowa, N.J.

[6] Dobson, R. C. J., Valegard, K., and Gerrard, J. A. (2004) The crystal structure of three site-directed mutants of *Escherichia coli* dihydrodipicolinate synthase: Further evidence for a catalytic triad, *Journal of Molecular Biology 338*, 329-339.

[7] Devenish, S. R. A., Gerrard, J. A., Jameson, G. B., and Dobson, R. C. J. (2008) The high-resolution structure of dihydrodipicolinate synthase from *Escherichia coli* bound to its first substrate, pyruvate, *Acta Crystallographica F 64*, 1092-1095.

[8] Dobson, R. C. J., Griffin, M. D. W., Devenish, S. R. A., Pearce, F. G., Hutton, C. A., Gerrard, J. A., Jameson, G. B., and Perugini, M. A. (2008) Conserved main-chain peptide distortions: A proposed role for Ile203 in catalysis by dihydrodipicolinate synthase, *Protein Science 17*, 2080-2090.

[9] Kefala, G., Evans, G. L., Griffin, M. D. W., Devenish, S. R. A., Pearce, F. G., Perugini, M. A., Gerrard, J. A., Weiss, M. S., and Dobson, R. C. J. (2008) Crystal structure and kinetic study of dihydrodipicolinate synthase from *Mycobacterium tuberculosis*, *Biochemical Journal 411*, 351-360.

[10] Fodje M.N.; Berg, R. B., G.; Grochulski, P., Janzen K. (2010) *Procedings of Personal Computers and Particle Accelerator Controls*, 130-132.

[11] Pflugrath, J. (1999) The finer things in X-ray diffraction data collection, *Acta Crystallographica D 55*, 1718-1725.

[12] Vagin, A., and Teplyakov, A. (2010) Molecular replacement with MOLREP, *Acta Crystallographica D 66*, 22-25.

[13] Matthews, B. W. (1968) Solvent content of protein crystals, *Journal of Molecular Biology 33*, 491-497.

[14] Adams, P. D., Afonine, P. V., Bunkoczi, G., Chen, V. B., Davis, I. W., Echols, N., Headd, J. J., Hung, L.-W., Kapral, G. J., Grosse-Kunstleve, R. W., McCoy, A. J., Moriarty, N. W., Oeffner, R., Read, R. J., Richardson, D. C., Richardson, J. S., Terwilliger, T. C., and Zwart, P. H. (2010) PHENIX: a comprehensive Python-based system for macromolecular structure solution, *Acta Crystallographica D 66*, 213-221.

[15] Emsley, P., and Cowtan, K. (2004) Coot: model-building tools for molecular graphics, *Acta Crystallographica D 60*, 2126-2132.

[16] Hayward, S., and Berendsen, H. J. C. (1998) Systematic analysis of domain motions in proteins from conformational change: New results on citrate synthase and T4 lysozyme, *Proteins 30*, 144-154.

[17] Hayward, S., Kitao, A., and Berendsen, H. J. C. (1997) Model-free methods of analyzing domain motions in proteins from simulation: A comparison of normal mode analysis and molecular dynamics simulation of lysozyme, *Proteins: Structure, Function, and Bioinformatics 27*, 425-437.
[18] Hayward, S., and Lee, R. A. (2002) Improvements in the analysis of domain motions in proteins from conformational change: DynDom version 1.50, *Journal of Molecular Graphics & Modeling 21*, 181-183.
[19] Poornam, G. P., Matsumoto, A., Ishida, H., and Hayward, S. (2009) A method for the analysis of domain movements in large biomolecular complexes, *Proteins 76*, 201-212.
[20] Edelsbrunner, H., M, E. P., #252, and cke. (1994) Three-dimensional alpha shapes, *Association of Computing Machinery Transactions on Graphics 13*, 43-72.
[21] Edelsbrunner, H., Facello, M., Ping, F., and Jie, L. (1995) Measuring proteins and voids in proteins, In *System Sciences, 1995. Proceedings of the Twenty-Eighth Hawaii International Conference on*, pp 256-264 vol.255.
[22] Edelsbrunner, H., and Shah, N. R. (1996) Incremental topological flipping works for regular triangulations, *Algorithmica 15*, 223-241.
[23] Facello, M. A. (1995) Implementation of a randomized algorithm for Delaunay and regular triangulations in three dimensions, *Computer Aided Geometric Design 12*, 349-370.
[24] Liang, J., Edelsbrunner, H., Fu, P., Sudhakar, P. V. and Subramaniam, S. (1989) Analytical shape computation of macromolecules: II. Inaccessible cavities in proteins, *Proteins 33*, 18-29.
[25] Connolly, M. (1983) Analytical molecular surface calculation, *Journal of Applied Crystallography 16*, 548-558.
[26] Lee, B., and Richards, F. M. (1971) The interpretation of protein structures: Estimation of static accessibility, *Journal of Molecular Biology 55*, 379-IN374.
[27] Sayle, R. A., and Milner-White, E. J. (1995) RASMOL: biomolecular graphics for all, *Trends in Biochemical Sciences 20*, 374-376.

Chapter 3 Results and Analysis

3.1 Crystallization of DHDPS

3.1.1 WT Crystallization with and without L-Lysine

Crystals of wt-DHDPS (PDB: 4LY8) were first obtained using commercial screens. The PEG-II suite from Hampton Research, USA was used for the sitting drop vapour diffusion method (drop size and well volume). Several positive hits were identified and optimized using the hanging drop vapour diffusion method. Iterative changes were made to the concentration of protein and precipitants, drop volumes, well volumes, temperature, and pH. The final crystallization condition (0.25 M sodium acetate, 18% PEG4000, 0.1 M TRIS, pH 8.5) afforded crystals of wt-DHDPS which diffracted to 1.6 Å. The cryoprotectant consisted of 10% ehthylene glycol, 30% PEG 400, and 60% precipitant solution.

Crystals grown under similar conditions (0.25 M sodium acetate, 20% PEG4000, 0.1M TRIS, pH 8.5) were used for soaking experiments with L-lysine (PDB: 4M19). wt-DHDPS crystals were looped from the mother liquor and placed into a solution of 10% ethylene glycol, 30% PEG 400, and 60% precipitant solution, with 10 mM of L-lysine. Crystals were soaked for 5-10 min; a short soak time was necessary as crystals were observed to degrade if soaked for longer periods. The L-lysine soaking solution also served as the cryoprotectant. The best diffracting crystals from this procedure were 2.0 Å.

The wt-DHDPS (PDB: 4LY8) was found to be of the space group $P2_12_12_1$, and was solved by molecular replacement using *Cj*-DHDPS (PDB: 3M5V) previously solved by the CSGID and refined to a resolution of 1.6 Å (Pertinent statistics can be found in Table A.1). The structure of *Cj*-DHDPS:pyr (4LY8) is similar to the structures deposited by the CSGID (PDB: 3LER & 3M5V)

with a Cα rmsd of 0.29 Å. As observed in other DHDPS structures, *Cj*-DHDPS crystallizes as a tetramer, composed of a dimer of tight dimers.

3.1.2 Y110F Crystallization with and without L-Lysine

Crystallization conditions for the Y110F mutant (PDB: 4MLJ) were adapted from those of the wt-DHDPS crystals described above. Y110F crystallized in a solution of 0.2 M sodium acetate, 18% PEG4000, 0.1M TRIS, pH 8.5, and using hanging drop vapour diffusion method at 287 ˚K. These crystals were looped and placed in a cryoprotectant of 10% ethylene glycol, 30% PEG 400, 60% precipitant solution. The best diffracting crystals had resolution of 2.1 Å. The Y110F crystal was found to be of the space group $P2_12_12_1$. The structure was solved by molecular replacement and was refined to a resolution of 2.1 Å. Pertinent refinement statistics are presented in Table A.1. The tetrameric structure was found to contain pyruvate at the active site. Comparison of the Y110F:pyr (4MLJ) structure with the wt:pyr (4LY8) structure indicates that they are nearly identical (Cα- rmsd of 0.25 Å). The position of F110 is un-altered relative to the position of Y110 in the wild-type structure.

As with the wt-DHDPS, crystals of Y110F:pyr:lys (PDB: 4MLR) were obtained with the soaking method. The crystals where grown in 0.15 M sodium acetate, 17 % PEG4000, 0.1M TRIS, pH 8.5, using hanging drop vapour diffusion method at 287 ˚K. Crystals were looped and soaked for 5 – 10 min in a solution of 10% ethylene glycol, 30% PEG 400, and 60% precipitant solution containing 30 mM of L-lysine. Higher concentration of L-lysine was necessary presumably because of weaker binding to the mutated allosteric site. The soaking condition also served as the cryoprotectant, and the best diffracting crystals had a resolution of 2.2 Å. The Y110F crystals soaked in L-lysine (PDB: 4MLR) were found to be of the space group $P2_1$. The structure was

solved using molecular replacement and refined to a resolution of 2.2 Å. Pertinent Data collection and refinement statistics can be found in Appendix A (Table A.1 and A.2).

3.1.3 Crystallization of apo-DHDPS

It had been found that wt (4LY8) and Y110F (4MLJ) DHDPS each co-purified and crystallized with pyruvate covalently bound to the active site. It was therefore necessary to treat protein preparations with excess ASA to ensure that all co-purified pyruvate had been reacted. Prior to crystallization, samples of DHDPS were incubated 30 minutes with 10 mM ASA, which is a sufficient excess to react all co-purified pyruvate. The sample was then dialyzed to remove all ASA and HTPA/DHDP from the solution.

The apo-DHDPS (PDB: 4R53) was then crystallized in a solution of 0.2 M sodium acetate, 20% PEG4000, 0.1 M TRIS, pH 8.5, using the hanging drop vapour diffusion method at 287˚ K. Crystals were looped into a cryoprotectant of 10% ethylene glycol, 30% PEG 400, 60% precipitant solution, and flash frozen in liquid nitrogen. The best diffracting apo-DHDPS crystals had a resolution of 2.0 Å. The apo-DHDPS crystals were found to be of the space group $P2_1$. The structure was solved using molecular replacement and refined to a resolution of 2.0 Å. Pertinent data collection and refinement statistics can be found in Appendix A (Table A.1 and A.2).

3.1.4 Crystallization of WT and Y110F with bislysine

Unsuccessful attempts were made to adapt the above soaking procedure for the synthetic inhibitor bislysine. It was concluded that the increased size of the inhibitor did not lend itself well to diffusion through protein crystal solvent channels. An alternative strategy was employed to co-crystallize DHDPS with bislysine.

Using the hanging drop vapour diffusion method wt-DHDPS co-crystallized with 10 mM (±)-bislysine (tetrahydrochloride salt; final concentration) in a solution of 16% P4000, 0.1 mM Tris (pH 8.5) at 287˚K. These crystals were cryoprotected in a solution of 10% ethylene glycol, 30% PEG400, 60% precipitant solution with 10 mM bislysine. Co-crystallization of wt-DHDPS and bislysine produced crystals diffracting to 1.6 Å (PDB: 4RT8). Co-crystals of wt-DHDPS:pyr:bislysine (PDB: 4RT8) were found to be of the space group $P2_12_12_1$. The structure was solved by molecular replacement and refined to a resolution of 2.2 Å. As with previous structures the tetrameric structure contained pyruvate at the active site, and the inhibitor bislysine was easily identified from the F_o-F_c map (Figure 3.1).

The mutant Y110F co-crystallized with 25 mM (±)-bislysine (tetrahydrochloride salt; final concentration) in a solution of 0.2 M sodium acetate, 16% PEG4000, 0.1 mM TRIS (pH 8.5). The hanging drop vapour diffusion method was used at 287 ˚K. The crystals were cryoprotected in a solution of 10% ethylene glycol, 30% PEG 400, 60% precipitant solution with only 20 mM (±)-bislysine (tetrahydrochloride salt) due to limited availability of bislysine. Despite similar binding affinities for bislysine in wild-type and Y110F DHDPS it was necessary to use twice as much bislysine to obtain crystal structures with Y110F-DHDPS. We speculate that the higher concentration of bislysine required is somehow related to the loss of one hydrogen bond in the allosteric site. The best diffracting co-crystals of Y110F-bislysine had resolution of 2.35 Å (PDB: 4RT9). The Y110F-bislysine crystalized in the space group $P2_12_12_1$, and was solved by molecular replacement and refined to 2.35 Å (PDB: 4RT9). Rather uncharacteristically, the enzyme does not have pyruvate bound at the active site. However, bislysine is easily identified in the allosteric site from the F_o-F_c map (Figure 3.2). With the exception of the missing hydroxyl at F110 there is no obvious structural differences from wt-DHDPS:bislysine (4RT8).

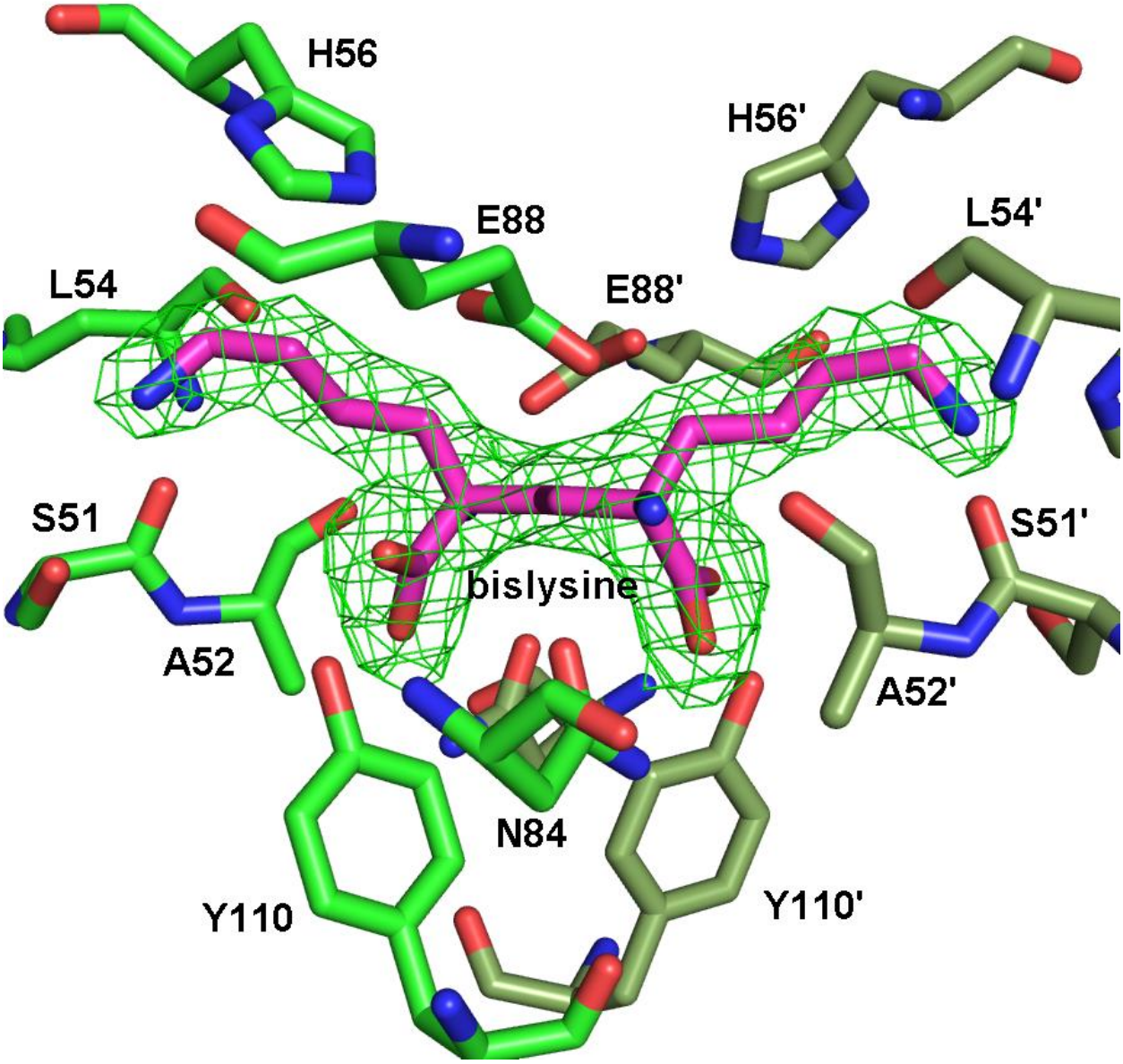

Figure 3.1 – **Electron Density of bislysine in wt-DHDPS** Purple bislysine bound to the allosteric site of wt-DHDPS in green (PDB: 4RT8). The Green Mesh is the electron density omit map scaled at 3.0 σ.

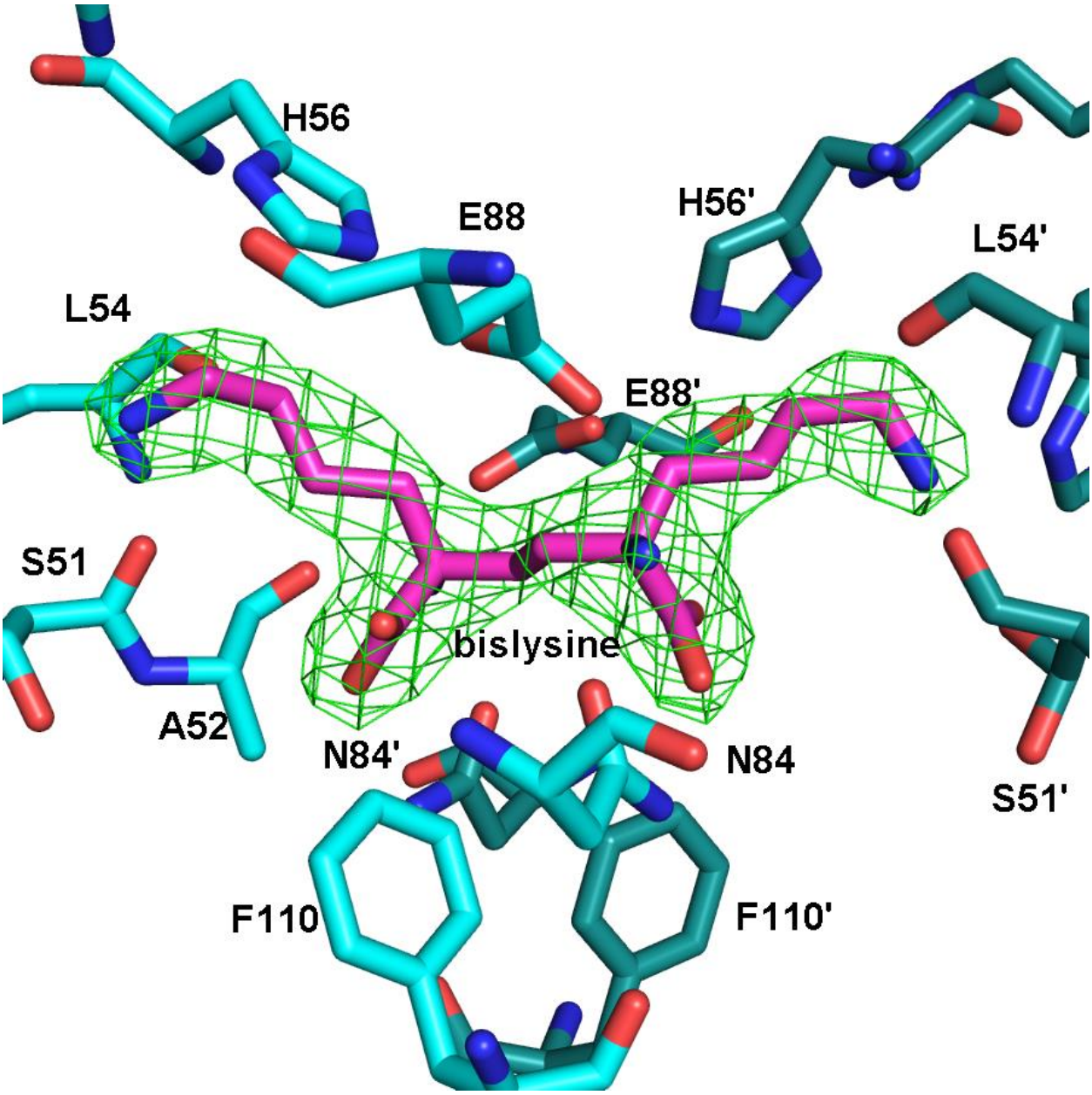

Figure 3.2 – **Omit map for bislysine bound in the allosteric site of Y110F-DHDPS.** Purple bislysine bound to the allosteric site of Y110F-DHDPS in blue (PDB:4RT9). The Green Mesh is the electron density omit map scaled at 3.0 σ.

3.1.5 Crystallization of wt-DHDPS with L-Thialysine

Crystals of wt-DHDPS with L-thialysine were obtained using the ligand-soaking technique. Crystals were grown in a solution of 0.2 M sodium acetate, 20% PEG 4000, 0.2 M Tris, pH 8.5 using the hanging drop vapour diffusion method at 287 ˚K. The cryoprotectant was 30 µL PEG 400, 10 µL ethelyne glycol, 60 µL well solution and included 30 mM L-thialysine; the best diffracting crystals had a resolution of 1.9 Å. The crystals were found to be of the space group $P2_1$, solved by molecular replacement and refined to 1.9 Å. Pyruvate was bound to the active site, and L-thialysine could be easily identified from the F_o-F_c map (Figure 3.3). The electron density associated with the inhibitor L-thialysine was less well defined than previously solved crystal structures with L-lyisine, which suggests a lower occupancy.

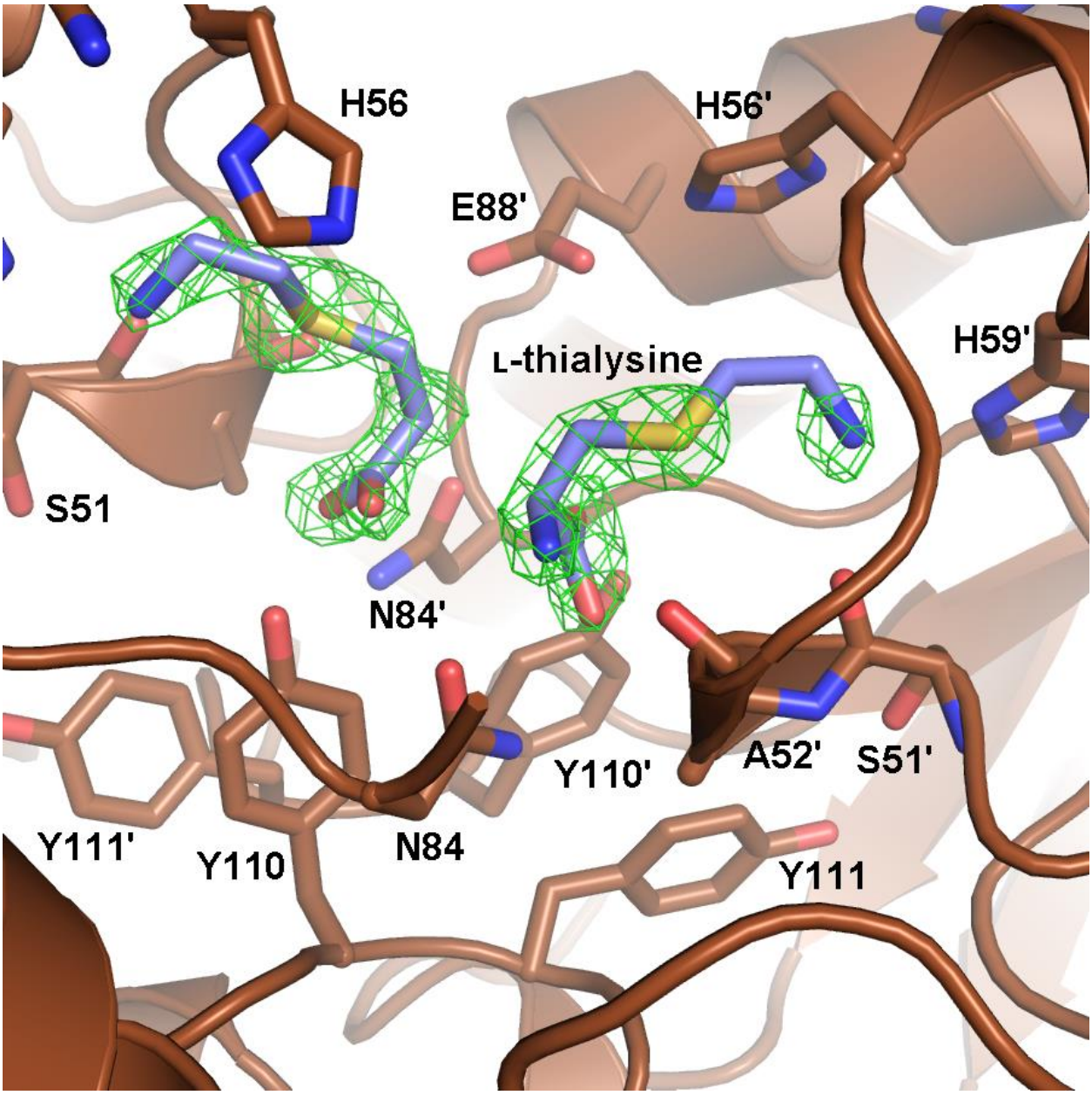

Figure 3.3 – **Omit map for thialysine bound in the allosteric site of wt-DHDPS.** wt-DHDPS is shown in brown, and L-thialysine is depicted in grey. The green mesh represents the electron density of the F_o-F_c Omit map rendered at 3.0 σ. The shape of the electron density is not as clearly defined as for L-lysine or bislysine; however, it is convincingly attributable to L-thialysine.

3.1.6 Crystallization of wt-DHDPS with ASA

The method for crystallizing DHDPS with ASA in the active site requires several preliminary steps prior to setting up the actual crystallization experiments. The protein sample is first incubated

for 30 min with excess pyruvate (30 mM), to ensure 100% active site occupancy. Following this, the active site Schiff base (pyruvate-K166 double bond) is reduced by treatment with $NaCNBH_3$ (BH) for 2 hours. The sample is then dialyzed to remove all excess and reacted reagents.

The reduced BH-DHDPS:lac is then co-crystallized with 100 mM ASA in a solution of 0.16 M di-ammonium tartrate, 12% PEG 3350 at 287 ˚C using the hanging drop vapour diffusion method. Crystals proved highly unstable in a variety of cryoprotectant solutions; fortunately, the mother liquor proved to be a suitable cryoprotectant. Crystals from these preparations diffracted to 1.93 Å in the absence of ASA and 2.37 Å when co-crystallized with ASA. The final resolution of refinement was also 1.93 Å in the absence of ASA and 2.37 Å when co-crystallized with ASA. Pertinent diffraction and refinement statistics can be found in Appendix A (Table A.1 and A.2).

3.1.7 DHDPS from *C. jejuni* co-purifies with Pyruvate

Pyruvate was not added to any sample of DHDPS during either purification or crystallization; with the exception of treatment with sodium cyanoborohydride. In all cases we observed that pyruvate was present in the active site (Figure 3.4), with the exception of Y110F:bislysine (PDB: 4RT9). Since pyruvate was not added to any samples of DHDPS this indicates that it must co-purify, and then co-crystallize with DHDPS, suggesting that the F-form of the enzyme, with pyruvate bound, is likely the preferred state of the enzyme.

The one exception is the crystal structure of Y110F-DHDPS:bislysine where there is no indication of pyruvate at the active site. It has been shown in *Cj*-DHDPS that L-lysine enhances the affinity of the enzyme for pyruvate.[1-3] Several possibilities exist to explain the absence of pyruvate in Y110F-DHDPS:bislysine. Some aspect of the crystallization condition may have changed the equilibrium to favor unbound pyruvate. Since bislysine can bind to either the 'E-form' or 'F-form' of the enzyme, it is possible that conditions used here selectively crystalize the Y110F-

DHDPS:bislysine without pyruvate. Finally, it may be that bislysine, unlike L-lysine, influences the mutant enzyme to favor a vacant active site.

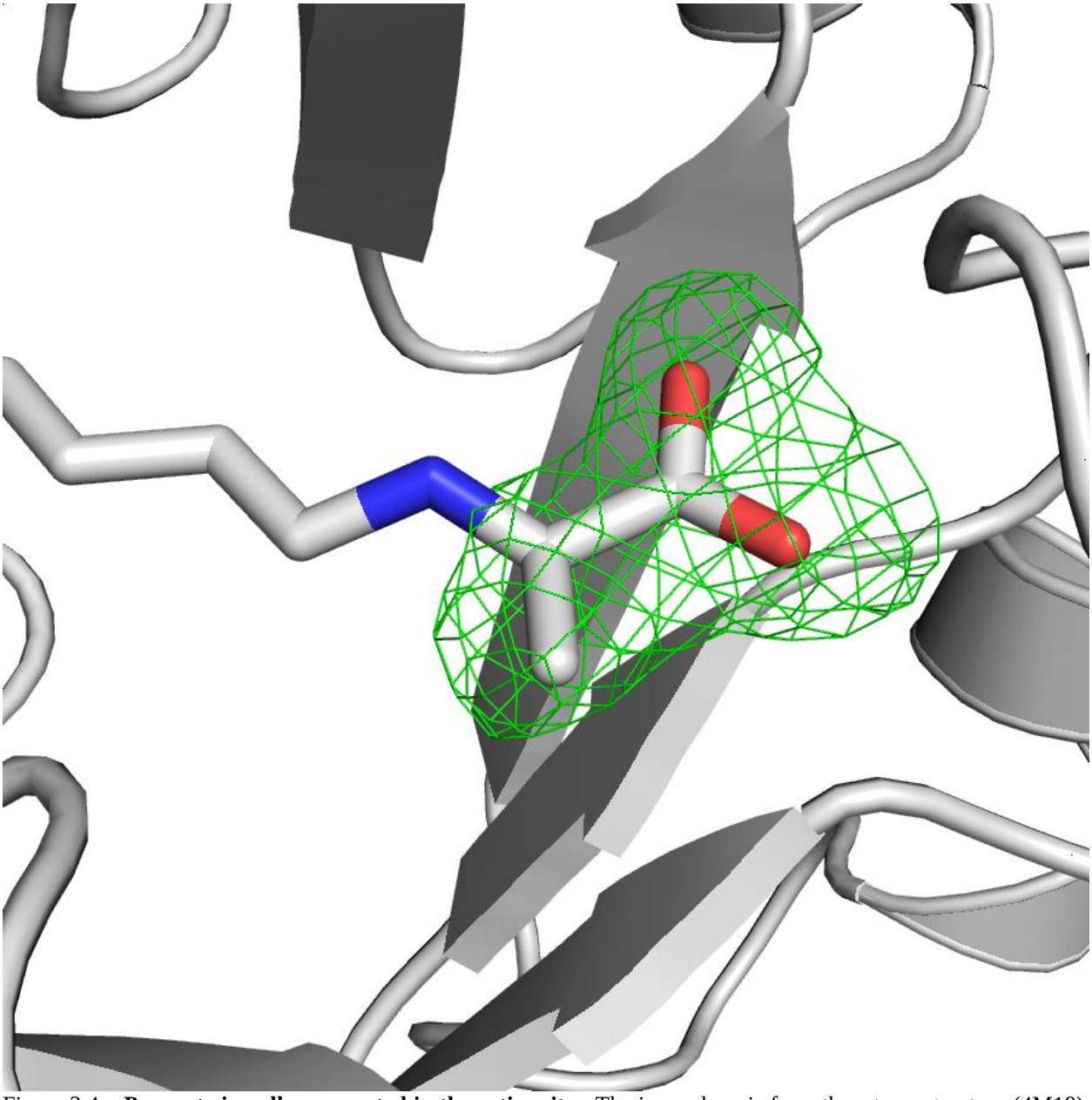

Figure 3.4 – **Pyruvate is well represented in the active site.** The image here is from the wt:pyr structure (4M19). The Green mesh is the F_o-F_c omit map (scaled at 3.0 σ) and is representative of electron density observed in the active site of all DHDPS crystal structures presented in this thesis.

3.2 Structural effects of L-lysine on wt-DHDPS

3.2.1 Structure of wt-DHDPS with L-Lysine in the allosteric site

The wt-DHDPS:pyr:lys (PDB: 4M19) crystals occupy the space group $P2_1$. The structure was solved by molecular replacement and refined to a resolution of 2.0 Å (Table A.2). As with DHDPS:pyr (PDB: 4LY8), the active site was found to contain pyruvate bound to K166, without intervention. L-Lysine was clearly identified by the outline of its electron density in the F_o-F_c map. As observed in DHDPS from other species L-lysine binds to the allosteric site in a 'head-to-head' orientation, that is, with α-carbons in close proximity, in the allosteric site.

The allosteric binding site exists at the tight-dimer interface and the binding site for a single L-lysine molecule is comprised of residues from both monomers. Consistent with other DHDPS, two L-lysine molecules bind in a head-to-head fashion with 2-fold symmetry (Figure 3.5, panel A), and each L-lysine makes hydrogen bond interactions with both monomers.[4-7] A list of lysine hydrogen bond interactions is presented in Table 3.1 and depicted graphically in Figure 3.5, panel B.

For a L-lysine molecule bound to the allosteric site of monomer A, the carboxyl of L-lysine is hydrogen bonded to Tyr110 in monomer A. The α-amino group is hydrogen bonded to Ala52 from monomer A, and Asn84/Glu88 from monomer B. The ε-amino group forms hydrogen bonds with His59, and the back-bone carbonyls of Ser51 and Leu54 of monomer A. The two fold symmetry of *Cj*-DHDPS results in the same interactions for the L-lysine bound to monomer B. This is consistent with L-lysine binding patterns reported from homologous species.[8]

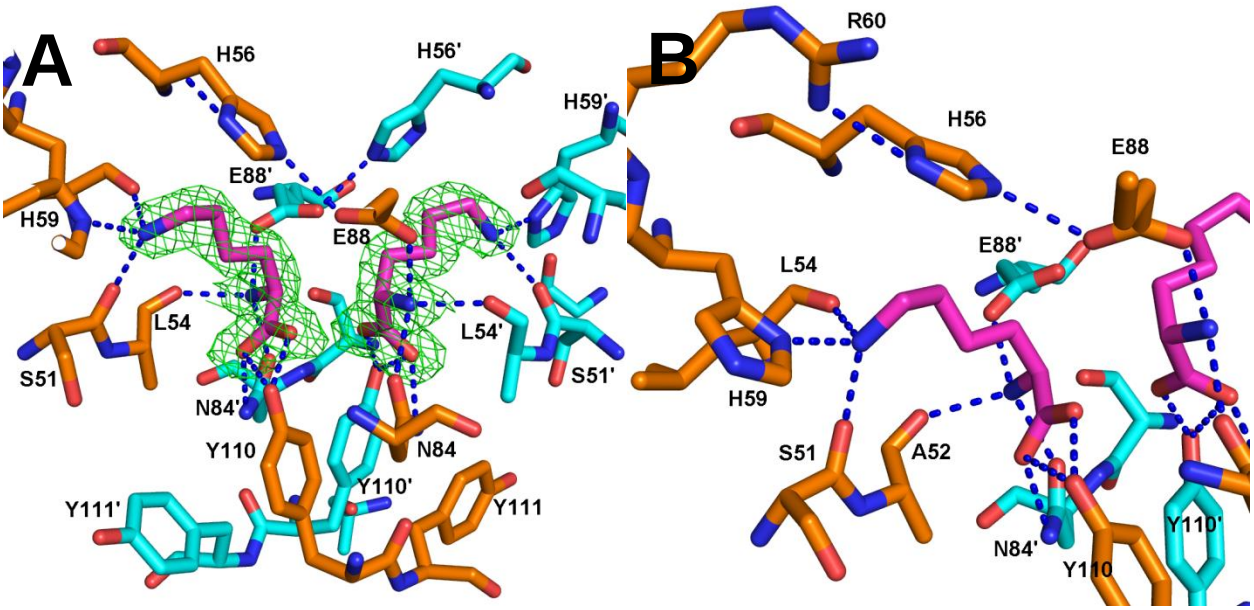

Figure 3.5 – **Difference Density and Hydrogen bonding interactions completed by L -lysine in the allosteric site.** L-Lysine bound DHDPS, monomer A in orange, monomer B (primed residues) in blue. Panel A shows the omitt map for L-lysine bound to the allosteric site of wt-DHDPS (4LY8). Green electron density map represents the SA omit map with no L-lysine present, contoured at 3 σ. Panel B is a close up of one L-lysine highlighting the newly formed hydrogen bonds. A single L-lysine molecule forms hydrogen bonds with residues from both monomers and the second L -lysine binds with two fold symmetry.

Table 3.1 – **List of all hydrogen bonds made by L-lysine in the Allosteric Site**

Hydrogen Bond	Distance
L-lysine-N to N84'	2.8 Å
L-lysine-N to E88'	2.8 Å
L-lysine-O to N84'	3.0 Å
L-lysine-O to Y110	3.3 Å
L-lysine-OXT to Y110	2.6 Å
L-lysine-Nζ to H59	3.0 Å
L-lysine-Nζ to S51(CO)	2.8 Å
L-lysine-Nζ to L54(CO)	3.3 Å

3.2.2 Comparison of wt-DHDPS with and without L-Lysine

A comparison of the *Cj*-DHDPS:pyr:lys (PDB: 4M19) structure to the *Cj*-DHDPS:pyr (PDB: 4LY8) structure reveals several side chain movements to accommodate L-lysine in the allosteric site (Figure 3.6). Furthermore there are notable shifts in the backbone Cα's in helices flanking the allosteric site. It appears as if the helices shift into the allosteric site when L-lysine is bound.

The principle interest is the effect that L-lysine has on the active site; however, there are only minor changes observed between the active sites of *Cj*-DHDPS:pyr (4LY8) and *Cj*-DHDPS:pyr:lys (4M19) upon binding of L-lysine to the allosteric site. Small but measurable changes in the distance between pairs of residues are seen for the following pairs: Y137 – T47 (3.4 Å to 2.9 Å), Y137 – Y111' (4.7 Å to 4.2 Å), and C1 of the pyruvyl Schiff base and the carbonyl of I207 and G190 (3.8 Å to 4.5 Å and 4.7 Å to 3.7 Å respectively).

Interestingly the largest structural changes occur in side chains at the weak dimer interface. The secondary structures at the weak dimer interface remain largely intact. The notable movements include significant shifts in Cα positions and side chain orientations. Historically, this region of the protein structure has received the least attention, but will be critical in understanding reports of inhibitor cooperativity across the weak dimer interface.

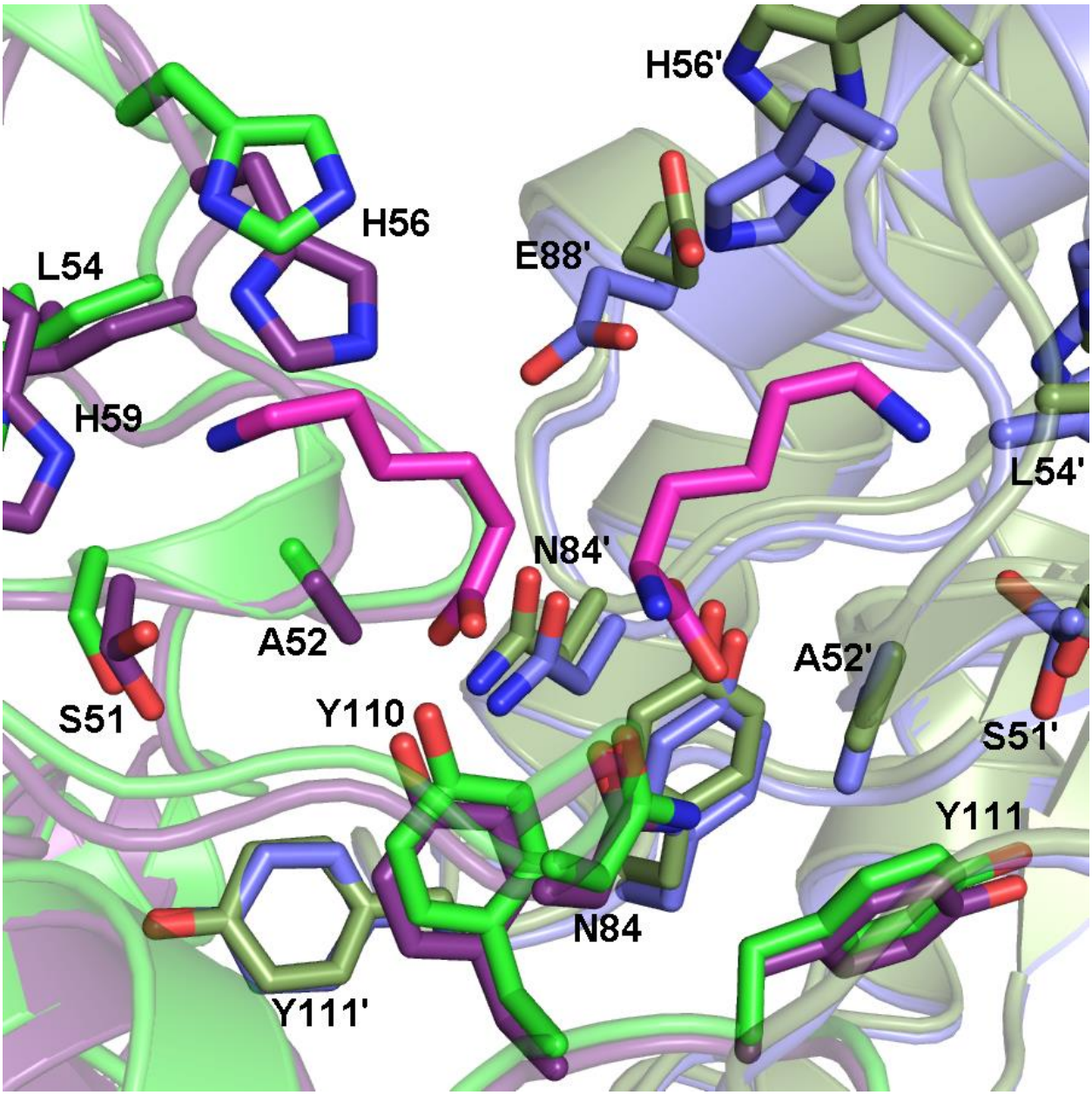

Figure 3.6 – **Superposition of *Cj*-DHDPS:pyr:lys and wt:pyr.** The *Cj*DHDPS:pyr:lys structure (PDB: 4M19) is shown in green, and the *Cj*-DHDPS:pyr structure (PDB: 4LY8) is shown in puple (different shades indicate each monomer). There is some disorder introduced at the side-chain of S51, therefore two possible positions are represented. The superposition highlights that many residues make minor shifts to accommodate the binding of L-lysine (shown in magenta).

3.2.3 Determination of Dynamic Domains

While the structure *Cj*-DHDPS:pyr:lys (4M19) was very similar to the *Cj*-DHDPS:pyr (4LY8) structure, crystal quality was observed to degrade when L-lysine was included in the cryoprotectant solution, but remained stable when L-lysine was absent from the cryoprotectant. These observations suggest L-lysine may induce certain conformational changes. Close examination of the superimposed structures revealed notable misalignment and contracted helices. We used the program DynDom to reveal a subtle concerted domain movement.[9-11] DynDom identifies domains based on vector movements and determines the average vector movements based on a reference structure. Each identified domain is matched to the equivalent section in the unbound protein using a root mean square difference (rmsd) of Cα's. Our analysis of the *Cj*-DHDPS:pyr:lys (4M19) structure demonstrated that there is a concerted domain movement caused by the binding of L-lysine. The fixed domain is comprised of the N and C terminus, residues 1-80 and 188-298. The moving domain consists of residues 104 to 184. At the interface of moving and fixed domains are residues which lie on or very near the bending axis. Identified domains are highlighted on a single monomer and on the tight dimer formation in Figure 3.7.

The bending axis is defined by a closure value of 0.798, which represents the amount of hinging as opposed to twisting. A value greater than 0.5 indicates a predominantly hinged motion rather than a screw axis.[9-11] The moving domain shifts 3.8˚ on its hinge axis resulting in maximal Cα displacement of 2.0 Å at Thr115. Domain movements indicate that half of each monomer rotates toward the allosteric site (Figure 3.7). The domain shifts are consistent with the closing of the helices around the L-lysine in the allosteric site.

The moving domain extends from the allosteric site to the weak dimer interface, and at its center includes the aromatic residues Y110/111. Notably Y110 is one of only 3 residues (Y110, N84, and

E88) in the moving domain that makes a direct hydrogen bond to the inhibitor L-lysine. The neighboring residue Y111 interdigitates across the tight dimer interface to complete the catalytic triad in the active site of the neighboring monomer (Figure 3.8). This is an important observation because Y110/111 has been critically implicated in the mechanism of allostery and presents a probable link between the allosteric site and the active site via domain movement.[1, 3] Therefore Y110/Y111 was identified as a possible link between the allosteric site and the active site. It appears that the movements of the very rigid Y110/111 are the result of domain movements, or possibly that domain movements are the result of shifts to the aromatic core. Furthermore, inhibition of *Cj*-DHDPS demonstrates cooperativity across the weak dimer interface.[1, 2] The dynamic domains identified here apparently link the allosteric site to the weak dimer interface and may play some role in the mechanism of cross dimer communication.

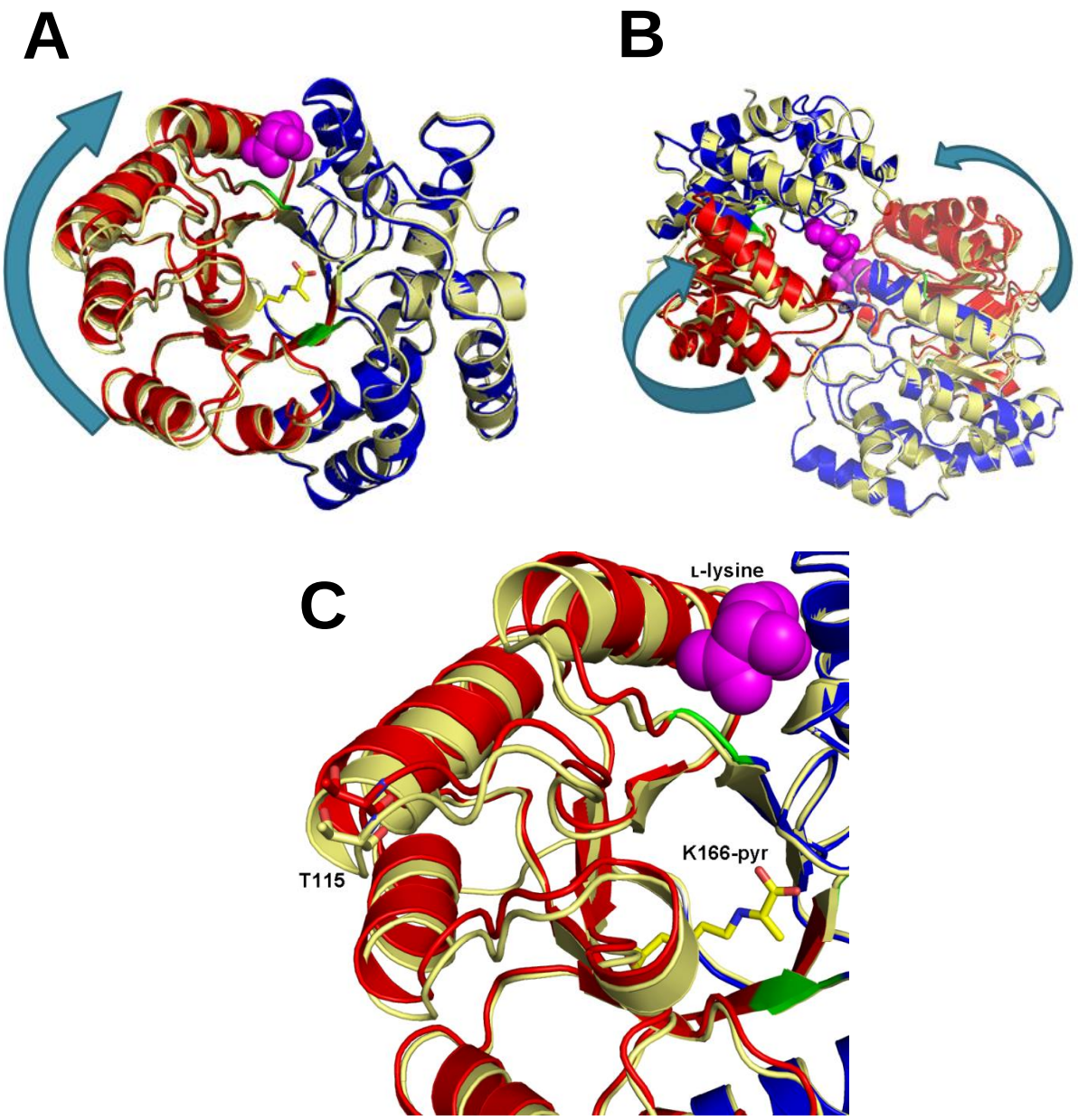

Figure 3.7 – **Domain movements in wild type *Cj*-DHDPS.** Panel A shows the highlighted domains in a superposition of *Cj*-DHDPS:pyr:lys (4M19) and *Cj*-DHDPS:pyr (4LY8). On the *Cj*-DHDPS:pyr:lys structure (PDB: 4M19) the fixed domain is blue, moving domain is red and hinging residues are in green. The *Cj*-DHDPS:pyr structure (PDB: 4LY8) is shown in yellow. L-Lysine bound to the allosteric site (magenta) belongs to the blue and red structure. The blue arrow shows the monomeric hinging action where the moving (red) domain shifts to close the allosteric site. Panel B shows the interplay of monomers at the tight dimer interface. Identical domain movements in each monomer close the allosteric site around two L-lysine molecules. Panel B shows a close up of the active site and allosteric site. The moving domain (red) moves towards the allosteric site with a maximal Cα displacement of 2.0 Å at T115.

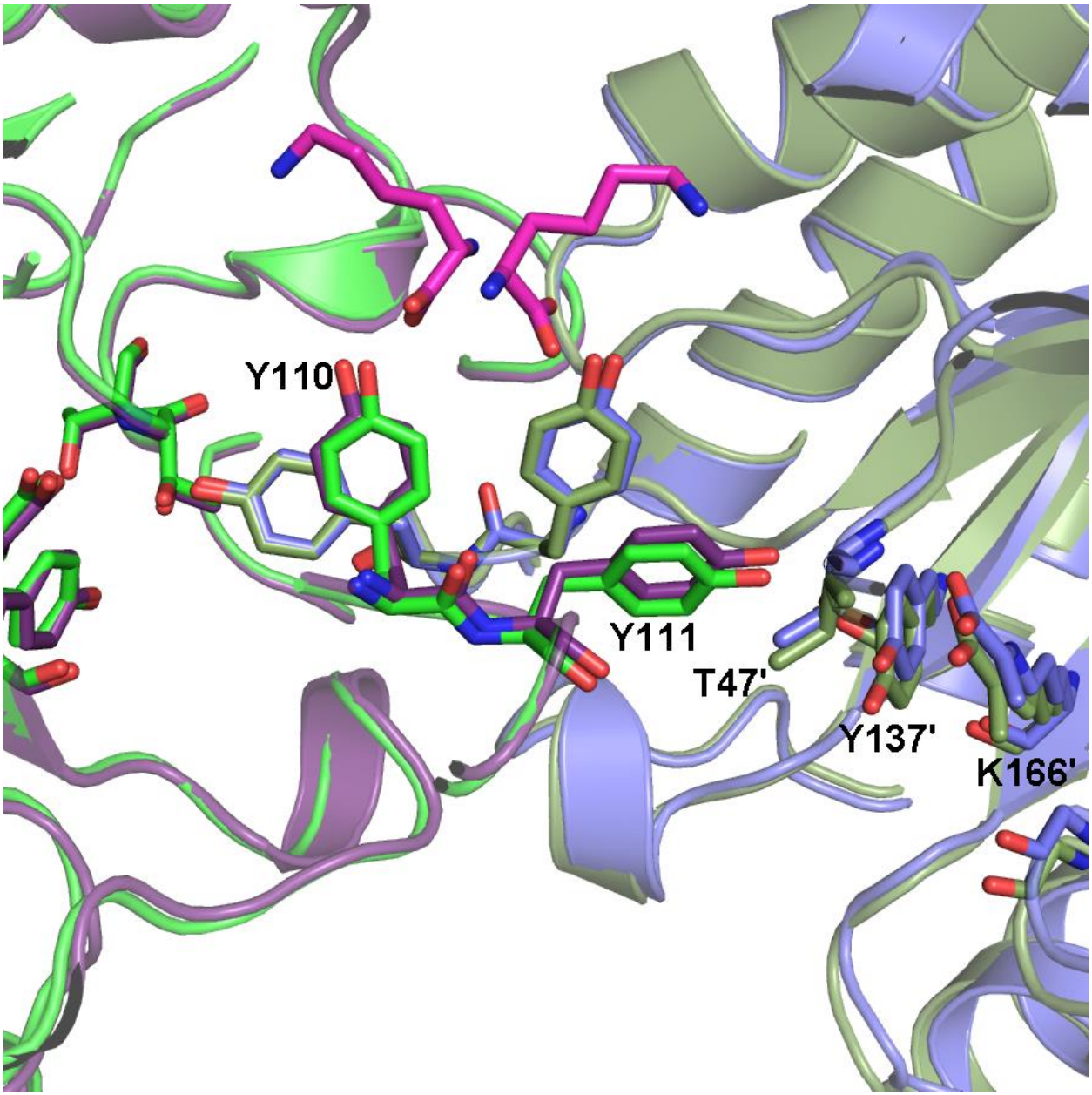

Figure 3.8 – **The aromatic pair Y110/Y111 links the allosteric site and the active site.** *Cj*-DHDPS:pyr:lys (PDB: 4M19) shown in purple with L-lysine in magenta, and *Cj*-DHDPS:pyr (PDB:4LY8) is in green (different shades indicate each monomer). The aromatic pair of Y110/Y111 links the carboxyl of the inhibitor L-lysine to the catalytic triad of the active site.

3.2.4 Analysis of Cavity Volumes

The observed domain movements appear to be coupled with closure of the allosteric site when L-lysine binds; reflected in the changing Cα positions of helices comprising the allosteric site. This observation led us to measure the volume of the active site and allosteric site in each of our wild type crystal structures. Using CASTp[12, 13] we compared the solvent accessible volume of active sites and allosteric sites in apo-*Cj*-DHDPS (4R53), *Cj*-DHDPS:pyr (4LY8), *Cj*-DHDPS:pyr:lys (4M19). Calculations of the allosteric site were done with L-lysine removed from the model. When calculating the volume of the active site pyruvate was included in the model, since it defines the active site available for ASA. These comparisons reveal that the binding of each ligand changes the volume of both the active site and the allosteric site (Table A.3). The binding of pyruvate to apo-*Cj*-DHDPS (4R53) decreases the active site volume by 44% from 36 $Å^3$ to 20 $Å^3$. Additionally, the allosteric site is reduced by 16% to 417 $Å^3$ from 494 $Å^3$. The reduction in allosteric site volume could improve the affinity of the allosteric site for L-lysine by both improving the orientation of binding groups and providing an entropic effect of limiting L-lysine conformations.

Binding of L-lysine reduces the volume of the allosteric site by a further 43% from 417 $Å^3$ to 239 $Å^3$. At the active site, the volume increases by 30% from 20 $Å^3$ to 26 $Å^3$ upon L-lysine binding. An image representative of the change in allosteric site volume from apo-*Cj*-DHDPS (4R53) to *Cj*-DHDPS:pyr:lys (4M19) was generated using the program Hollow[14] and is shown in Figure 3.9; overall the cavity is observed to shrink in all dimensions as the surrounding helices and residues move towards the center of the cavity. The increased volume at the active site may play a crucial role in the inhibition of the enzyme, likely by reducing the affinity of the active site for ASA.

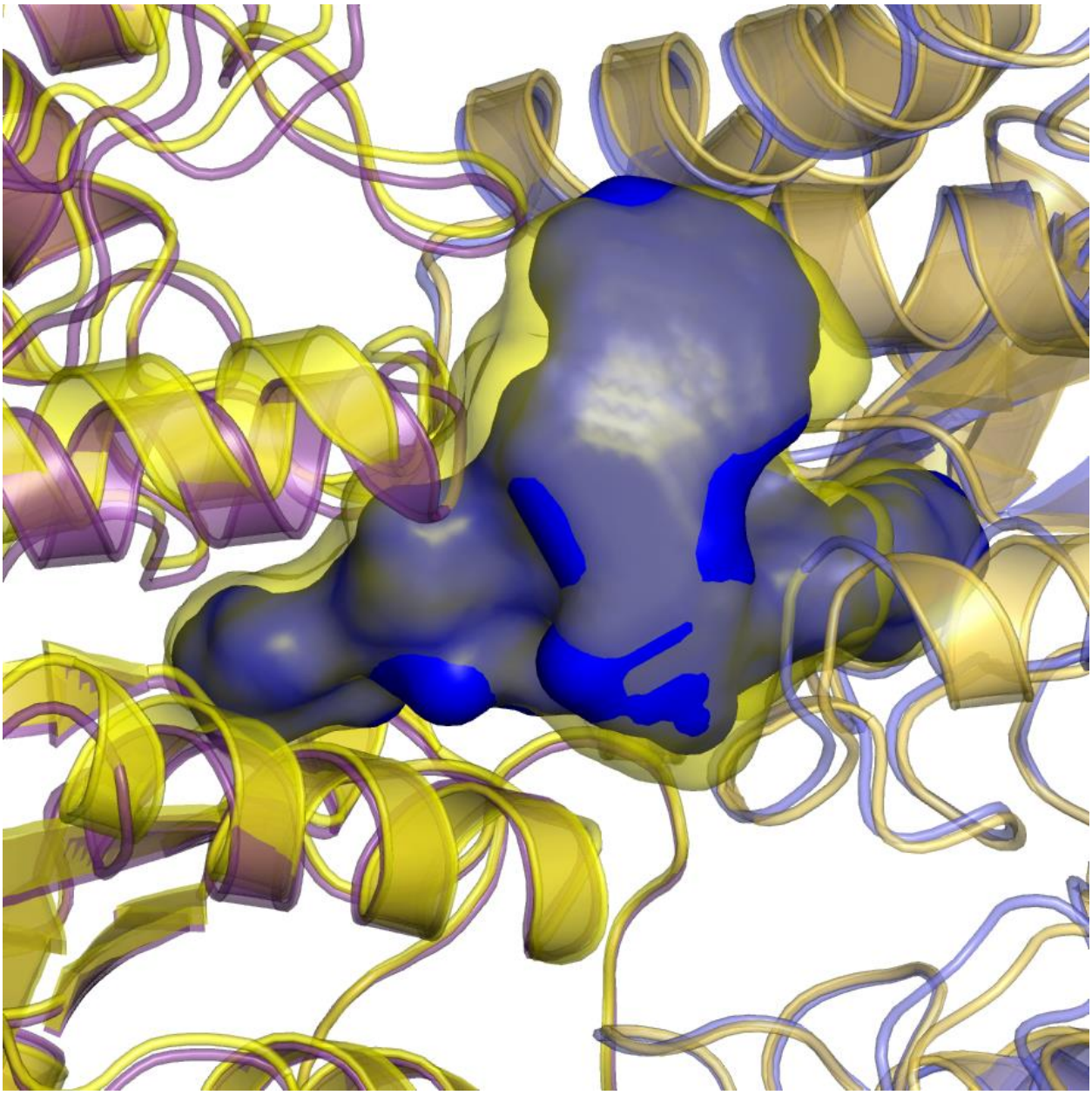

Figure 3.9 – **Volume change of the allosteric site.** The calculated allosteric cavity is rendered with the program Hollow[14] for apo-*Cj*-DHDPS (4R53) in transparent yellow (larger), and *Cj*-DHDPS:pyr:lys (4M19) in blue (smaller). The structure of apo-*Cj*-DHDPS (4R53) is in yellow, and *Cj*-DHDPS:pyr:lys (4M19) is in blue. The allosteric site is observed to shrink in all dimensions as the surrounding helices and side chains move toward the center of the cavity.

3.2.5 Effects at the Dimer-Dimer Interface

The moving domain includes significant contacts at the region of both the tight and weak dimer interface. The tetrameric structure is critical for natural activity and inhibition.[15] It is well documented that at the tight dimer interface, two L-lysine molecules bind cooperatively in each allosteric cleft.[4-7] Additionally, we have shown that L-lysine binding in *Cj*-DHDPS is cooperative *across* the weak dimer interface, as indicated by Hill coefficients > 2.[2] The moving domain extends from the allosteric site into the weak dimer interface. At this interface, we find several cross-dimer interactions that have shifted in the DHDPS:pyr:lys (4M19) structure. Rearrangements include the breaking of several hydrogen bonds: H181'/N242, and D173'/Y241 (Figure 3.10, panel A); disruption of hydrogen bonds between N201'/D238, N201'(CO)/K234, and S200'(CO)/Y196 (Figure 3.10, panel B). Furthermore, upon binding L-lysine at the allosteric site there is significant rearrangement of a hydrophobic pocket (I172, I194, I172', I194',V176; Figure 3.10, panel C) at the weak dimer interface, where each residue moves by 1.5 – 2.0 Å. These residues may be implicated in the weak dimer cooperativity signal and should be examined as a part of future work.

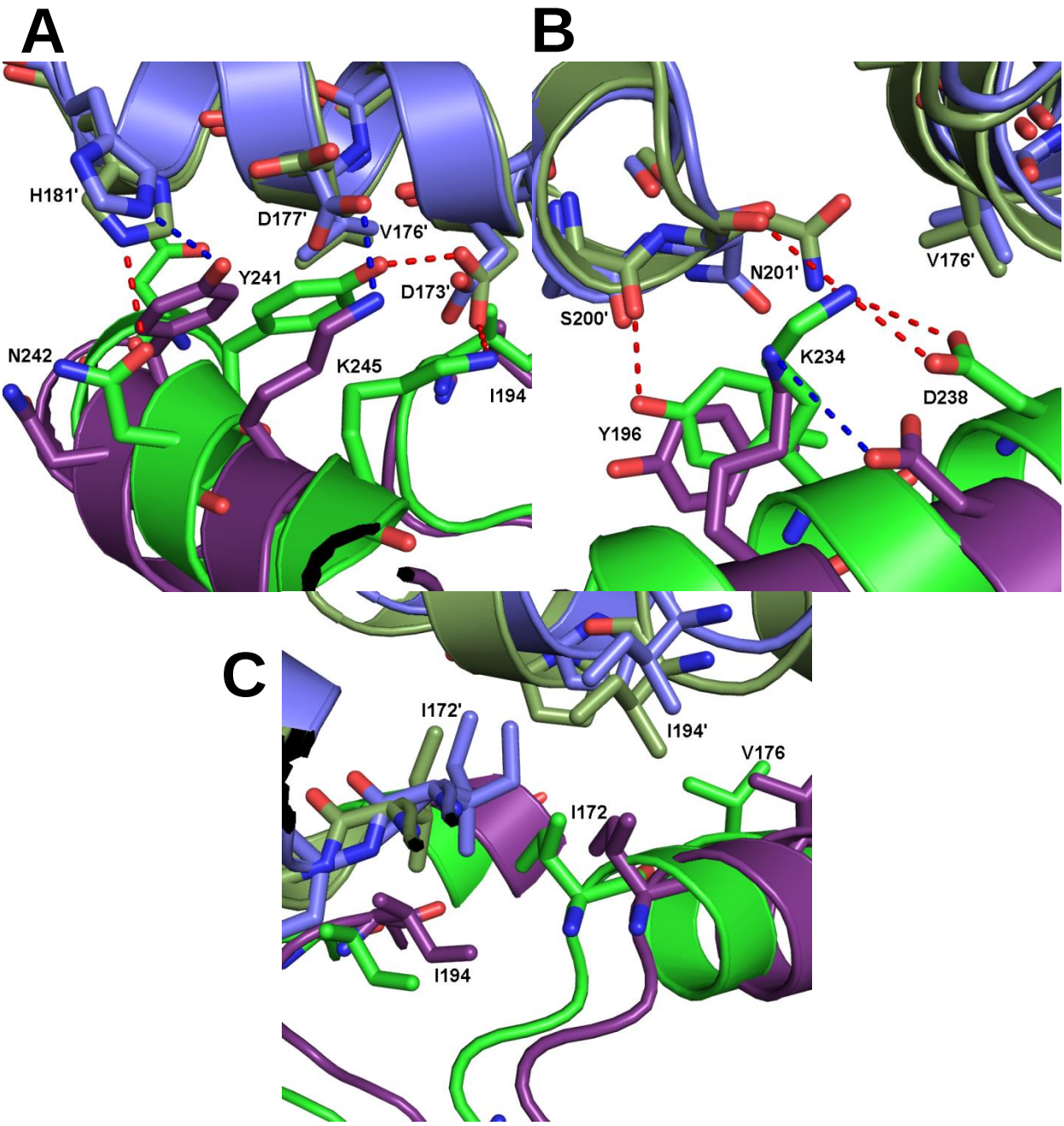

Figure 3.10 – **Changes at the dimer-dimer interface.** *Cj*-DHDPS:pyr:lys (PDB: 4M19) shown in green and *Cj*-DHDPS:pyr (PDB: 4LY8) shown in purple (different shades indicate each monomer). The dashed blue line denotes hydrogen bonds which are only present in the DHDPS:pyr:lys structure (4M19), while the red dashed line denotes hydrogen bonds only present in the DHDPS:pyr structure (4LY8). Panel A depicts the breaking of a hydrogen bond between H181' to N242, and D173' to Y241; and formation of hydrogen bonds between H181' to Y241, and another between D177' to K245. Panel B shows the disruption of hydrogen bonds between N201' to D238, N201'(CO) to K234, and S200'(CO) to Y196; the residues K234/D238 move together to retain their hydrogen bond. Panel C shows the rearrangement of a hydrophobic pocket formed by I172, I194, I172', I194' and V176. These changes may contribute to the cooperativity observed between four L-lysine binding sites.

3.3 Structural effects of L-lysine on Y110F-DHDPS

As described in section 1.5.5 the Y110F mutation of *Cj*-DHDPS greatly diminishes the enzymes sensitivity to inhibition by L-lysine.

3.3.1 Analysis of Y110F-DHDPS with L-Lysine

As in the *Cj*-DHDPS:pyr:lys (4M19) structure, L-lysine was clearly seen in the initial F_o-F_c electron density map, and is bound in the allosteric site in a head-to-head orientation in the Y110F:pyr:lys (4MLR) structure. All side chain positions and hydrogen bonding networks observed in the *Cj*-DHDPS:pyr:lys (4M19) structure are preserved in the Y110F:pyr:lys (4MLR) structure with the exception of the missing tyrosine hydroxyl group. This result reveals that L-lysine still binds to the mutant Y110F despite the fact that there is little to no attenuation of catalytic activity. The Y110F-DHDPS is insensitive to L-lysine inhibition, and yet the crystal structure affirms that the inhibitor binds to the enzyme in the same position and conformation as it does in the wild-type DHDPS. The observation that the inhibitor binds to the allosteric site, and enzyme activity remains high suggests that the hydrogen bond between the inhibitor L-lysine and Tyr110 is of critical importance in the effective allosteric signal transduction.

3.3.2 Comparison of Y110F-DHDPS with and without L-Lysine

As with the wild type enzyme, binding of L-lysine to the Y110F allosteric site induces several small side chain movements. There is some shifting observed in the backbone carbonyls of the helices flanking the allosteric site; although it is not to the same extent as the wt-DHDPS (4LY8). Similar to the wt-DHDPS, L-lysine appears to induce very little structural change at the active site.

There are only minor changes observed between the active sites of Y110F:pyr (4M19) and Y110F:pyr:lys (4MLR) upon binding of L-lysine to the allosteric site. Small but measurable

changes in the distance between residues are seen for the following pairs: Y137 – Y111' (4.6 Å to 5.1 Å) increases in length (the opposite effect from wild type); and C1 of the pyruvyl Schiff base and the carbonyl of G190 (and 4.5 Å to 4.2 Å respectively). Several movements observed between wt:pyr and wt:pyr:lys are not observed in the comparison of Y110F:pyr and Y110F:pyr:lys, including: Y137 – T47 (3.5 Å to 3.5 Å), and C1 pyruvyl Schiff base to the carbonyl of I207 (3.8 Å to 3.8 Å).

As with L-lysine binding in the wild type DHDPS, we observe rearrangement of several residues located at the allosteric site of Y110F-DHDPS when L-lysine binds. The distance between E88-H56 is reduced (decreasing from 3.7 Å – 3.2 Å), R60 side chain moves (decreasing from 9.1 Å to 3.1 Å) to support the side chain of H56 in its new position, and the R60 side chain forms a new hydrogen bond (decreasing from 5.6 Å to 3.4 Å) with the back bone H56(CO). Furthermore, R60 side chain has moved from 11.4 Å – 3.8 Å relative to G91(CO) to form a new hydrogen bond. As the allosteric site contracts, G80(CO) can form a hydrogen bond to H59 (distance decreasing form 4.0 Å – 2.7 Å). Unlike the wild-type DHDPS, the distance between E88-E88', which is reduced in wt-DHDPS, remains unchanged when L-lysine binds to Y110F, suggesting the size of the allosteric site does not decrease to the same extent as the wild type.

In wt-DHDPS (4M19), L-lysine has a considerable effect at the weak dimer interface. However, when Y110F:pyr:lys (4MLR) is compared to Y110F:pyr (4MLJ), an examination of the weak dimer interface reveals little to no change due to binding of L-lysine at the allosteric site. This may be due to either weaker binding of L-lysine, or disruption of the mechanism for inducing such a change.

3.3.3 Absence of Domain-Scale Movements in Y110F:pyr:lys

Although the helices flanking the allosteric site shift when L-lysine is bound in Y110F, the domain scale movements noted by DynDom for *Cj*-DHDPS:pyr:lys (4M19) are absent in the Y110F:pyr:lys (4MLJ) structures. That is to say, although there are obvious shifts in secondary structures and in side chains, as a whole the changes do not occur in concerted vectors. When Y110F:pyr (4MLJ) is compared to wt:pyr:lys (4M19) DynDom identifies the same domain movements observed for both wild-type structures. However, when comparing Y110F:pyr:lys (4MLR) to the wt:pyr:lys (4LY8), again we observe no domain movements. This suggests that the Y110F structure may exist between the two wild-type states; or, that it does not contain identifiable domains. That is, the sum of any changes cannot be defined as either a hinge or a screw axis.

Close inspection of the domains identified in the wt-DHDPS reveals that Y110 is located in the middle of the moving domain. According to B-factors and allowed Ramachandran angles, this is one of the most rigid regions of the enzyme. It stands to reason that with the absence of the Tyr110 hydroxyl, this region may not move as it does in the wild type structure; exclusion of this region may reduce the size, unity, or magnitude of movement in identifiable domains to less than the detection threshold of DynDom. This would suggest that the hydrogen bond from Y110 to the inhibitor is critically important for proper domain movement. It is possible that domain movement simply cannot occur without involvement of Y110. Or, perhaps the mobile domain no longer moves as a unit and conformational changes in *Cj*-DHDPS cannot be defined on a domain scale.

In wt-DHDPS, the moving domain extends from the active site to the weak dimer interface (Figure 3.11). When examining Y110F with and without L-lysine we observe no domain movement and no changes at the weak dimer interface. Therefore, domain movement induced by

L-lysine binding at the allosteric site may be necessary to alter the arrangement at the weak dimer interface; and potentially signal cooperative L-lysine binding at the antipodal allosteric binding site. Absence of dynamic domains in Y110F-DHDPS implies that interaction of the inhibitor with the hydroxyl of Y110 is a prerequisite for domain movement and therefore, possibly cross dimer cooperativity.

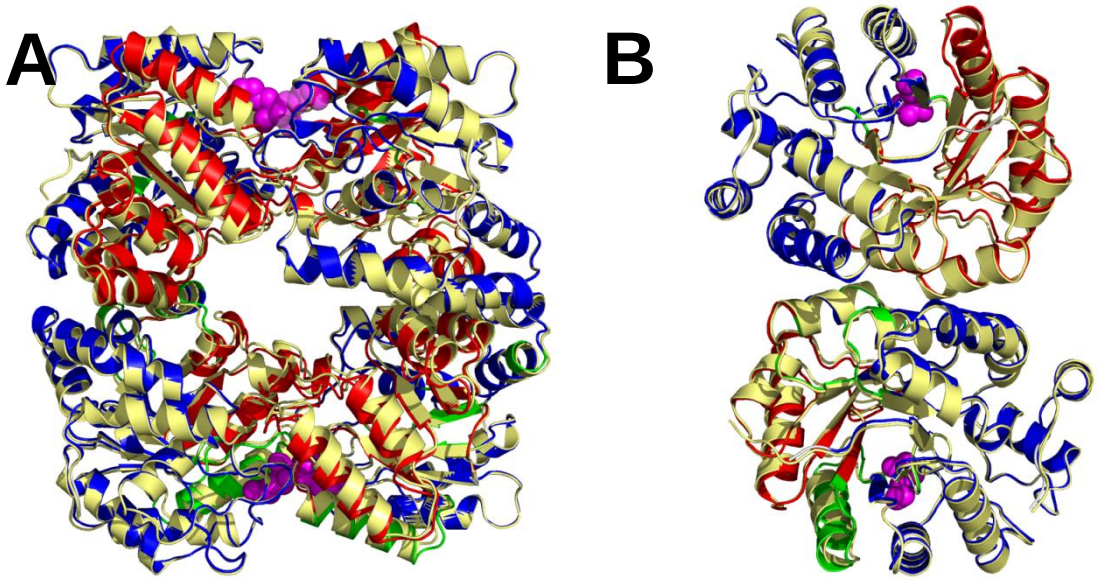

Figure 3.11 – **Quaternary relationship of Dynamic Domains.** On the *Cj*-DHDPS:pyr:lys structure (PDB: 4M19) the fixed domain is blue, moving domain is red and hinging residues are in green. The *Cj*-DHDPS:pyr structure (PDB: 4LY8) is shown in yellow. L-Lysine bound to the allosteric site (magenta) belongs to the blue and red structure. Panel A shows the tetrameric arrangement of DHDPS. It is clear from this angle that the red moving domain comes into contact with other monomers at both the weak and tight dimer interface. Panel B shows the interplay of monomers at the weak dimer interface where the moving domain of each monomer meats the fixed domain of the neighbor.

3.3.4 Y110F is Still Inhibited at High Concentrations of L-Lysine

Kinetic analysis of the Y110F mutant DHDPS was conducted by Yulia Skovpen.[1] Similar to wild-type, Y110F displays ping-pong kinetics, and demonstrates approximately half the enzymatic activity of wild-type.[1, 3] The L-lysine IC_{50} for Y110F was found to be approximately 40 mM (figure 3.8), which indicates that the Y110F mutation drastically changes the ability of the enzyme to be inhibited by L-lysine. This makes the enzyme insensitive to L-lysine regulation at its

physiological concentrations, however; when sufficiently saturated (> 80 mM) the Y110F enzyme displays partial allosteric L-lysine inhibition (Figure 3.8). Due to very weak L-lysine inhibition cooperativity coefficients where not estimated.[1]

3.3.5 Analysis of Y110F Cavity Volumes

Using CASTp, [12, 13] we calculated the volume of the allosteric site and active site in DHDPS Y110F both with and without L-lysine. Although there is no domain movement associated with L-lysine binding in the Y110F mutant, we do observe a decrease in solvent accessible volume in the allosteric site and movement of Cα positions which are similar to those observed between wt-DHDPS:pyr and wt-DHDPS:pyr:lys. The volume of the allosteric site of Y110F:pyr:lys (4MLR) is reduced by only 26% from 446 $Å^3$ to 332 $Å^3$ (compared to 43% in the wild-type enzyme) and the active site volume decreases by only 6% from 22 $Å^3$ to 20 $Å^3$ (compared to an increase of 22% in wild type; Table A.3). The magnitude of L-lysine's effect on the allosteric site is clearly less than that observed in wild type structures.

3.3.6 L-Lysine Binds to Y110F-DHDPS with Minimal Structural Effects

With the exception of the missing hydrogen bond at the F110 position, L-lysine adopts the same conformational side chain positions. Hydrogen bonding networks observed in the *Cj*-DHDPS:pyr:lys (4M19) structure are preserved in the Y110F:pyr:lys (4MLR) structure. As in the *Cj*-DHDPS:pyr:lys (4M19) structure, L-lysine was clearly seen in the initial F_o-F_c electron density map, and is bound in the allosteric site in a head-to-head orientation in the Y110F:pyr:lys (4MLR) structure. As for the structures without L-lysine, comparison of the Y110F:pyr (4MLJ) structure with the wt:pyr (4LY8) structure shows that they are nearly identical (Cα rmsd of 0.25 Å). Therefore from a structure-function perspective the lack of hydroxyl at F110 must play a significant role in the observed dynamics of catalysis and inhibition.

Phe110 is unable to form a hydrogen bond with L-lysine, and the structure displays few of the shifts associated with the *Cj*-DHDPS:pyr:lys (4M19) structure. Although the helices flanking the allosteric site shift when L-lysine is bound in Y110F, the changes noted for wt-*Cj*-DHDPS at the weak dimer interface are missing in the Y110F:pyr:lys (4MLR) structure. Additionally, the domain scale movements noted by DynDom for *Cj*-DHDPS:pyr:lys (4M19) are absent in the Y110F:pyr:lys (4MLJ) structure. Therefore we can conclude that the Y110F:pyr:lys (4MLR) structure is more similar to the *Cj*-DHDPS:pyr (4LY8) structure than to the *Cj*-DHDPS:pyr:lys (4M19) structure. Finally, the changes to solvent accessible volume at the allosteric, and active sites are significantly less upon L-lysine binding in Y110F compared to wt-*Cj*-DHDPS.

It is remarkable that all structural changes associated with L-lysine binding in wt-*Cj*-DHDPS have been significantly reduced, or eliminated with the loss of a single hydrogen bond in the allosteric site. The kinetic data indicates that Y110 is important for L-lysine inhibition; while the crystal structures clearly demonstrate that L-lysine binds, but has muted structural effects on the enzyme. Therefore the hydrogen bond between the inhibitor L-lysine and Tyr110 is of critical importance in the effective allosteric signal transduction.

3.4 Structure of WT and Y110F-DHDPS with Bislysine

The history and efficacy of the bislysine inhibitor is described in section 1.5.6.

3.4.1 Secondary Bislysine Binding Site

In addition to bislysine at the allosteric site, two more bislysine molecules were found within the crystal's asymmetric unit. The secondary bislysines were bound to the same surface site in two out of four monomers. The secondary binding site is located at the opposite end of the β-barrel from the enzyme's active site. The binding site is composed of random surface loops, with

minimal rearrangement to accommodate the binding of bislysine (Figure 3.12). On the other monomers one secondary binding site was buried by crystal contacts from a symmetry related molecule and the other is open to solvent space. Examination of the protein structure does not reveal any logical link from the secondary bislysine binding site to either the active site or the known allosteric binding site. Throughout all inhibition studies there has not been any indication of either secondary inhibitor binding or effect. Therefore, it is reasonable to conclude that this secondary binding site is an artifact of the crystallization conditions.

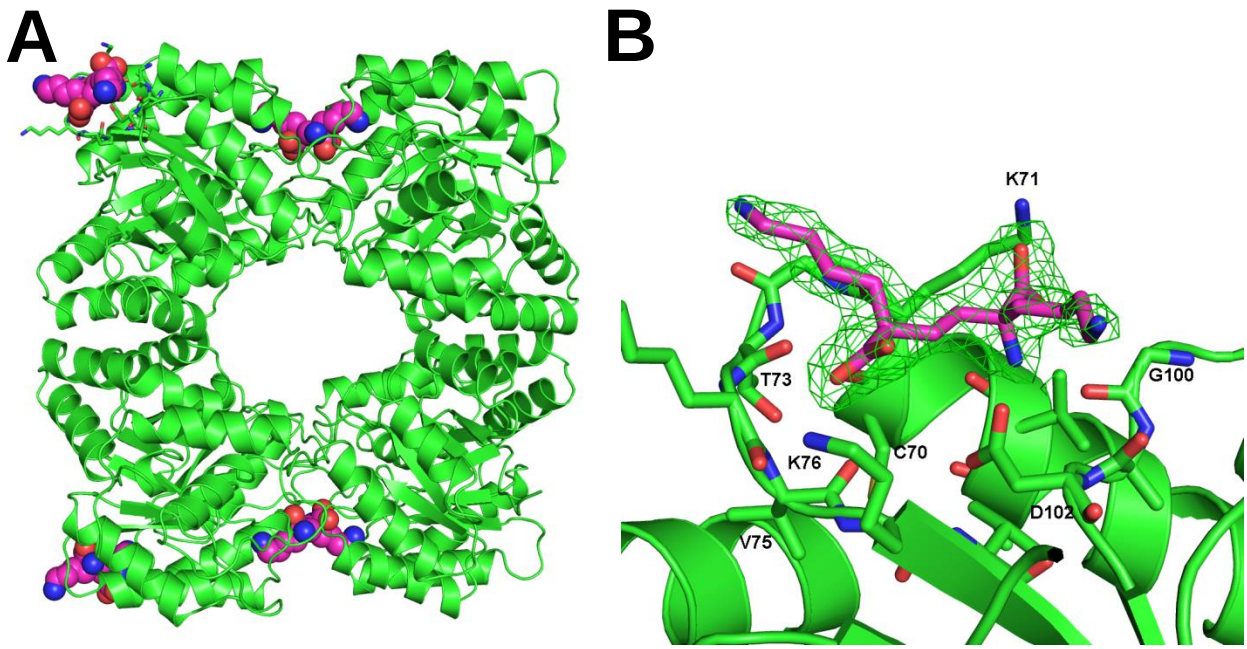

Figure 3.12 – **An Artifactual binding site for bislysine.** Panel A gives a global view of the DHDPS tetramer indicating the location of four bound bislysine molecules (PDB: 4RT8). Two bislysine are bound in the known allosteric site and two bislysine are bound at a newly identified site. Panel B shows F_o-F_c electron density omit map of bislysine and highlights the residues forming this secondary binding site.

3.4.2 Effects of Bislysine on wt-DHDPS

A comparison of the *Cj*-DHDPS:pyr:bislysine (4RT8) structure to the *Cj*-DHDPS:pyr (4LY8) structure reveals several side chain movements to accommodate bislysine in the allosteric site (Figure 3.13). There is notable contraction around the allosteric site; it appears as if the helices shift into the allosteric site when bislysine is bound, as noted by the backbone Cα's in helices

flanking the allosteric site. Using CASTp, we calculate the solvent accessible volume of the allosteric site to be 214 $Å^3$, which represents a 49% reduction in volume from the wt:pyr structure (4LY8).

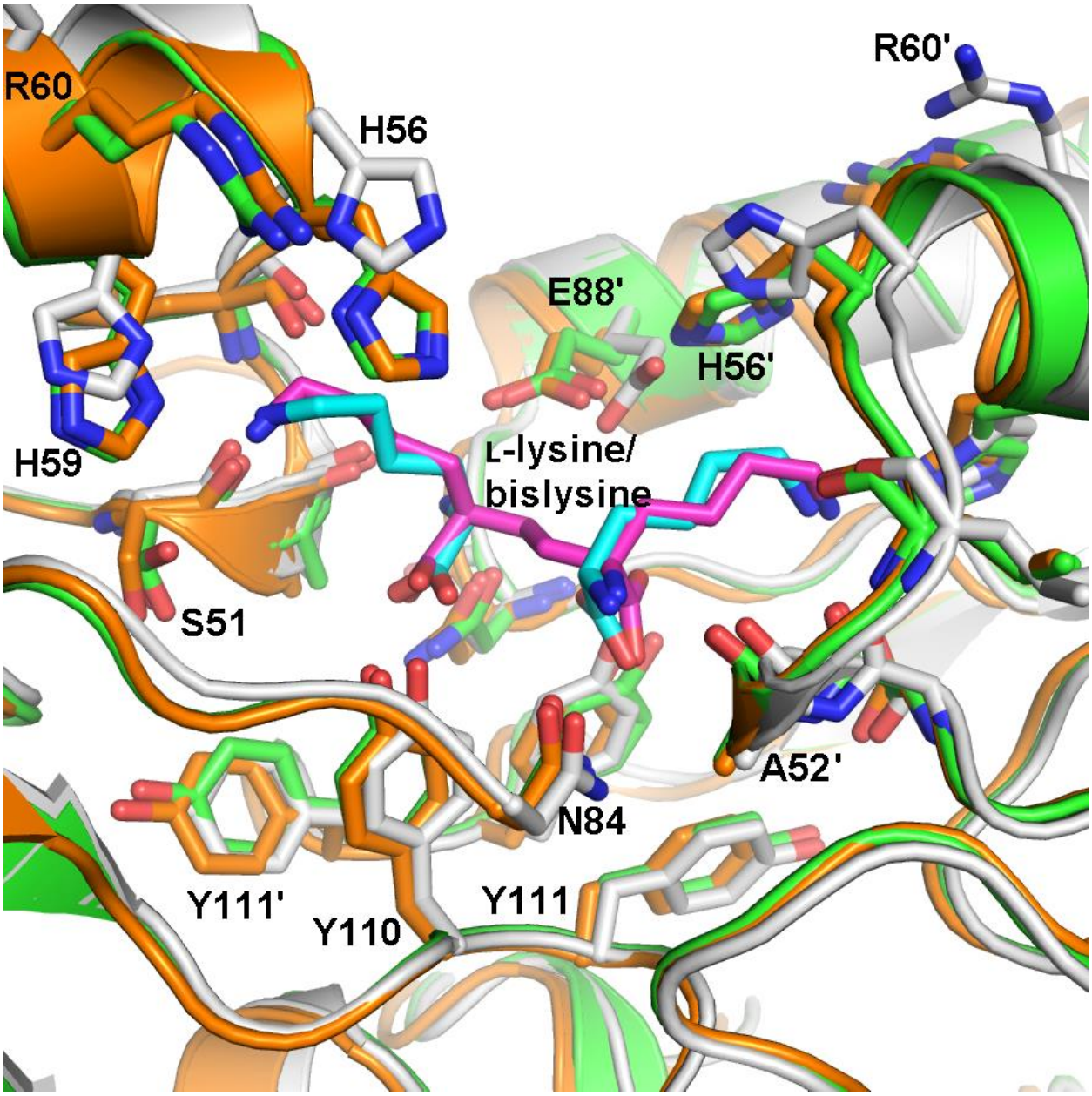

Figure 3.13 – **Superposition of wt:pyr:bislysine with wt:pyr:lys and wt:pyr.** The structure of wt:pyr (4LY8) is depicted in sliver, wt:pyr:lys (4M19) is orange with L-lysine in blue, and wt:pyr:bislysine (4RT8) is green with bislysine in purple. Upon binding of bislysine DHDPS undergoes the same conformational changes at the allosteric site as it does when binding L-lysine.

Since bislysine is a 300-fold more effective inhibitor than L-lysine, we anticipated either enhanced structural affects in the active site or stronger binding affinity, or both. However, contrary to the effects of L-lysine; bislysine induces only one change to the geometry of the catalytic triad: the hydrogen bond distance of two residues, Y137 – T47, in the catalytic triad is reduced (3.4 Å to 3.0 Å; Figure 3.16, panel C). However, the solvent accessible active site volume increases 35% from 20 $Å^3$ to 27 $Å^3$ (Table A.3). These observations underscore the significance of the catalytic triad, and the importance of a proper-sized active site.

Inhibition studies indicate that two bislysine molecules exhibit binding cooperativity across the weak dimer interface.[1] For this reason comparisons were made on the conformation of the weak dimer interface in wt:pyr (4LY8), and wt:pyr:bislysine (4RT8). At the weak dimer interface, the secondary structures remain largely intact; indeed, there is less rearrangement than observed for wt:pyr:lys (4M19). The effects that L-lysine has at the weak dimer interface are not captured in the wt:pyr:bislysine crystal structure, and yet cooperativity is observed across the weak dimer interface, making the structural basis for cooperativity particularly difficult to explain.

3.4.3 Comparison of wt-DHDPS with L-lysine and with Bislysine

As expected, bislysine occupies the binding site of two L-lysine molecules within one allosteric site. The bislysine completes all of the hydrogen bonds and side chain accommodations as described previously for L-lysine binding to wt-DHDPS. Indeed, of all the hydrogen bonds formed between the enzyme and inhibitor, only one is significantly different from those in the wt:pyr:lys (4M19). The bond between the L-lysine-Nζ, and the carbonyl oxygen of Leu54 is longer in the bislysine structure (4.2 Å) than in wt:pyr:lys (3.3 Å; Figure 3.14).

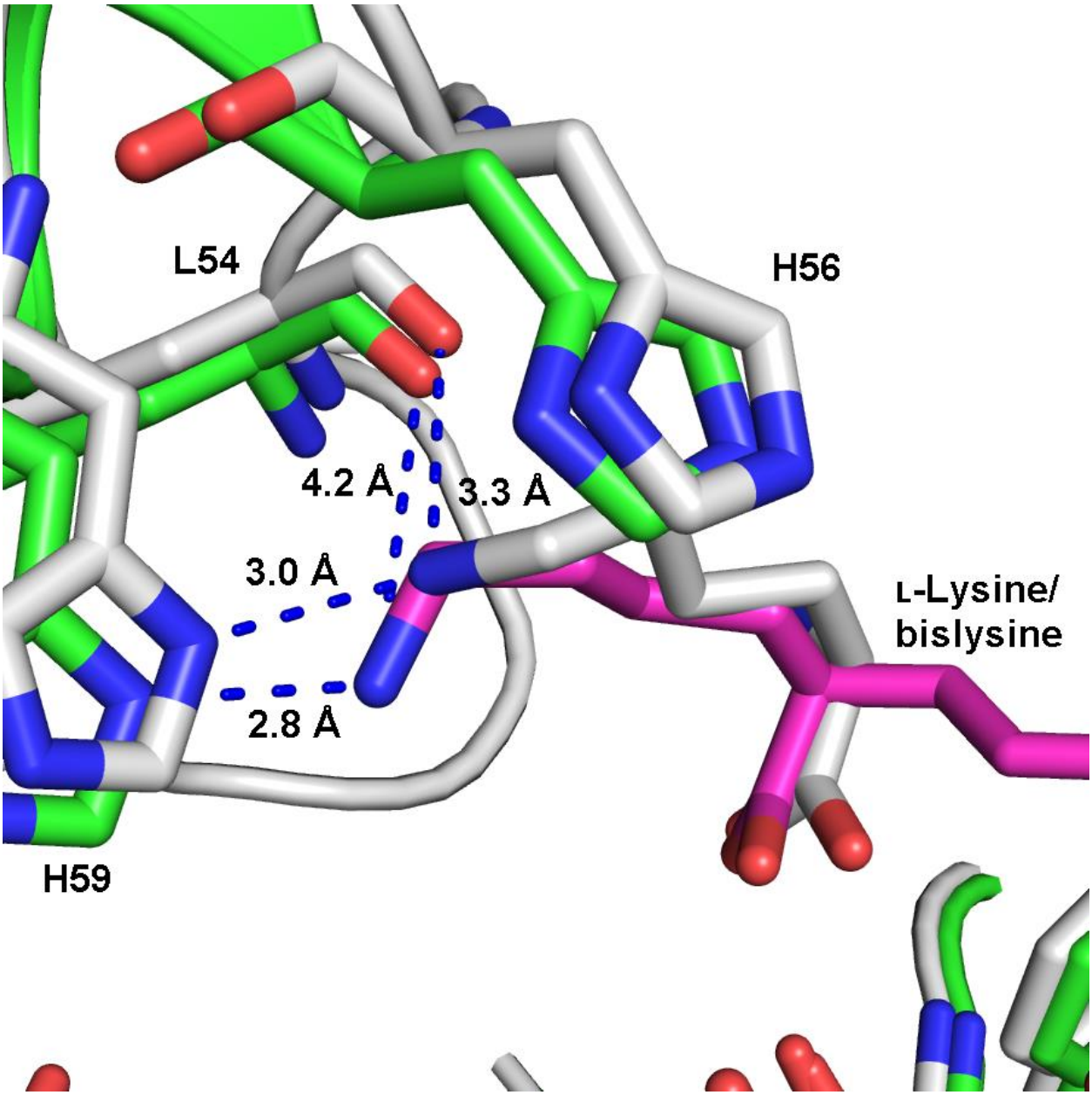

Figure 3.14 – **A small difference in hydrogen bonding at the Nζ of L-lysine vs bislysine.** Thewt:pyr:bislysine structure (4RT8) is shown in green with bislysine in purple. The wt:pyr:lys structure (4M19) is shown in grey with L-lysine also in grey. There is an obvious change in length for the hydrogen bond from Nζ to L54(CO). However, the hydrogen bond difference between Nζ to H59 cannot be considered significant.

Bislysine is known to inhibit wt-DHDPS 300 times more effectively than the natural inhibitor, L-lysine.[1] One possibility is that any structural changes critical to inhibition would be enhanced or become more obvious. However, a number of structural changes observed when L-lysine binds to wt-DHDPS are not seen when bislysine binds to DHDPS. Notably there is no detection of

concerted domain movements, despite the obvious movement in helices close to the allosteric site. It is possible that the structural distortions caused by bislysine do not induce unified domain movement. Or, perhaps that domains labeled in the binding of L-lysine have become too small or distorted to be considered proper domains.

As noted above, the allosteric site of wt:pyr:bislysine (4RT8) is 49% smaller than that of the wt:pyr structure (4LY8). Whereas the wt:pyr:lys (4M19) allosteric site is only 43% smaller than the solvent accessible volume of the wt:pyr structure (4LY8). At the active site, bislysine increases the solvent accessible volume by 35% from that of wt:pyr (4LY8), while the natural inhibitor L-lysine induces only 27% increase in solvent accessible volume. This observation leads us to believe that the volume of the active site may be critical to effective catalysis, and therefore a potential control mechanism.

When comparing the active site of the wt:pyr:lys (4M19) structure to the wt:pyr (4LY8) structure, a number of small changes were noted (Section 3.2.3). Interestingly, many of these small changes are not observed when comparing the active site of the wt:pyr:bislysine (4RT8) structure to the wt:pyr (4LY8) structure. Active site changes which are not observed between wt:pyr:bislysine and wt:pyr are: Y137 – Y111' (4.7 Å to 4.7 Å); the C1 of the pyruvyl Schiff base and the carbonyl of I207 (3.8 Å to 3.8 Å); and G190 (and 4.7 Å to 4.5 Å). The major changes to the catalytic triad (Y137 – T47; 3.4 Å -> 2.9 Å) are affected by both L-lysine and bislysine. Many prior studies have indicated the importance of the catalytic triad by eliminating one or more residues.[4, 16] However, it would appear that the length of hydrogen bonds between members of the catalytic triad may be as important as their identity and presence.

Both L-lysine, and bislysine have been shown to exhibit cooperativity across the weak dimer interface. Comparison of this region between wt:pyr (4LY8) and wt:pyr:lys (4M19) revealed several dramatic rearrangements potentially facilitating cooperativity between allosteric sites cross the weak dimer interface. Interestingly, none of these structural changes are present in the wt:pyr:bislysine structure (4RT8). Changes identified in the wt:pyr:lys structure (4M19) are potentially involved in cross dimer communication; however, their absence in the wt:pyr:bislysine (4RT8) is contradictory and the cooperativity phenomenon remains difficult to explain.

3.4.4 The Effects of Bislysine Binding to Y110F DHDPS

The point mutation Y110F is particularly interesting as the loss of a single hydroxyl group at the allosteric site results in extreme insensitivity to the natural inhibitor L-lysine. The IC_{50} for Y110F-DHDPS with L-lysine is approximately 40 mM, which is 600 times weaker than the 65 µM IC_{50} of wt-DHDPS with L-lysine. The synthetic inhibitor bislysine is capable of strongly inhibiting the Y110F mutant DHDPS.[1] Evidently, the hydroxyl of Y110 is important to the mechanism of allosteric inhibition but, the efficacy of bislysine indicates that there must be other structure-function links between the allosteric site and the active site; therefore, the structure of Y110F-DHDPS with bislysine in the allosteric site should reveal communication between the allosteric and active site which are not attributable to tyrosine 110.

Unique to the crystal structure of Y110F:bislysine (4RT9) is the fact that the K166-pyruvate Schiff base adduct did not resolve within the active site. It cannot be ruled out that crystallization with bislysine may be selective for a pyruvate-free active site or drives pyruvate release. As with other DHDPS structures, pyruvate was never introduced to the enzyme prior to crystallization. In addition to possible inhibitory effects, there may have been a shift in equilibrium due to differences in crystallization conditions or cryoprotection which are not present in other DHDPS workups.

Both L-lysine and bislysine have been shown to enhance the binding of pyruvate,[1] and thus a likely explanation is one of low occupancy due to crystallization conditions, rather than an inhibitory effect.

3.4.4.1 Absence of Domain Movement in Y110F:bislysine

Bislysine binds to Y110F-DHDPS in the same manner as bislysine in wt-DHDPS; which, for both wt-DHDPS and Y110F-DHDPS bislysine occupies the same space as two L-lysines do in either wild-type or Y110F-DHDPS. The same network of new hydrogen bonds is completed in all structures. As with structures described previously, the helices flanking the allosteric site, in Y110F-DHDPS, appear to move towards the inhibitor bislysine, as judged by Cα positions (Figure 3.15). We used DynDom to examine Y110F:bislysine (PDB: 4RT9) for domain scale movement. Similar to the case of Y110F-DHDPS with L-lysine, DynDom does not detect any domain scale movements. In the wild-type DHDPS, Y110 is at the heart of the moving domain, and is observed to move more than 1 Å to accommodate the inhibitor in the allosteric site. In Y110F-DHDPS this accommodation is absent. It is possible that without the movement of the aromatic core, the integrity of the domain has been lost such that moving regions have become too small or movement vectors are no longer synchronous and thus dynamic domains cannot be defined. Whatever the case may be, it appears that Y110 is correlated to domain movement, and said domain movement is not critical to the inhibition of the enzyme.

At the active site, there is only one notable change: the distance between Y111' and Y137 has increased from 4.6 Å to 5.0 Å (Figure 16, panel A). Interestingly, this is the same change observed for L-lysine bound to Y110F-DHDPS, but not observed in any wt-DHDPS with either L-lysine or bislysine (Figure 16 panels B, C, D). In the case of wt:pyr:lys (PDB: 4M19) the same distance between Y111' - Y137 is reduced from 4.7 Å to 4.2 Å (Figure 16, panel D). The changes observed

in the catalytic triad of wt:pyr:lys are all distinctly different from those changes observed in wt:pyr:bislysine (4RT8), where the catalytic triad shifts in the hydrogen bond between Y137-T47 from 3.4 Å to 3.0 Å (Figure 16, panel C). Nevertheless, it appears that in all cases of inhibitor-binding to DHDPS, the geometry of the catalytic triad has been affected.

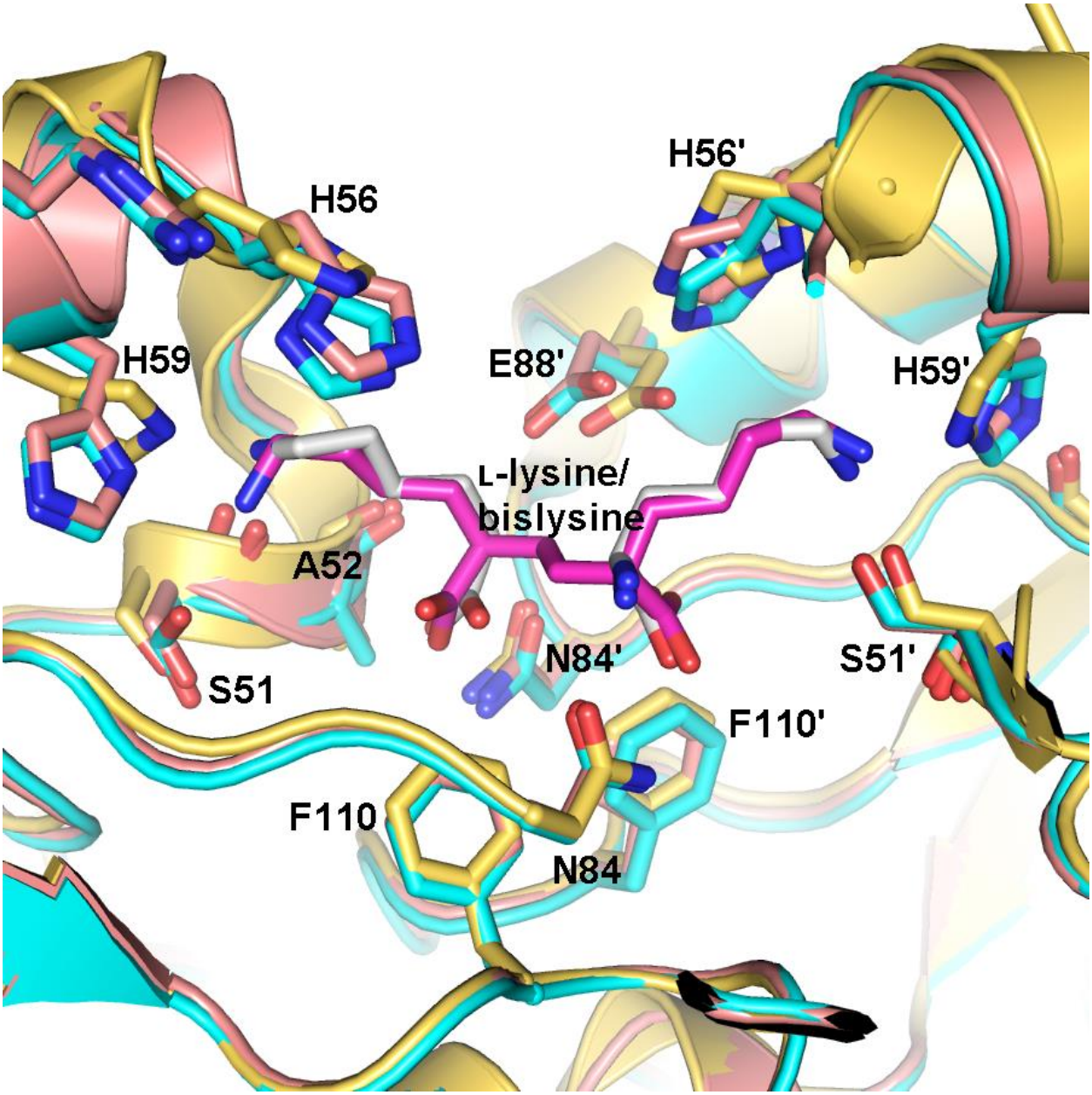

Figure 3.15 – **Superposition of Y110F:bislysine with Y110F:pyr:lys and Y110F:pyr** The structure of Y110F:pyr (4MLJ) is depicted in yellow, Y110F:pyr:lys (4MLR) is pink with L-lysine in white, and Y110F:pyr:bislysine (4RT9) is blue with bislysine in purple. Upon binding of bislysine, Y110F-DHDPS undergoes the same conformational changes at the allosteric site as it does when binding L-lysine. We note the Cα of flanking helices move towards the allosteric site; however, there is no concerted domain movements.

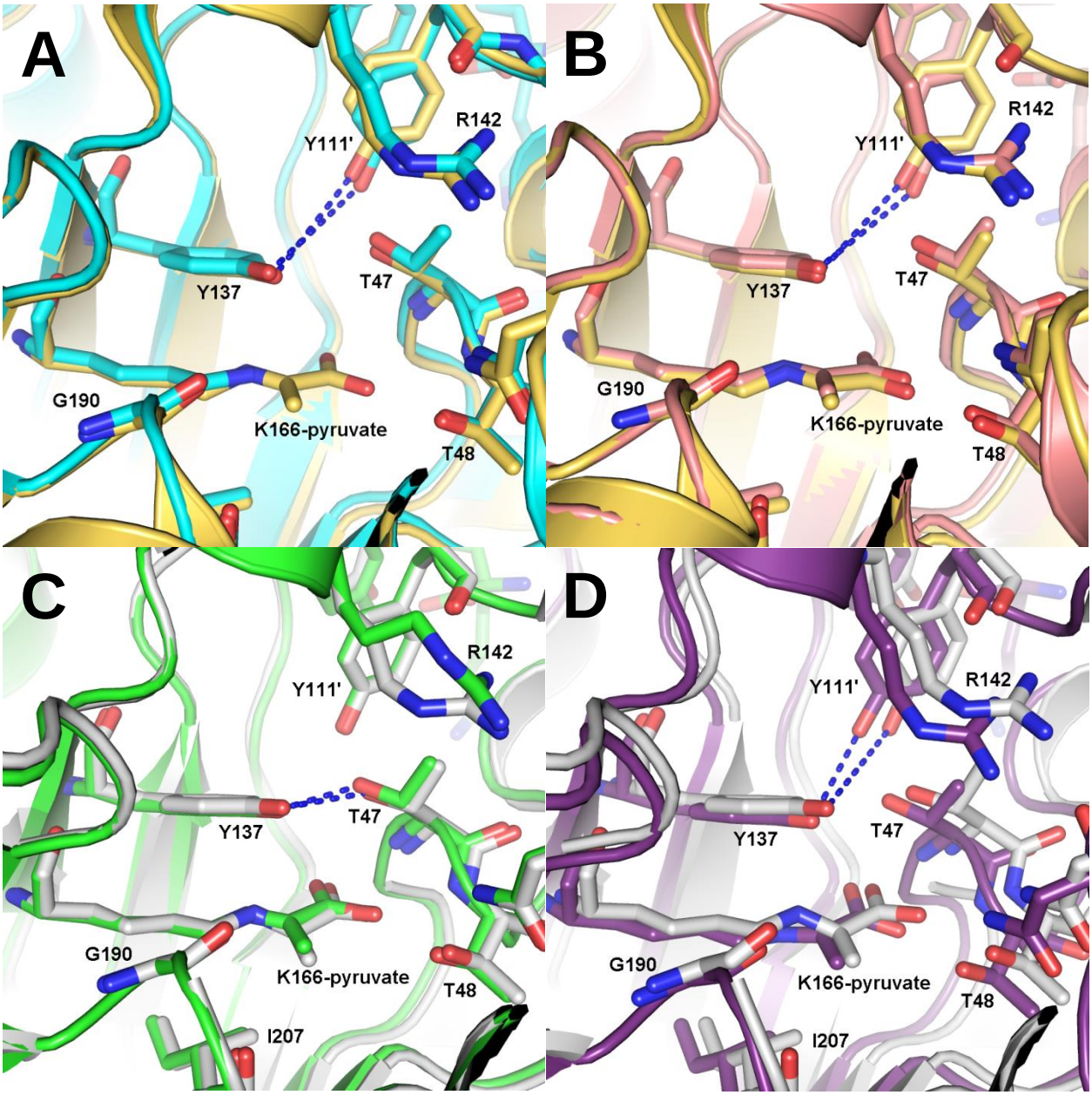

Figure 3.16 – **Allosteric effect at the active site.** Panel A shows Y110F:bislysine (PDB: 4RT9) in blue superpositioned on Y110F:pyr (4MLJ) shown in yellow. The distance between Y137/Y111' is increased from 4.6 – 5.0 Å when bislysine binds. Panel B shows Y110F:pyr:lys (4MLR) in pink superimposed on Y110F:pyr (4MLJ) in yellow. Here, we also see he distance between Y137/Y111' has increased from 4.6 – 5.0 Å. Panel C shows wt:pyr:bislysine (4RT8) in green superimposed on wt:pyr (4LY8)shown in silver. In the wild type structure we see the distance between Y137/Y111' is unchanged, and the distance between Y137/T47 is decreased 3.4 – 3.0 Å when bislysine binds. Panel D shows wt:pyr:lys (4M19) in purple and wt:pyr (4LY8) in silver. We see that when L-lysine binds it affects the distance between Y137/Y111'; however, the bond is shortened 4.7 - 4.2 Å rather than lengthened as we see in other structures.

3.4.4.2 Cavity volumes in Y110F:bislysine

As with other structures, the shifting Cα positions around the allosteric site was readily apparent. We therefore examined the solvent accessible volume of both the active site and allosteric site using CASTp. The solvent accessible volume of the Y110F:bislysine (PDB: 4RT9) allosteric site is 278 $Å^3$, which is 33% smaller than wt:pyr (4LY8), 38% smaller than Y110F:pyr (4MLJ), 16% smaller than Y110F:pyr:lys (4MLR), and 16% larger than wt:pyr:lys (4M19; Table A.3). Unfortunately, Y110F:bislysine (PDB: 4RT9) did not crystallize with pyruvate at the active site. This makes direct comparisons of the active sites between all DHDPS structures difficult. Using CASTp we measured the pyruvate free active site volume of Y110F:bislysine (4RT9) as 42 $Å^3$. We can compare this directly to the active site volume of the apo-DHDPS (PDB: 4R53), which is 36 $Å^3$; thus bislysine induces a 17% increase in the active site volume over that of apo-DHDPS.

If we assume that changes in active site volume between apo-DHDPS (PDB: 4R53) and each of wt:pyr (4LY8), and Y110F:pyr (4MLJ) are exclusively due to the presence of pyruvate and not rearrangement of the enzyme, then we can hypothesize the effects bislysine may have on the active site of Y110F:bislysine (4RT9). The average difference between the active site volume of wt-apo-DHDPS and wt/Y110F:pyr is 15 $Å^3$, which we determine to be the volume occupied by the pyruvate adduct, based on previous assumptions. Based on this, 15 $Å^3$ is subtracted from the measured active site volume of Y110F:bislysine (41.8 $Å^3$), and the remaining volume if pyruvate was present would be approximately 26 $Å^3$. From this analysis the active site volume of 26 $Å^3$ represents a 18% increase from the active site volume of 22 $Å^3$ in Y110F:pyr (4MLJ). Thus Y110F:pyr:lys (PDB: 4MLR) demonstrates little to no change in active site volume relative to Y110F:pyr (4MLJ) which corresponds with little to no inhibition; whereas bislysine restores the

trend for increasing the volume of the active site when strong inhibition is observed. These results reinforce the correlation noted between strong inhibition and increasing volume at the active site.

3.4.5 Discussion: Possible Contributions to Stronger Bislysine Inhibition

Bislysine inhibits wt-DHDPS 100,000 times stronger than the natural inhibitor L-lysine.[1] Despite near incomplete insensitivity to L-lysine, Y110F-DHDPS is inhibited by bislysine at nearly the same potency as wt-DHDPS. Stronger inhibition may be attributable to tighter binding or enhanced activation of allosteric mechanisms. It was anticipated that crystallization of the synthetic inhibitor bislysine, with each of wild-type and Y110F-DHDPS would provide insight into the mechanism for enhanced inhibition, and therefore natural inhibition of L-lysine.

It must be considered that entropy of binding is the most obvious contribution to enhanced inhibition. Results of Isothermal Titration Calorimetry experiments performed by Phenix and Palmer indicate that binding of L-lysine has a large entropic component.[17] Combining two L-lysine molecules with a 2-carbon linker will decrease the entropic barrier for binding of the second inhibitor molecule to occupy both sides of the allosteric site. The result is a greater increase in entropy for the binding event, which would lead to an overall greater decrease in free energy.[1, 17]

Furthermore, inhibition studies of DHDPS with bislysine indicate that binding of bislysine is a slow two-step process.[1] The crystal structure indicates that much of the bislysine inhibitor is buried within the allosteric site, with H56 acting as a cap. One can imagine that a series of conformational changes must occur to both the enzyme and inhibitor as bislysine slides into each half of the allosteric site (Figure 3.17). It is highly likely that a similar sequence of conformational changes must happen during dissociation. Therefore, it is likely that dissociation is an equally slow two-

step process which contributes favorably to enhanced inhibition. The H56 probably plays a very important role when capping the allosteric site.

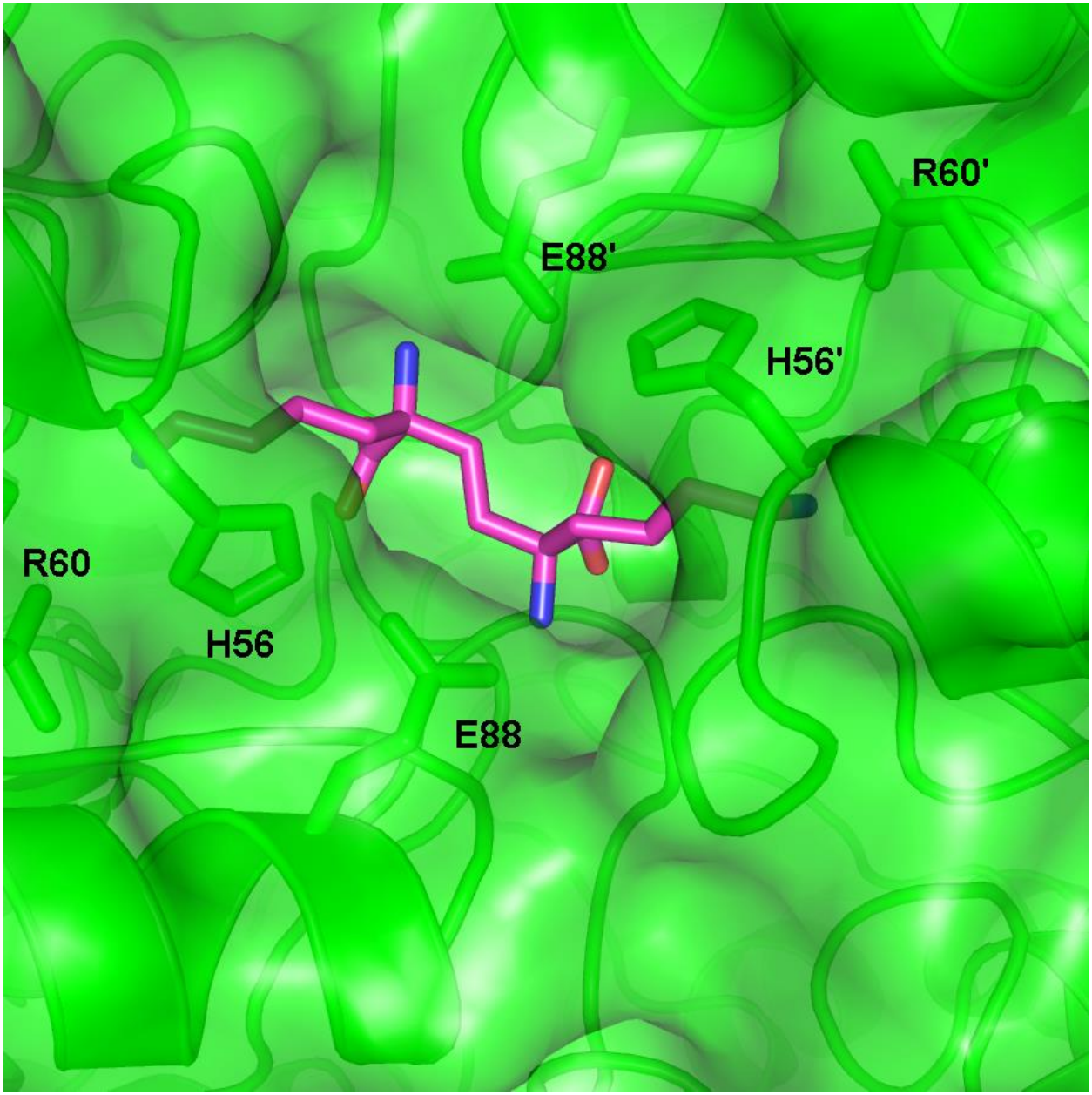

Figure 3.17 – **Molecular Surface around the DHDPS allosteric binding pocket.** The figure depicts bislysine (purple) bound within the allosteric site of wt-DHDPS (PDB: 4RT8) in green. Select residues are shown which form a "lid" on the allosteric site. One can envision that a series of conformational changes are required for bislysine to either bind or dissociate from the allosteric site.

In addition to arguments for tighter binding of bislysine, consideration must be made for enhancement of the allosteric signal for inhibition. Although increased binding affinity may contribute the most to enhanced inhibition there are subtle differences between the structures of DHDPS with L-lysine or bislysine which suggest enhancement or changes to the structural mechanism of inhibition. Structural analysis of DHDPS with bislysine are considerably less numerous than the myriad of effects noted for the binding of L-lysine. That is to say, in the case of bislysine we observe only a handful of specific structural changes upon binding of bislysine to either wild type, or Y110F-DHDPS. One can envision two dynamic structural states of the enzyme which exist in equilibrium: an uninhibited state, and a maximally inhibited state. It is possible that the diverse changes of the wt:pyr:lys (PDB: 4M19) structure, relative to wt:pyr (PDB: 4LY8) represents an incomplete shift in equilibrium towards the maximally inhibited structure; whereas, the stronger inhibitor, bislysine, will drive the enzyme to be dominated by a fully inhibited conformation. If inhibition of DHDPS is indeed dependent on an equilibrium of dynamic conformations then protein dynamics may play a large role which we have not empirically examined. Logically those structural changes which are observed for both L-lysine and bislysine should be considered more important to the mechanism of allostery than those structural changes which are observed only in the case of L-lysine.

In a comparison of six structures (wt:pyr, 4LY8; Y110F:pyr, 4MLJ; wt:pyr:lys, 4M19; Y110F:pyr:lys, 4MLR; wt:pyr:bislysine, 4RT8; Y110F:bislysine, 4RT9) we can identify two changes to the active site common to the binding of both the allosteric inhibitors L-lysine and bislysine (Figure 3.16). Both inhibitors induce changes in the geometry of the catalytic triad (Y137, T47, Y111'), though the specific change is unique to either wt-DHDPS or Y110F-DHDPS. In wt-DHDPS we note that both L-lysine, and bislysine decrease the hydrogen bond distance

between Y137-T47 from 3.4 Å to 2.9 Å, and 3.0 Å respectively. In contrast, binding of L-lysine or bislysine to Y110F-DHDPS increases the distance between Y111'-Y137 from 4.6 Å to 5.1 Å and 5.0 Å respectively. Interestingly, in the wt-DHDPS the distance between Y111'-Y137 is decreased from 4.7 Å to 4.2 Å when L-lysine is bound, but is unaffected when bislysine is bound. Deletion of any residue involved in the catalytic triad has been shown to have a dramatic effect on the enzymes activity.[4, 16] The observations suggest that modification of local pKa's in an inherently dynamic catalytic triad may be integral to inhibition, as well as catalysis. Unfortunately, consideration of the catalytic triad alone cannot fully explain the difference in inhibitor sensitivity between Y110F:pyr:lys and Y110F:bislysine.

Regarding the phenomenon of antipolar cooperation, there are select residue movements at the weak dimer interface observed when L-lysine binds to wt-DHDPS suggesting possible means for cross dimer communication. However, no such residue movements are observed in either wt:pyr:bislysine (PDB: 4RT8) or Y110F:bislysine (4RT9). This is drastically different from the multiple rearrangements observed in wt:pyr:lys (4M19), making it impossible to draw any convincing conclusions.

Interestingly, the absence of domain movement in structures with bislysine suggests that domains highlighted when L-lysine binds to wt-DHDPS have only coincidental importance. Domain movements are clearly outlined when comparing the structures of wt:pyr (PDB: 4LY8) with wt:pyr:lys (4M19). However, there are no domain movements observed when either L-lysine or bislysine binds to Y110F-DHDPS. It is possible that the central location of the point mutation Y110F splits the domain such that the bulk of the enzyme does not move as a whole. However, the structure of wt:pyr:bislysine (4RT8) is also lacking in well-defined domain movements relative to wt:pyr (4LY8), despite the intact hydrogen bond to Y110, which is more difficult to rationalize.

Bislysine remains a highly effective inhibitor and the simplest conclusion is that domain movements are not critical for reducing catalytic activity of DHDPS. This gives more weight to local effects at the active site; such as solvent accessible volume, and the arrangement of the catalytic triad.

The dynamic domains likely have some peripheral role. Perhaps dynamic domains contribute to the mechanism of cross dimer cooperativity, or govern the inherent dynamics and stability of *Cj*-DHDPS. Based on inhibition analysis and Hill coefficients, subtle differences may be anticipated in the cooperativity of L-lysine vs bislysine;[1] which may result in slightly different structural effects.

The most profound correlation is that of solvent accessible volume in the active site and allosteric site relative to the strength of inhibition. At the allosteric site the greatest enzyme inhibition is correlated to the greatest decrease in solvent accessible volume (Figure 3.18). Considering the dynamic model of protein-ligand binding this would appear to be intuitively linked to the strength of inhibitor binding. However, we must also consider that, although the mechanism of allostery is unknown, the magnitude of structural displacement at the allosteric site is likely to have effects throughout the protein, including the active site. The volume phenomenon at the allosteric site is mirrored at the active site, where the strength of the inhibitor is correlated to increasing solvent accessible volume. The active site volume of wt:pyr (PDB: 4LY8) and Y110F:pyr (4MLJ) are effectively the same, at 20 $Å^3$ and 22 $Å^3$ respectively. When an inhibitor is bound to DHDPS the solvent accessible volume of the active site is increased relative to wt:pyr: Y110F:pyr:lys ±0%, wt:pyr:Lys +30%, Y110F:bislysine +30%, and wt:pyr:bislysine +35%. Clearly, the solvent accessible volume of the active site is strongly correlated to the activity of the enzyme. Unlike the previously noted changes to the geometry of the catalytic triad, which may

affect the reactivity of ASA, changes in the volume of the active site are likely to affect the binding affinity of ASA.

The increased volume of the active site may reduce the enzymes affinity for ASA or destabilize the catalytically competent conformation of ASA. When bislysine is bound the active site volume increases on par with wt-DHDPS:pyr:bislysine. Since the mutant enzyme is inhibited to the same extent as the wild-type enzyme then changes in the volume of the active site very likely play an important role in the mechanism of inhibition. The changes noted for the active site suggest that inhibition of DHDPS may be a combined result of perturbations to the catalytic triad and increase in solvent accessible volume of the active site.

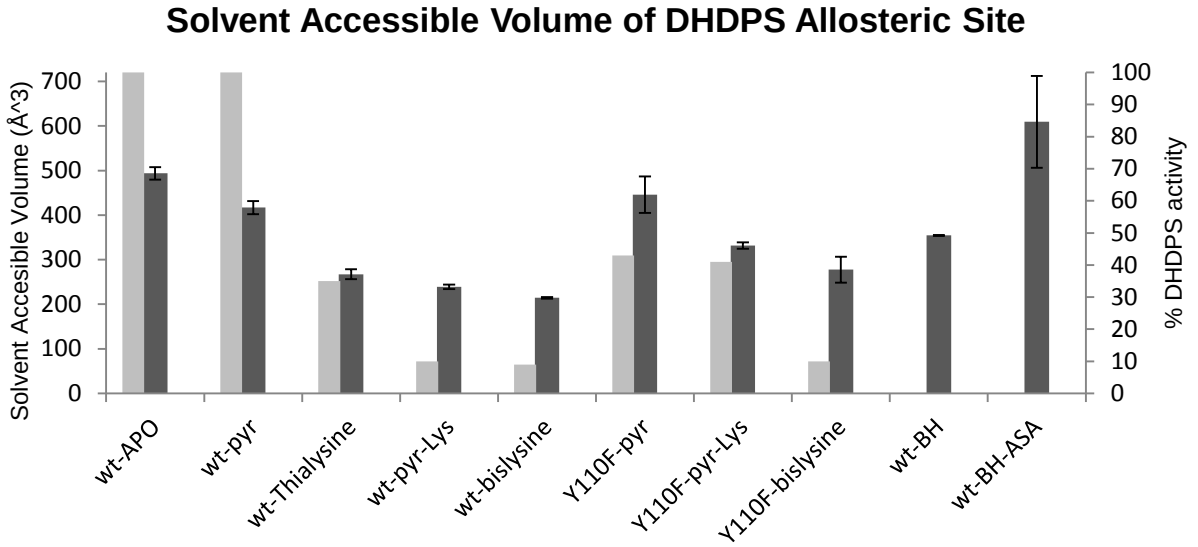

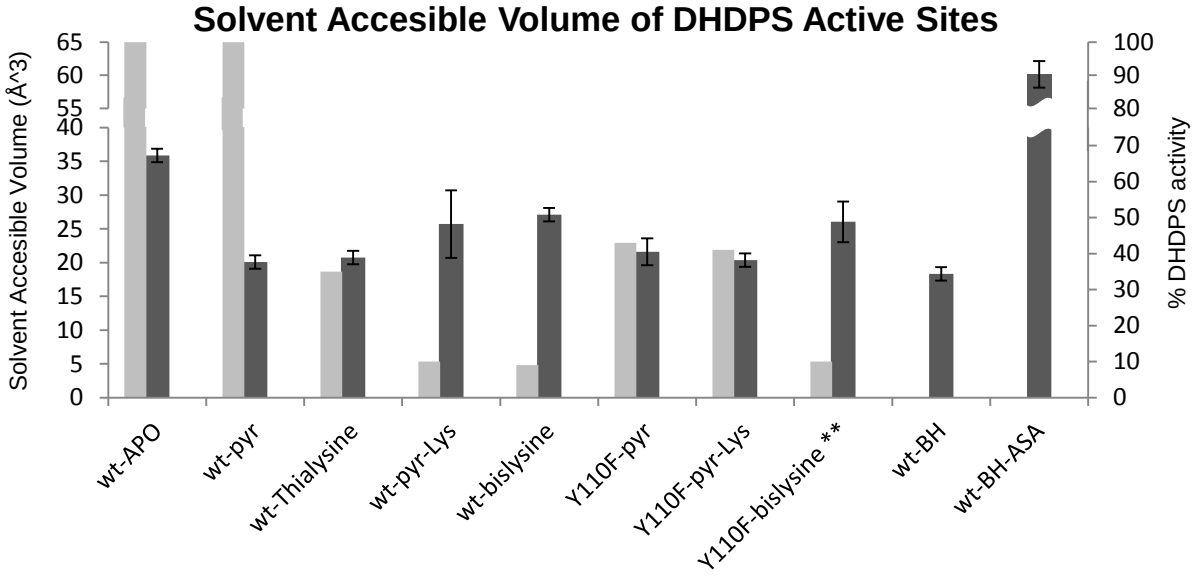

****** Estimated solvent accessible volume if pyruvate had been present in the active site.

Figure 3.18 – **Bar Charts depict volume changes at the active site and allosteric site.** Solvent accessible volumes calculated using CASTp[12, 13] as described in the text, and excluding L-lysine from the model. Changes to the solvent accessible volume are correlated to the strength of inhibition. (■) Cavity Volume; (■) % DHDPS activity.

3.5 Structure of wt-DHDPS with L-Thialysine

L-Thialysine is a weak inhibitor of DHDPS. Despite its similarities with the natural inhibitor L-lysine, L-thialysine has an IC_{50} of only 2 mM, which is 30 times weaker than L-lysine (IC_{50} 65 µM).[1] It is unclear why such a similar molecule should be so ineffective as an inhibitor. Structural studies will help to reveal the subtleties of inhibitor strength.

3.5.1 wt-DHDPS with L-Thialysine

Despite weaker electron density, L-thialysine is readily modeled into the allosteric site. Two L-thialysine molecules bind in each dimeric allosteric site in a "head-to-head" fashion, with two fold symmetry (Figure 3.3). Superficially, L-thialysine appears to bind in the very same fashion as that of L-lysine. The strongest argument for weak inhibition would appear to be the strength of binding; this is supported by weak electron density, in the F_o-F_c map, indicating low occupancy, and the higher concentration of L-thialysine which was required to obtain the crystal structure relative to L-lysine.

3.5.2 Comparison of wt-DHDPS with and without L-Thialysine

As with L-lysine and bislysine, we first compare the wt:pyr:thialysine structure to that of wt:pyr. From a global perspective there is remarkably little structural difference, with an rmsd of 0.38 Å. Whereas comparison of wt:pyr:thialysine to wt:pyr:lys (PDB: 4M19) has an rmsd of 0.40 Å. There is of course some movement of side chains in and around the allosteric site to accommodate L-thialysine (Figure 3.19). We can also see the Cα's of helices closing the allosteric site; although, not as pronounced as observed for L-lysine or bislysine. As was performed for other DHDPS structures, we examine the structures for domain movement, and made measurements of the volume of the allosteric and active sites.

Structural analysis of wt:pyr:thialysine and wt:pyr (PDB: 4LY8) using DynDom reveals domain movements only in one of eight wt:pyr:thialysine monomers. Although the pattern of moving and stationary domains is the same as that for wt:pyr:lys (4M19), a one in eight representation can only be considered inconclusive at best, and is more than likely anomalous. Optimistically, examination of symmetry related molecules reveals that there is no reason to believe that this is a result of crystal packing, and therefore low representation of domain movement may be correlated to the low occupancy of L-thialysine.

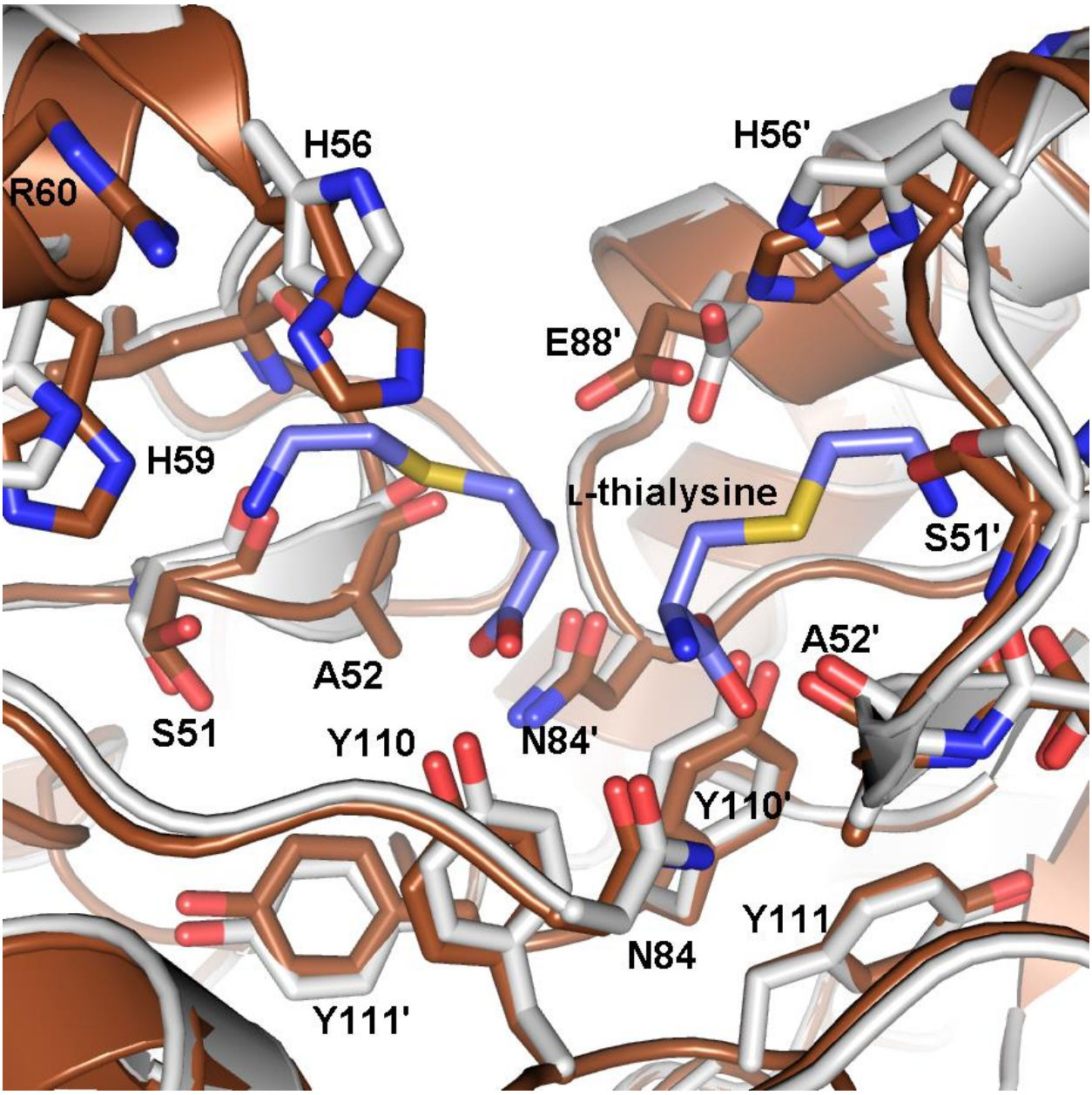

Figure 3.19 – **Superposition of wt:pyr:thialysine with wt:pyr.** The structure of wt:pyr (PDB: 4LY8) is depicted in white, wt:pyr:thialysine is brown with L-lysine in blue. Upon binding of thialysine wt-DHDPS undergoes the same conformational changes at the allosteric site as it does when binding L-lysine. We note the Cα of flanking helices move towards the allosteric site; however, only 1 in 8 monomers suggests any domain movements.

Using CASTp we can measure the solvent accessible volume of the wt:pyr:thialysine active site and allosteric site. The allosteric site has a solvent accessible volume of 267 $Å^3$, and the active site has a solvent accessible volume of 21 $Å^3$. Each of these measurements agrees with the previously noted correlations between strength of inhibitor and solvent accessible volume at the

active site (Table A.3). When L-thialysine binds to wt:pyr (PDB: 4lY8), the allosteric site decreases in size by 36%, while the active site solvent accessible volume is effectively unchanged. Therefore, although L-thialysine binds to DHDPS, it does not induce the principal change at the active site that we associate with strong inhibition. This suggests that the relationship between inhibitor strength and active site volume is indeed one of cause and effect and a necessity for successful inhibition.

Not surprisingly, there is very little movement of individual residues within the active site of wt:pyr:thialysine, and an examination of the weak dimer interface of wt:pyr:thialysine compared to wt:pyr (4LY8) revealed no changes. The only notable rearrangement is within the catalytic triad. The hydrogen bond between Y137 and T47 is reduced from 3.4 Å, to 2.9 Å (Figure 3.20). The same movement for these residues is seen in the structure of wt:pyr:lys (4M19), and interestingly, is also the sole residue movement observed in the active site of wt:pyr:bislysine (4RT8). The limited inhibition observed for L-thialysine is probably attributable to this change at the catalytic triad, while volume changes serve to enhance the effects of L-lysine and bislysine.

The reduction of the hydrogen bonding distance between Y137 to T47 is observed with three allosteric inhibitors of varied efficacy, suggesting that the length of this bond is critical to the mechanism of allosteric inhibition. However, despite observing the same residue movement when each inhibitor is bound, the efficacy of each is highly variable. This suggests the observed change in hydrogen bonding length is not solely responsible for inhibition of the enzyme. Regardless of the inhibitory magnitude attributable to this one hydrogen bond, the observations reinforce our conviction that modifications to the geometry of the catalytic triad are required for effective enzyme inhibition.

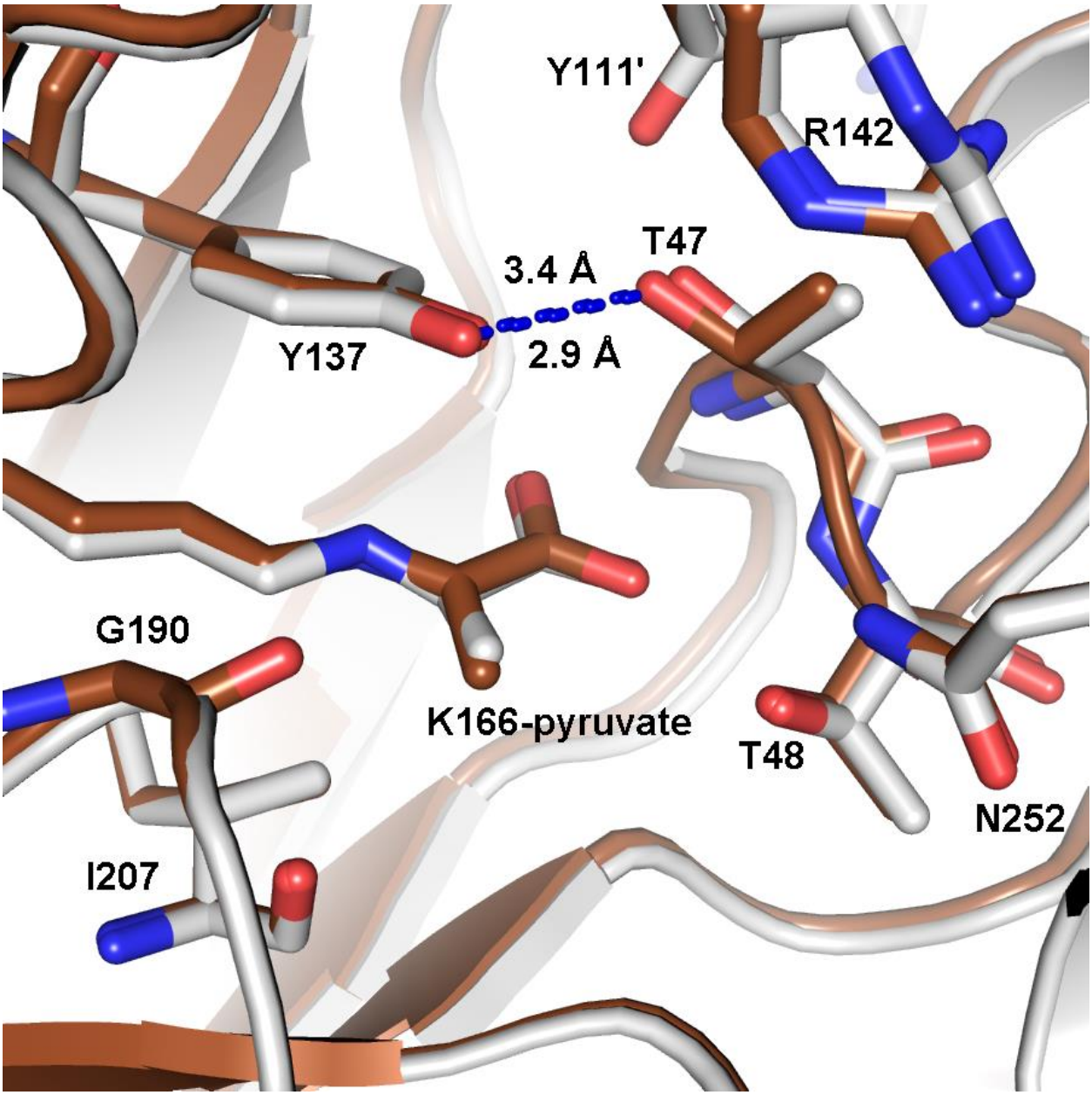

Figure 3.20 – **Allosteric effect at the active site of wt:pyr:thialysine.** This figure depicts wt:pyr:thialysine (brown) super-positioned on wt:pyr (4LY8) shown in whit. The hydrogen bond between Y137/T47 is decreased 3.4 – 2.9 Å when thialysine binds. Which is analogous to the allosteric effect of bislysine; where the hydrogen bond between Y137/T47 is reduced 3.4 – 3.0 Å. In contrast the allosteric effect of L-lysine is to reduce the distance between Y137/Y111': 4.7 – 4.2 Å.

3.5.3 Comparison of WT-DHDPS with L-Lysine and L-Thialysine

As mentioned previously (section 3.5.1), L-thialysine appears to bind to DHDPS in the same manner as L-lysine. Only a handful of structural changes are conserved between binding of L-lysine or L-thialysine; however, in many cases the magnitude of the effect is less. Many of the

structural effects noted for binding of L-lysine to wt-DHDPS are entirely absent in wt:pyr:thialysine. It is for this reason that one might describe the changes observed between wt:pyr (PDB: 4LY8) and wt:pyr:thialysine as incomplete.

The most obvious trend is the effect that L-thialysine has on cavity volumes at the allosteric site and at the active site. Whereas L-lysine induces a 43% reduction in the volume of the allosteric site and a 30% increase in the volume of the active site; the effect of L-thialysine binding is less intense, with a 36% reduction in volume at the allosteric site, and no significant change at the active site (Figure 3.18). This observation supports the previously identified correlation between the strength of an inhibitor and its effect on solvent accessible volume of the active site and allosteric site. Furthermore, at the active site we identify one change which is common to the L-thialysine and L-lysine structures. At the active site, the hydrogen bond between Y137 and T47 is reduced from 3.4 Å to 2.9 Å. As members of the catalytic triad, the Y137-T47 pair is of significant importance to the enzyme's catalytic mechanism.

3.5.4 Discussion

As a weak inhibitor (IC_{50}), L-thialysine provides a necessary contrast to the structural examination of the natural inhibitor L-lysine, and the super inhibitor bislysine. Logically, the role of structural changes induced by both L-thialysine and other stronger inhibitors should be discounted in their contribution to enzyme inhibition. However, if the strength of the binding interaction is the primary reason for weaker inhibition, then it would be reasonable to expect that overwhelming concentrations of a weak inhibitor should activate the same structural mechanism for allosteric inhibition. In essence, the argument is either for mechanical non-activation of allostery, or non-inhibition due to non-binding of the inhibitor.

The inhibitor L-thialysine bears remarkable similarity to the natural inhibitor L-lysine, and is known to inhibit DHDPS at sufficiently high concentrations.[1] Examination of crystal structures in this study reveals that L-thialysine occupies the same binding site and conformation as the natural inhibitor. It should be noted that occupancy of L-thialysine is less than L-lysine, despite using three times the concentration in the crystallization conditions. Structural changes noted between wt:pyr (PDB: 4LY8) and wt:pyr:thialysine (though muted) are common to both wild-type and mutant structures containing L-lysine or bislysine.

The structure of wt-DHDPS:pyr:thialysine suggests that certain structural changes are incompletely stimulated by L-thialysine. Therefore, it would appear that weak inhibition of L-thialysine is attributable to weak binding rather than non-activation of the allosteric mechanism. Weak binding may be attributable to two factors, each related to the inclusion of sulfur at the C-4 position: the length and volume of the side chain due to a larger atomic radius of sulfur, and the pK_a of the terminal amino group which is 9.52 in L-thialysine and 10.53 in L-lysine.[1]

3.6 Crystallization of wt-DHDPS with (S)-ASA

3.6.1 DHDPS with Reduced Schiff Base

Prior to crystallization, DHDPS was incubated with pyruvate followed by sodium cyanoborohydride (BH). Under these conditions, pyruvate will bind to the enzyme forming an sp^2 hybridized Schiff base, and sodium cyanoborohydride will reduce the Schiff base to a dead-end sp^3 hybridized tetrahedral adduct (BH-DHDPS:lac; Scheme 3.1). After treatment with sodium cyanoborohydride the enzyme activity was found to be zero according to the assay methods of Skovpen *et al*. outlined in section 2.2.5.2.3 of the Methods Chapter in this thesis.[1, 2] After dialysis, crystals of the reduced BH-DHDPS:lac crystallized as previously described. Examination of the

F_o-F_c map around K166-pyr in the active site indicates successful sp^3 hybridization, which is further reinforced by a complete absence of enzymatic activity.

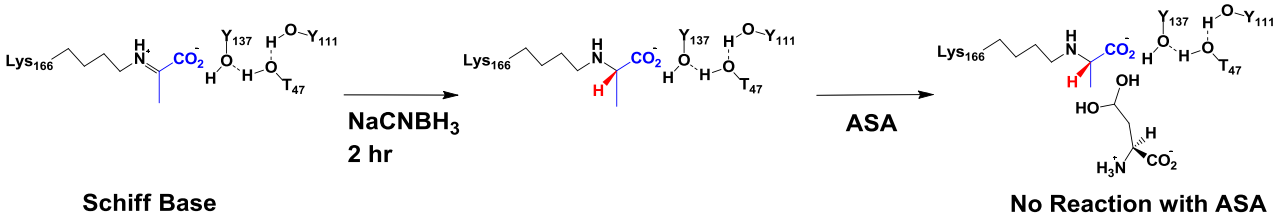

Scheme 3.1 – **Reaction Scheme for the reduction of the K166-pyruvate Schiff Base.** Using sodium cyanoborohydride the DHDPS:pyr Schiff Base is reduced to an sp^3 hybridized dead-end complex BH-DHDPS:lac.

Comparison of the reduced BH-DHDPS:lac with the wt:pyr (PDB: 4LY8) structure reveals a high degree of similarity: 0.195 Cα rmsd. Despite this, we can identify two key structural changes involving the catalytic triad and the solvent accessible volume of active and catalytic sites. At the active site of wt-BH-DHDPS:lac, the solvent accessible volume is reduced 10% relative to the wt:pyr (4LY8); from 20 $Å^3$ to 18 $Å^3$. Interestingly, examination of the catalytic triad reveals changes similar to those observed when L-lysine binds to the allosteric site in wt:pyr:lys (4M19). The hydrogen bond between Y137-T47 is reduced from 3.4 Å to 2.9 Å, and the distance between Y111'-Y137 is reduced from 4.7 Å to 4.1 Å. At the allosteric site, we see a 15% reduction in solvent accessible volume from 417 Å in wt:pyr:lys (4M19), and to 355 Å to BH-wt:pyr.

The observations outlined above present a perplexing contradiction, since no inhibitor is present in the allosteric site. Therefore consideration must be given to what may be cause and effect. Previously we proposed that binding of L-lysine induced the noted structural changes. Alternatively, changes observed may be attributed to stabilization of enzyme dynamics, rather than the nature of the inhibitor. If we consider that reducing the Schiff-base to a dead end complex may result in a stabilizing effect on the enzyme, then we may be artificially inducing similar structural

changes as binding a stabilizing inhibitor. Unfortunately, the reduced form of DHDPS is not catalytically competent, which limits any biochemical insight of the observed structure; therefore, it is not clear if structural changes observed in BH-DHDPS would not result in inhibition if the enzyme were catalytically competent.

3.6.2 DHDPS with Reduced Schiff Base and ASA

The reduced DHDPS:pyr enzyme was co-crystallized in the presence of 100 mM ASA as previously described in this thesis (section 2.2.5.2 and 3.1.6). At the active site the sp^3 hybridized K166-lactate adduct is well-resolved. There is also the addition of a strong, but poorly defined, blob of electron density at the position where ASA might be expected to bind. Due to the amorphous nature of the electron density, it is not clear how ASA should be modeled (Figure 21, panel A).

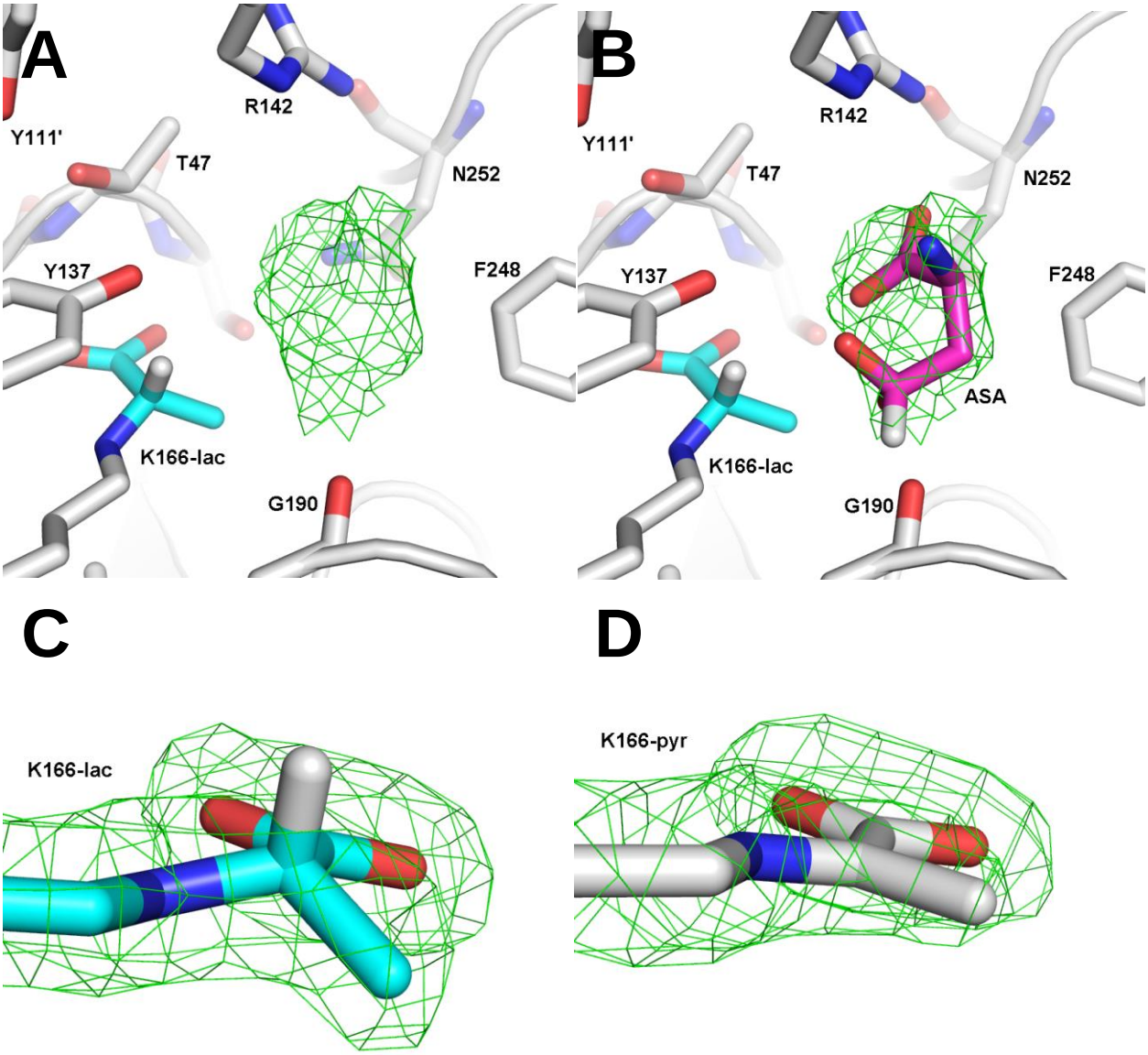

Figure 3.21 – **Preliminary modelling of ASA in the active site using F_o-F_c Map.** Panel A: Amorphous electron density occupying the likely binding location of ASA. F_o-F_c Omit map rendered at 0.5 σ. Panel B: ASA modeled as the hydrate into the amorphous F_o-F_c omitt map at 0.5 σ prior to the use of the FEM algorithm. Panel C: Shows the F_o-F_c omit map for K166-lac scaled at 3 σ. Proton positions are predicted for K166-lac and ASA. For comparison Panel D shows the Fo-Fc map for K166-pyr (pdb: 4LY8) scaled at 3 σ.

3.6.3 Identification of ASA in the Active Site

The density blob in the active site is not attributable to any solvent molecules, or protein residues, and occupies the expected binding site for ASA. When the electron density is scaled

between 0.5 – 0.7 σ it takes on the approximate size and shape of ASA (Figure 21, panel A). We attempted to model ASA into the omit map, but the specific conformation is not obvious (Figure 21, panel B). The Phenix suite of crystallography software includes a program for calculating Feature Enhanced Maps (FEM).[18, 19] The FEM program uses a series of algorithms to enhance the signal-to-noise ratio of the electron density map.[19] The FEM program was run using the original MTZ map, and a fully refined protein model with ASA excluded to limit modeling bias. The output feature-enhanced map is remarkably sharper than the standard omit map (Figure 22, panel A). The amorphous electron density previously assumed to belong to ASA at 0.5 – 0.7 σ is now representative of a single conformation of ASA at 1.0 -1.5 σ (Figure 22, panel B).

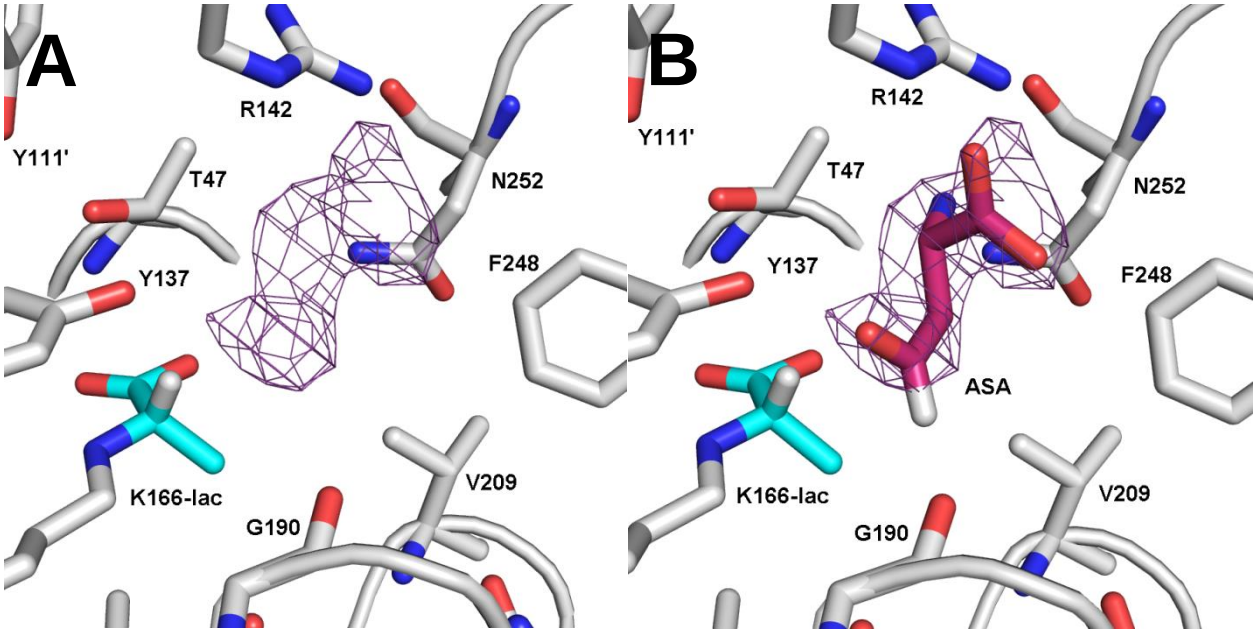

Figure 3.22 – **Modeling ASA at the active site using the FEM algorithm** Panel A: Feature Enhanced Map (FEM) of unidentified electron density in the active site displayed 1.0 σ. The shape of the electron density is less ambiguous than the standard Omit map. Panel B: ASA modeled as the aldehyde into the Feature Enhanced Map. Proton positions are predicted for K166-lac and ASA.

3.6.4 Occupancy and Conformation of ASA

Several attempts were made to co-crystalize DHDPS with ASA at lower concentrations of ASA that did not come to fruition. In order to observe even amorphous ASA electron density it was

necessary to use 100 mM of ASA. Under these conditions ASA occupancy is calculated to be 80% which gives confidence to the model. The amorphous nature of the original F_o-F_c map may be the result of weak transient binding, or an averaging of several contributing conformations.[20] Furthermore, alteration of the enzymes active site by modifying K166-pyr from trigonal planar to tetrahedral may weaken the strength of binding, or provide "looseness" for alternative conformations.

Indeed, the natural catalytic mechanism may be such that the incoming ASA reacts in a Theorell-Chance mechanism, where no stable complex is formed without reaction; therefore, two possibilities exist. The first is that in its natural state, ASA is in a rapid equilibrium between bound and unbound states, where the unbound state is greatly favoured; however, once condensation occurs the reaction is driven downhill to cyclization, forming HTPA. Thus, in the modified enzyme where no reaction is possible, ASA would favour the unbound over the bound state and the result will be lower and/or ambiguous occupancy. The second possibility is that the reductive modification of the enzyme active site has altered the geometry or protein dynamics of the binding site such that ASA no longer has a high affinity.

The reduction of the K166-pyr Schiff base from a trigonal planar to a tetrahedral conformation will of course alter the geometry and/or protein dynamics of the active site. As well, loss of the double bond may have some effect on enzyme-substrate electrostatic interactions. The FEM algorithms are designed to enhance the signal-to-noise ratio in the model of electron density. Should the original amorphous shape of ASA density be the average result of several conformations then the FEM algorithm is expected to extract the dominant conformation.[19] We must remain open-minded that the dominant conformation may not be the requisite reactive conformation. Furthermore, the modifications that have been made to the active site may have

altered the equilibrium of bound ASA conformations (such that a non-reactive conformation has become dominant), or that enzyme modifications have created the environment in which multiple bound conformations are possible.

3.6.6 Comparison of DHDPS with and without ASA

The dead end complex of DHDPS with ASA is the first of its kind, and gives us the opportunity to examine the structure function relationship of ASA in catalysis and inhibition. It has been shown that ASA will reduce the enzyme's affinity for the natural inhibitor L-lysine, and vice-versa.[1, 2] Through an examination of the structure containing ASA we hope to better understand not only catalysis, but also inhibition of the enzyme.

Superficially, there is little difference between the structures of DHDPS with ASA and without ASA. The tetramer and all secondary structures remain intact. Superposition of BH-DHDPS:ASA with wt:pyr reveals a 0.378 Cα rmsd, and no obvious structural rearrangements. As with previous structure examination we leveraged several tools to examine key themes of structural rearrangement.

Using CASTp we measured the solvent accessible volume of the active site and allosteric site. We determined the volume of the allosteric site to be 610 $Å^3$ which represents a 46% increase in volume from the structure of wt:pyr (PDB: 4LY8; 417 $Å^3$), and a 72% increase from the BH-DHDPS (355 $Å^3$; Figure 3.18). This observation reveals an interesting branch to a previously noted trend. In all structures containing an inhibitor at the allosteric site, we noted decreases in allosteric site volume proportional to the strength of inhibition. We know that ASA reduces the enzyme's affinity for L-lysine, and here the crystal structure presents one possible explanation:

binding ASA induces expansion of the allosteric site volume which likely reduces the enzymes affinity for inhibitory molecules.

The solvent accessible volume of the active site was determined using CASTp. Here, the implications of our observations are less clear. In previous structures with various inhibitors there is a trend in active site volume correlated to the strength of inhibition; however, the active site volume of BH-DHDPS:ASA is 60 $Å^3$, which is 200% larger than the active site in wt:pyr (20 $Å^3$; PDB: 4LY8), and 233% larger than the active site of BH-DHDPS (18 $Å^3$).

This observation appears to directly contradict the previously noted trend, implying that a larger active site is necessary for ASA binding rather than a factor of inhibition. Another possibility is that of a dynamic model of induced fit, wherein a small active site is necessary to invite binding after which ASA induces a better fit with a larger active site. Furthermore, one would expect obvious and significant structural rearrangement to accompany such a magnitude of volume increase.

Of all residues within the active site, there are no notable changes relative to the structure of wt:pyr (PDB: 4LY8). However, relative to the structure of BH-DHDPS there are two changes to the geometry of the catalytic triad. The hydrogen bond between Y137-T47 and geometric distance between Y111'-Y137 are lengthened from 2.9 Å to 3.5 Å and 4.1 Å to 4.7 Å respectively. With changes limited to the geometry of the catalytic triad, the most likely explanation for increased volume is that binding of ASA has induced some minor topological anomaly which allows the CASTp algorithm to expand its definition for the active site cavity.

An examination of the weak dimer interface reveals a cross dimer hydrogen bond which is broken upon binding of ASA. In wt:pyr (PDB: 4lY8), D173 forms a hydrogen bond (2.8 Å) with

K245' across the weak dimer interface (Figure 3.23). In the BH-DHDPS:ASA structure, this hydrogen bond has been broken (6.9 Å) and K245' extends away from the enzyme into solvent space. The implications of breaking this hydrogen bond are not obvious. The catalytic mechanism is known to be cooperative throughout the tetramer, and any structural changes at the weak dimer interface may be implicated in the mechanisms of cooperativity. Therefore, K245 and D173 may have some role to play in attenuating the cooperativity observed between allosteric sites.

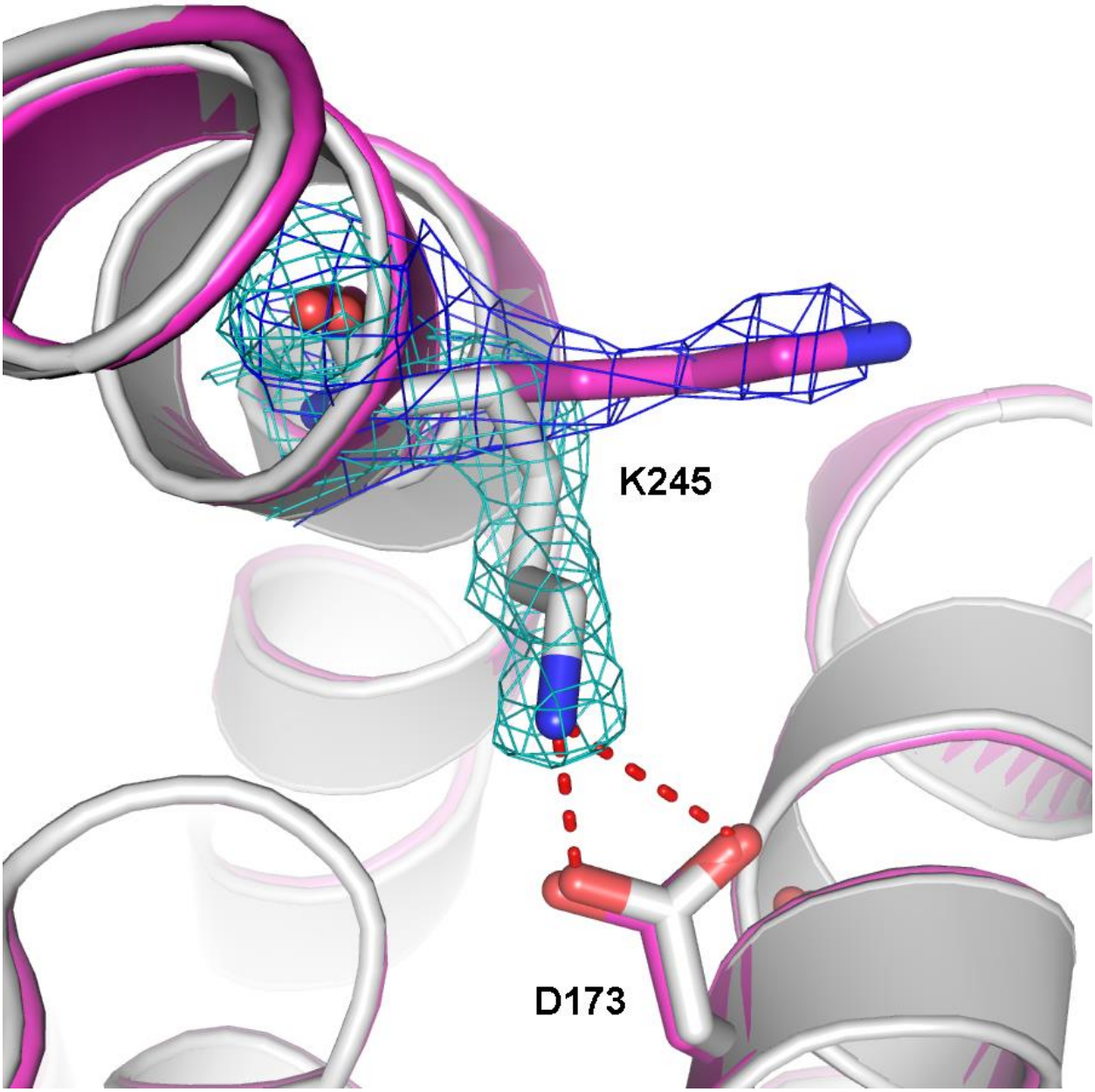

Figure 3.23 – **Disruption of a hydrogen bond at the weak dimer interface of wt-BH-ASA.** This figure depicts wt-BH-ASA in purple which is superimposed on the grey wt:pyr structure. For each structure the $2F_o$-F_c is shown scaled at 1 σ. The hydrogen bond shown in red is disrupted in the wt-BH-ASA structure and may have a role in cross dimer communication.

3.6.7 Comparison of DHDPS with ASA and DHDPS with L-Lysine

Throughout this study there is an emerging trend suggesting opposing structural effects of DHDPS binding L-lysine or ASA. Superposition allows direct structural comparisons between wt:pyr:lys (pdv: 4M19) and BH-DHDPS:ASA, where the contrasting structural details may

provide insight into the biochemical opposition of ASA and the inhibitor L-lysine. When comparing the structure of BH-DHDPS to wt:pyr:lys (4M19) there is almost all of the same Cα and side chain movements at the allosteric site; as in the comparison of wt:pyr (4LY8) with wt:pyr:lys (4M19), with one exception. In wt-DHDPS the hydrogen bond between E88-H56 supports a network of hydrogen bonds, and is speculated to act as a cap on the allosteric site after L-lysine binds (Figure 24). In wt:pyr (4LY8) the length of this hydrogen bond is 3.2 Å, and upon L-lysine binding is reduced to 2.8 Å; however, this hydrogen bond is eliminated (7.2 Å) as H56 flips away from E88 when ASA is bound to the DHDPS active site. The hydrogen bond network which was proposed to cap the allosteric site has been eliminated (Figure 24). Without H56 capping of the allosteric site, the enzyme's affinity for L-lysine may be reduced: this is one possible explanation for ASA reducing the affinity of L-lysine.

Furthermore, the solvent accessible volume of the allosteric site appears to be strongly affected by the binding of ASA. There is an emerging trend wherein the volume of the allosteric site decreases, upon inhibitor binding, proportional to the strength of inhibition. This is perhaps directly related to the tightness of inhibitor binding. Interestingly, in the structure of BH-DHDPS:ASA the volume of the allosteric site is 46% larger than that of wt:pyr (PDB: 4LY8), and a full 155% larger than wt:pyr:lys (4M19). This would appear to offer an explanation for why ASA reduces the enzyme's affinity for L-lysine; although, tracing the exact mechanism for inducing the volume increase is unclear.

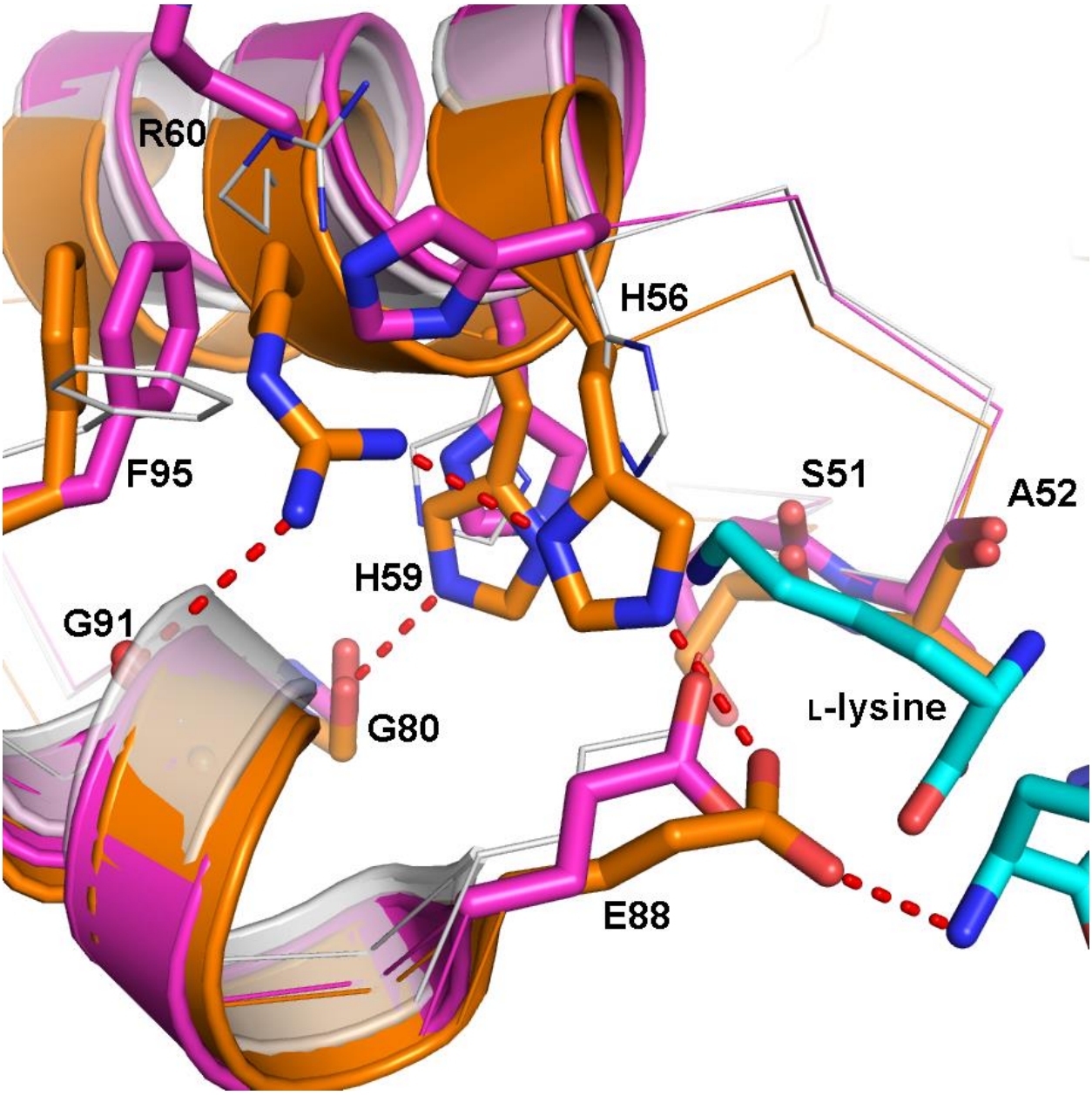

Figure 3.24 – **ASA disrupts Hydrogen Bonds at the allosteric site.** This figure depicts wt:pyr:lys (PDB: 4M19) in orange with L-lysine in blue and wt-BH-ASA is superimposed in purple. A number of hydrogen bonds (shown in red) which are found in wt:pyr:lys (4M19) are completely disrupted in wt-BH-ASA. It appears that ASA creates a number of conformational changes which are very opposite to the conformational changes induced when L-lysine binds. The ghost white wt:pyr (PDB: 4LY8) structure is included as a reference.

For most inhibitors there is an increase in the solvent accessible volume at the active site proportional to the strength of inhibition (Figure 3.18). For instance, the active site of wt:pyr:lys (4M19) is 30% larger than that of wt:pyr (4LY8). The correlation between cavity volumes and

inhibitor strength indicates an increase in active site volume may contribute to inhibition of the enzyme. Surprisingly, there is an even greater increase in active site volume upon binding of ASA to the active site. The active site of BH-DHDPS:ASA is 200% larger than that of wt:pyr (4LY8), and 131% larger than wt:pyr:lys (4M19). Such a dramatic change suggests significant structural rearrangement, however there is little evidence of this, which leads us to believe that minor changes have allowed CASTp an alternative definition of the active site cavity (Figure 25). In particular a subtle difference in the orientation of K113' appears to be strongly correlated to the overflow of the active site identified by CASTp. After manual rearrangement of K113' from wt-BH-ASA to match that of K113' from wt-BH the CASTp definition of the active site cavity returns to that which is typical of other DHDPS crystal structures: with a measured solvent accessible volume of 22 $Å^3$. This manual manipulation is not supported by the observed electron density, leading to the conclusion that K113' may be of some biological importance for the binding of ASA or its condensation with pyruvate.

The active site of BH-DHDPS:ASA is very similar to that of wt:pyr (PDB: 4LY8). It is not surprising then that all of the same minor residue changes are found between BH-DHDPS:ASA and wt:pyr:lys (PDB: 4M19). Small but measurable changes in the distance between pairs of residues are seen for the following pairs: Y137 – T47 (3.5 Å to 2.9 Å), Y137 – Y111' (4.7 Å to 4.2 Å), and C1 of the pyruvyl Schiff base to each of the carbonyls of I207 and G190 (3.6 Å to 4.5 Å, and 4.5 Å to 3.7 Å respectively). Perhaps more interesting is to also consider the structure of BH-DHDPS.

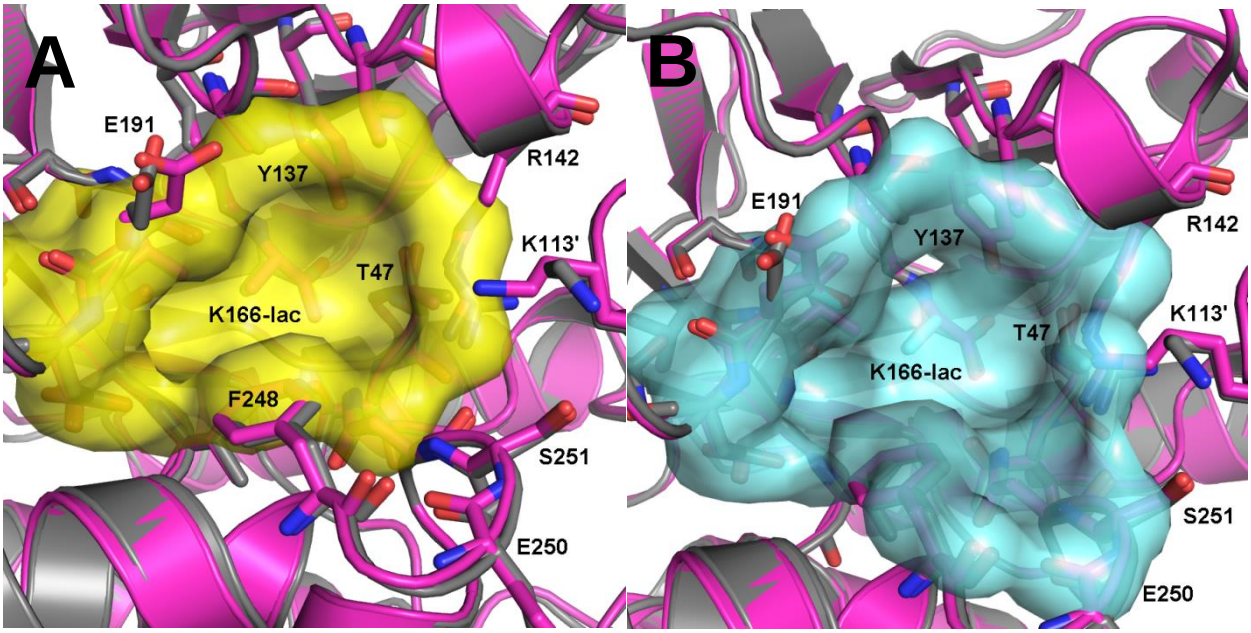

Figure 3.25 – **CASTp defines a different active site when ASA is bound to BH-DHDPS.** This figure depicts a super position of wt-BH-ASA (purple) on wt-BH (grey). Panel A depicts the surface of the active site as defined in wt-BH (surface in yellow, wt-BH in grey). Panel B depicts the surface of the active site as defined in wt-BH-ASA (surface in blue, wt-BH-ASA in purple) the yellow active site surface shown in panel A is typical for all DHDPS crystal structures except wt-BH-ASA. The blue active site surface is only identified in the wt-BH-ASA crystal structure.

As outlined above, the BH-DHDPS structure reveals two changes in hydrogen bonds of the catalytic triad relative to wt:pyr (PDB: 4LY8). The hydrogen bonds between Y137-T47 and between Y111'-T47 each become shorter, however the length of each of these hydrogen bonds is restored upon binding of ASA, matching that of the wt:pyr structure (4LY8). The significance of this observation is unclear.

In the structure of wt:pyr:lys (PDB: 4M19) the largest structural changes relative to wt:pyr (4LY8), occur at the weak dimer interface. These structural changes have been previously discussed in section 3.2.6 wt:pyr:lys (4M19) shows the most variance in this region of any structure. Upon ASA binding there appears to be a single cross-dimer hydrogen bond (2.8 Å) between D173-K245' which is broken (6.9 Å; Figure 23).

3.6.8 Discussion

This study presents the first ever DHDPS crystal structure with ASA bound at the active site, although there are uncertainties which make drawing definitive conclusions challenging. Nevertheless, when this structure is compared to each previous DHDPS structures it provides new insights and possible leads for better understanding catalysis and inhibition in the future.

The initial electron density associated with ASA was amorphous and difficult to interpret. The FEM algorithm proved useful to enhance the signal to noise and identify a single conformation of ASA. The ambiguous F_o-F_c electron density of ASA is most likely attributable to weak or transient binding. The extreme (100 mM) concentration of ASA that was required is further indicative of weak binding.

It is very likely that the tetrahedral geometry of the K166-lactate adduct has a profound effect on the enzymes ability to properly bind ASA. This could be an unfavourable change to the shape, enzyme dynamics or electrostatic profile of the active site. Weak ASA occupancy may also suggest a Theorell-Chance mechanism wherein binding of ASA is inherently unfavourable, but once the reaction is initiated it will proceed downhill to the products. Since no reaction is possible in the BH-DHDPS then binding cannot be driven by subsequent condensation.

Comparing the structure of wt-BH-ASA with other DHDPS structures reveals an interesting relationship relative to previously noted structural trends. In particular the effects that ASA has on the solvent accessible volumes as well as subtle changes to hydrogen bonding at the allosteric site and in the catalytic triad.

Using CASTp to measure cavities has revealed a trend where the volume of the allosteric site of DHDPS is substantially reduced in the presence of inhibitors, and the volume at the active site

is marginally increased. Inspection of the raw measurement for solvent accessible volume suggests that ASA induces a dramatic increase in the volume of both the allosteric site and the active site. A closer visual inspection using the CASTp pymol plugin reveals that the increased volume of the allosteric site in wt-BH-ASA appears to be the result of changing hydrogen bond network involving E88, H56, and R60 (Figure 3.24). These residues define how the allosteric site meets the bulk solvent, and may act as a lid on the allosteric site when L-lysine is bound. These observations may play a significant role in the mechanism through which ASA would reduce the enzymes affinity for L-lysine. These structural changes may explain the relationship between ASA and L-lysine, where L-lysine reduces the enzymes affinity for ASA, but ASA reduces the enzymes affinity for L-lysine.[1, 2]

The effects of ASA at the active site are considerably more perplexing. The trend noted in other DHDPS structures had indicated that changes to the geometry of the catalytic triad coupled with marginal increases in the volume of active site are correlated to binding allosteric inhibitors. Yet, in the structure of wt-BH-ASA we note similar changes to the geometry of the catalytic triad and massive change to the solvent accessible volume (Figure 25). However, close inspection of the structures and the CASTp output reveals an algorithmic explanation for the increase in solvent accessible volume.

It appears that a subtle change in the orientation of K113' has allowed the CASTp algorithm to change its definition of active site cavity. This is confirmed by manually manipulating the conformation of K113' wherein the calculated active site volume and definition of the active site again resembles that of every other DHDPS. However, such manual manipulation is not supported by the observed electron density. Therefore, the altered definition for the active site may not be

an artifact, and would suggest some undetermined biological role of K113' in binding or condensation of ASA.

As with the wt:pyr:lys (PDB: 4M19) structure there are subtle changes at the weak dimer interface. Although the changes noted in wt-BH-ASA are distinct from those noted for wt:pyr:lys (4M19), it is possible that there may be some role in the known cross dimer cooperativty of inhibition. In either case, it is not apparent upon examination of crystal structures what link these residues have to either the allosteric site or the active site.

The conformation determined for ASA in the active site of *Cj*-DHDPS:lac suggests that condensation should produce the (R)-isomer of HTPA. This contradicts previous studies of substrate mimetic molecules with *Ec*-DHDPS which suggest formation of the (S)-isomer of HTPA (Figure 3.26).[21-23]

Although contradictory each interpretation is not without the need for circumstantial consideration. The structure reported with succinate semi-aldehyde is based on the reaction of a substrate mimetic, which may be an imperfect estimation of the preferred stereochemistry of ASA. However, the structure of DHDPS:lac:ASA has a modified enzyme active site which may allow (or favor) a non-reactive conformation. Ultimately, when HTPA is released from the DHDPS active site it will dehydrate in solution to form DHDP regardless of stereochemistry.[4, 24, 25] Therefore stereo-selectivity of HTPA may be inconsequential to the evolved enzymatic function of DHDPS.

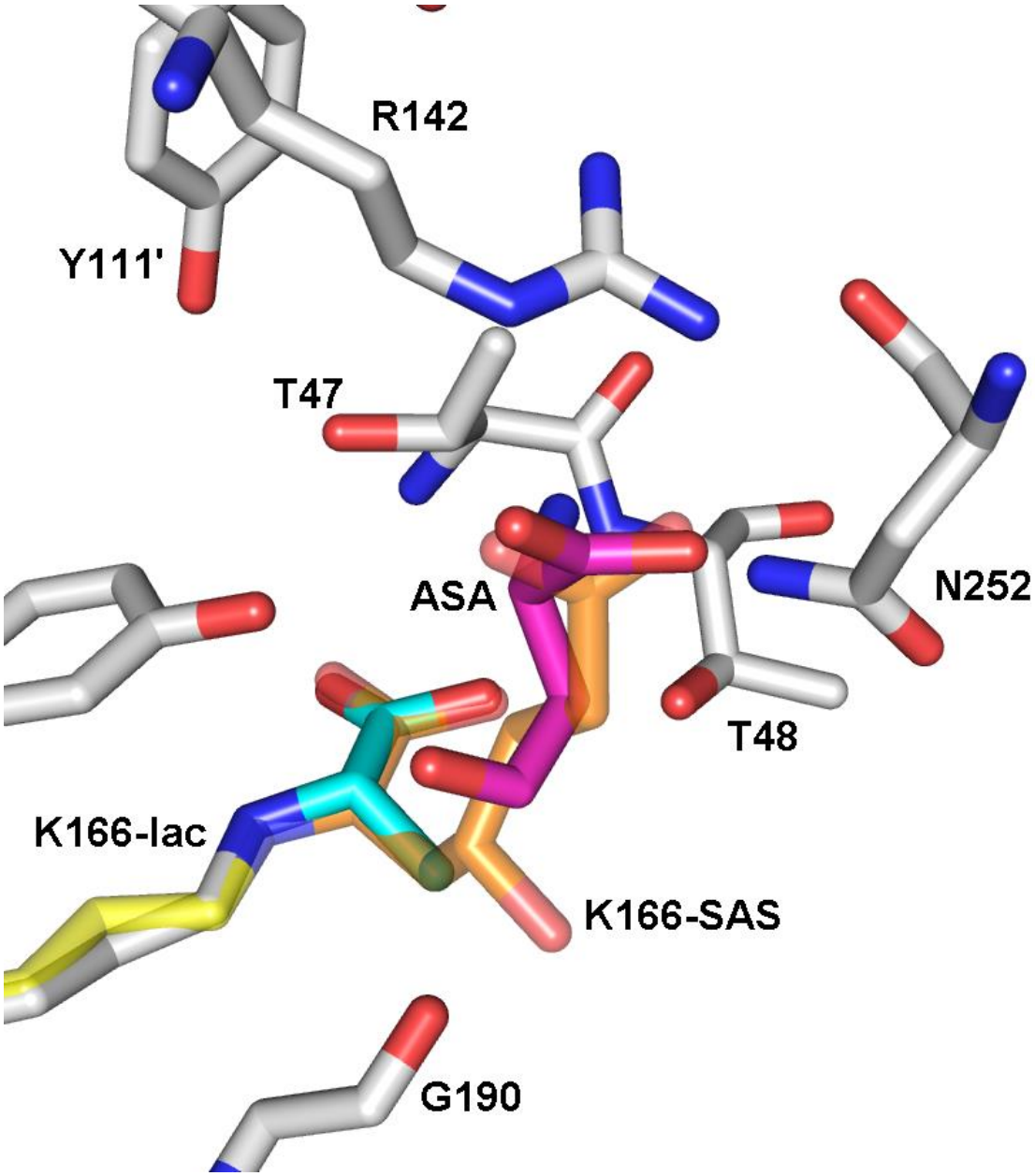

Figure 3.26 – **Superposition of *Cj*-DHDPS:lac:ASA with *Ec*-DHDPS:SAS.** The structure of *Cj*-DHDPS:lac:ASA is white, with ASA in magenta, and indicates that condensation would form R-HTPA. The structure of *Ec*-DDPS:SAS is yellow, with SAS in orange, and demonstrates that condensation with SAS has formed the S-isomer.

3.7 References

[1] Skovpen, Y. (2014) *Novel inhibitors of dihydrodipicolinate synthase*, (Doctor of Philosphy). Retrieved from Department of Chemistry, University of Saskatchewan

[2] Skovpen, Y. V., and Palmer, D. R. J. (2013) Dihydrodipicolinate synthase from *Campylobacter jejuni*: kinetic mechanism of cooperative allosteric inhibition and inhibitor-induced substrate cooperativity, *Biochemistry*, 5454-5462.

[3] Conly, C. J. T., Skovpen, Y. V., Li, S., Palmer, D. R. J., and Sanders, D. A. R. (2014) Tyrosine 110 plays a critical role in regulating the allosteric inhibition of *Campylobacter jejuni* dihydrodipicolinate synthase by lysine, *Biochemistry 53*, 7396-7406.

[4] Dobson, R. C. J., Valegard, K., and Gerrard, J. A. (2004) The crystal structure of three site-directed mutants of *Escherichia coli* dihydrodipicolinate synthase: Further evidence for a catalytic triad, *Journal of Molecular Biology 338*, 329-339.

[5] Devenish, S. R. A., Gerrard, J. A., Jameson, G. B., and Dobson, R. C. J. (2008) The high-resolution structure of dihydrodipicolinate synthase from *Escherichia coli* bound to its first substrate, pyruvate, *Acta Crystallographica F 64*, 1092-1095.

[6] Dobson, R. C. J., Griffin, M. D. W., Devenish, S. R. A., Pearce, F. G., Hutton, C. A., Gerrard, J. A., Jameson, G. B., and Perugini, M. A. (2008) Conserved main-chain peptide distortions: A proposed role for Ile203 in catalysis by dihydrodipicolinate synthase, *Protein Science 17*, 2080-2090.

[7] Kefala, G., Evans, G. L., Griffin, M. D. W., Devenish, S. R. A., Pearce, F. G., Perugini, M. A., Gerrard, J. A., Weiss, M. S., and Dobson, R. C. J. (2008) Crystal structure and kinetic study of dihydrodipicolinate synthase from *Mycobacterium tuberculosis*, *Biochemical Journal 411*, 351-360.

[8] Dobson, R. C. J., Devenish, S. R. A., Turner, L. A., Clifford, V. R., Pearce, F. G., Jameson, G. B., and Gerrard, J. A. (2005) Role of arginine 138 in the catalysis and regulation of *Escherichia coli* dihydrodipicolinate synthase, *Biochemistry 44*, 13007-13013.

[9] Hayward, S., and Berendsen, H. J. C. (1998) Systematic analysis of domain motions in proteins from conformational change: New results on citrate synthase and T4 lysozyme, *Proteins 30*, 144-154.

[10] Hayward, S., and Lee, R. A. (2002) Improvements in the analysis of domain motions in proteins from conformational change: DynDom version 1.50, *Journal of Molecular Graphics & Modeling 21*, 181-183.

[11] Poornam, G. P., Matsumoto, A., Ishida, H., and Hayward, S. (2009) A method for the analysis of domain movements in large biomolecular complexes, *Proteins 76*, 201-212.

[12] Liang, J., Edelsbrunner, H., Fu, P., Sudhakar, P. V., and Subramaniam, S. (1998) Analytical shape computation of macromolecules: I. Molecular area and volume through alpha shape, *Proteins-Structure Function and Genetics 33*, 1-17.

[13] Liang, J., Edelsbrunner, H., Fu, P., Sudhakar, P. V., and Subramaniam, S. (1998) Analytical shape computation of macromolecules: II. Inaccessible cavities in proteins, *Proteins-Structure Function and Genetics 33*, 18-29.

[14] Ho, B. K., and Gruswitz, F. (2008) HOLLOW: generating accurate representations of channel and interior surfaces in molecular structures, *BioMed Central Structural Biology 8*, 49.

[15] Griffin, M. D. W., Dobson, R. C. J., Pearce, F. G., Antonio, L., Whitten, A. E., Liew, C. K., Mackay, J. P., Trewhella, J., Jameson, G. B., Perugini, M. A., and Gerrard, J. A. (2008)

Evolution of quaternary structure in a homotetrameric enzyme, *Journal of Molecular Biology 380*, 691-703.
[16] Dobson, R. C. J., Perugini, M. A., Jameson, G. B., and Gerrard, J. A. (2009) Specificity versus catalytic potency: The role of threonine 44 in *Escherichia coli* dihydrodipicolinate synthase mediated catalysis, *Biochimie 91*, 1036-1044.
[17] Phenix, C. P., and Palmer, D. R. J. (2008) Isothermal titration microcalorimetry reveals the cooperative and noncompetitive nature of inhibition of *Sinorhizobium meliloti* L5-30 dihydrodipicolinate synthase by (S)-lysine, *Biochemistry 47*, 7779-7781.
[18] Adams, P. D., Afonine, P. V., Bunkoczi, G., Chen, V. B., Davis, I. W., Echols, N., Headd, J. J., Hung, L.-W., Kapral, G. J., Grosse-Kunstleve, R. W., McCoy, A. J., Moriarty, N. W., Oeffner, R., Read, R. J., Richardson, D. C., Richardson, J. S., Terwilliger, T. C., and Zwart, P. H. (2010) PHENIX: a comprehensive Python-based system for macromolecular structure solution, *Acta Crystallographica D 66*, 213-221.
[19] Afonine, P. V., Moriarty, N. W., Mustyakimov, M., Sobolev, O. V., Terwilliger, T. C., Turk, D., Urzhumtsev, A., and Adams, P. D. (2015) FEM: feature-enhanced map, *Acta Crystallographica D 71*, 646-666.
[20] Kleywegt, G. J. (2007) Crystallographic refinement of ligand complexes, *Acta Crystallographica D 63*, 94-100.
[21] Dobson, R. C. J., Griffin, M. D. W., Roberts, S. J., and Gerrard, J. A. (2004) Dihydrodipicolinate synthase (DHDPS) from *Escherichia coli* displays partial mixed inhibition with respect to its first substrate, pyruvate, *Biochimie 86*, 311-315.
[22] Blickling, S., Renner, C., Laber, B., Pohlenz, H. D., Holak, T. A., and Huber, R. (1997) Reaction mechanism of *Escherichia coli* dihydrodipicolinate synthase investigated by X-ray crystallography and NMR spectroscopy, *Biochemistry 36*, 24-33.
[23] Boughton, B. A., Hor, L., Gerrard, J. A., and Hutton, C. A. (2012) 1,3-Phenylene bis(ketoacid) derivatives as inhibitors of *Escherichia coli* dihydrodipicolinate synthase, *Bioorganic & Medicinal Chemistry 20*, 2419-2426.
[24] Renwick C. J. Dobson, Michael D. W. Griffin, and, G. B. J., and Gerrard, J. A. (2005) The crystal structures of native and (S)-lysine-bound dihydrodipicolinate synthase from *Escherichia coli* with improved resolution show new features of biological significance, *Acta Crystallographica D D61*, 1116–1124.
[25] Devenish, S. R. A., Blunt, J. W., and Gerrard, J. A. (2010) NMR studies uncover alternate substrates for dihydrodipicolinate synthase and suggest that dihydrodipicolinate reductase is also a dehydratase, *Journal of Medicinal Chemistry 53*, 4808-4812.

Chapter 4 Conclusions

4.1 Conclusions

This study presents the high resolution crystal structures of wild type and Y110F *Cj*-DHDPS with various substrates and inhibitors. From a global perspective all structures are highly similar with little in the way of gross structural changes. As a body of work these structures begin to reveal the subtle structural changes required for enzymatic inhibition. At the outset of this work Y110 was emerging as a potential trigger point for inhibition of DHDPS. However crystallographic and kinetic data[1] of DHDPS with bislysine demonstrate that Y110F cannot be solely responsible for the mechanism of allostery. Furthermore inhibition of Y110F with bislysine indicates that Y110 is not necessary for inhibition of DHDPS.

There are at least three explanations for inhibition of Y110F-DHDPS by bislysine but not by L-lysine. 1) L-lysine and bislysine each inhibit DHDPS according to the same mechanism and the enhanced inhibition of bislysine is solely due to the enhanced binding affinity of bislysine. If this is the case then Y110F should have nothing to do with signal transduction and only contribute to binding affinity. 2) Bislysine inhibits DHDPS according to a completely different mechanism than L-lysine. This has not been reflected in available inhibition studies.[1] Furthermore, the structural similarities between L-lysine and bislysine suggest that the mechanism of inhibition would be very similar. 3) Inhibition of DHDPS is the sum of a number of contributing structural factors, each with variable importance. Bislysine is perhaps changing the significance away from Y110 and onto some other mechanism which is present to a lesser extent during inhibition by L-lysine. The evaluation of the above hypothesis should be the subject of future works.

Crystallographic results indicate inhibition of DHDPS appears to be due to a combination of changes to the geometry of the catalytic triad and changes in the solvent accessible volume of the active site. In general changes at the active site are restricted to the hydrogen bond lengths between members of the catalytic triad (T47, Y111', Y137), and typically 0.4-0.6 Å. The specific change at the catalytic triad is different in wild-type and Y110F, and when L-lysine or bislysine is bound. Changes to the length of hydrogen bonds between members of the catalytic triad is likely to affect the pK_a of Y137 and thus its ability to donate and accept protons during the condensation step of the enzymatic mechanism.[2] Although the means by which the inhibitor attenuates the geometry of the catalytic triad is not clear.

A trend emerged where solvent accessible volume of the active site is correlated to the strength of the inhibitor, and the volume of the allosteric site is inversely correlated to the strength of inhibitor. Increases to the volume of the active site are likely to affect the binding affinity of ASA. Furthermore, the presence of ASA in the active site appears to have the opposite effect on solvent accessible volumes: at least at the allosteric site. These changes to the solvent accessible volume at the allosteric site offer a potential explanation for the reduced binding affinity of lysine in the presence of ASA.

At the active site the solvent accessible volume is dramatically increased when ASA is bound to *Cj*-DHDPS. The majority of this change in volume is attributable to a small movement in the side chain of K113'. It is unclear if this has biological significance or if this movement is an anomaly of crystallization conditions. Although for a residue that crosses the dimer-dimer interface K113' is potentially interesting from an enzyme cooperativity perspective.

Binding of lysine induces domain movement in the wild-type enzyme not previously observed, suggesting that the hydrogen bond network created by the inhibitor molecules between subunits tethers the domain in place, preventing relaxation to a catalytically active conformation. This concerted domain movement seems to have relatively little effect on the observed positions of the active-site residues relative to the lysine-free structure. The Domain movements do not appear to be essential to the inhibition of DHDPS but likely play some peripheral role related to dimer-dimer communication or governing protein dynamics. The moving domains of individual monomers meet at the weak dimer interface, and a rearrangement of cross-monomer interactions takes place.

We have identified several residues at the weak dimer interface which may be involved in cross dimer communication. Several of these residues where identified when lysine binds to wt-DHDPS:pyr where cross monomer communication may be the result of domain movements: I172, D173, V176, I 194, Y196, S200, N201, K234, D238, Y241, N242. Furthermore, the super position of DHDPS:lac:ASA with DHDPS:pyr reveals two more residues at the weak dimer interface which are rearranged upon ASA binding: K245 and D173. Each of the aforementioned residues, in particular D173 which is common to both cases, may play some role in the cooperativity observed for inhibition by L-lysine in *Cj*-DHDPS.[1, 3] These residues are not implicated in any Y110F structure, however inhibitor cooperativity was not determined for the Y110F-DHDPS.[1] Bislysine does exhibit cooperative inhibition of wild-type *Cj*-DHDPS, however there are no changes to the weak dimer interface when comparing the structures of DHDPS:pyr:bislysine vs DHDPS:pyr. Therefore the potential role of these residues cannot be considered a certainty and should constitute a portion of future works. None of these residues have been implicated in prior studies examining the tetramerization of DHDPS.[4]

The series of crystal structures presented here, and in particular the structure of wt-DHDPS:pyr:thialysine, suggests that certain structural changes may be incompletely stimulated by weaker inhibitors. Therefore, it would appear that weaker inhibition is attributable to weaker binding rather than non-activation of the allosteric mechanism. DHDPS may be moving between two conformational states, an uninhibited catalytically competent state and a maximally inhibited state. Protein dynamics may play a significant role in the inhibition of DHDPS for which we have not yet been able to study.

4.2 References

[1] Skovpen, Y. (2014) *Novel inhibitors of dihydrodipicolinate synthase*, (Doctor of Philosphy). Retrieved from Department of Chemistry, University of Saskatchewan

[2] Harris, T. K., and Turner, G. J. (2002) Structural basis of perturbed pKa values of catalytic groups in enzyme active sites, *International Union of Biochemistry and Molecular Biology - Life 53*, 85-98.

[3] Skovpen, Y. V., and Palmer, D. R. J. (2013) Dihydrodipicolinate synthase from *Campylobacter jejuni*: kinetic mechanism of cooperative allosteric inhibition and inhibitor-induced substrate cooperativity, *Biochemistry*, 5454-5462.

[4] Griffin, M. D., Dobson, R. C., Gerrard, J. A., and Perugini, M. A. (2010) Exploring the dihydrodipicolinate synthase tetramer: how resilient is the dimer-dimer interface?, *Archives of Biochemistry & Biophysics 494*, 58-63.

Chapter 5 Future Work

5.1 Deconvolution of mechanisms contributing to inhibition of *Cj*-DHDPS

Increasingly the inhibition of DHDPS does not appear to be the result of any single chemical or structural change. Rather, successful inhibition is more likely the weighted aggregate result that all small changes will contribute to inhibition. Future work should focus on identifying which structural features are most important to catalysis and inhibition. The real challenge will lie in determining which of these mechanisms can be exploited when designing inhibitors, and also will be robust in the face of natural selection. Moreover, as suggested by bislysine, each new inhibitor may slightly change the importance of any one piece of the inhibition puzzle.

5.1.1 What role does protein dynamics play in inhibition of *Cj*-DHDPS

Protein dynamics is often discussed, as a catch all descriptor, to explain the sum of minor structural changes that contribute to enzyme function. However, protein dynamics should also be considered independently as one of many small changes contributing to the enzymes function, or dysfunction. Research studies on DHDPS from other sources have suggested that protein dynamics may be an important aspect of catalysis.[1-4] Protein dynamics may be modified by, or contribute to, the structural effects noted when various substrates and inhibitors bind to *Cj*-DHDPS. Protein dynamics for *Cj*-DHDPS in the context of effects observed at the catalytic triad, the role of dynamic domains, changes to cavity volumes, cross dimer communication, and as an independent structural phenomenon are currently being studied using Hydrogen Deuterium Exchange Mass Spectrometry (HDX-MS) in collaboration with Konerman *et al.* at The University of Western Ontario and may enhance the understanding of the known crystal structures.[5]

5.2 Mutagenesis to confirm the link between cooperativity and select residues at the weak dimer interface

Past research has focused on examining the structural integrity of the weak dimer interface; often with the goal of producing stable dimeric DHDPS. In these studies, residues where selected for mutation based on their potential to destabilize the dimer-dimer association. However, to examine the channels for cross-dimer cooperativity the weak dimer interface must remain intact while only highly suspect residues are selected for mutation. The crystal structures of DHDPS:pyr:lys and DHDPS:lac:ASA each present residues at the weak dimer interface which may play a role in cross dimer cooperativity rather than dimer-dimer stability. Candidate residues for mutation studies include: I172, D173, V176, H181, I194, Y196, S200, N201, K234, D238, Y241, N242, and K245. Interestingly none of these residues have been previously examined in studies of dimer-dimer stability.

5.3 Mutagenesis to confirm the role of K113' in either catalysis or inhibition of *Cj*-DHDPS

Examination of the structure of DHDPS:lac:ASA lead to the serendipitous identification of K113' as potentially involved in normal functions of DHDPS. When ASA is bound to the active site the side chain of K113' shifts slightly to change the shape of the active site mouth. Although this movement may be anomalous it is worth exploring the role of K113' for two reasons. First, the small movement of K113' when ASA is bound to the enzymes active site is supported by clear electron density. Second, similar to Y111', K113' crosses the tight dimer interface to join the active site of the opposite monomer; therefore, K113' may have evolved for a specific role in catalysis or structural integrity of the active site.

5.4 Confirmation of the stereochemistry of HTPA produced by *Cj*-DHDPS

The crystal structure of *Cj*-DHDPS:lac:ASA indicates that ASA binds in a conformation that would produce the (S)-isomer of HTPA. However, studies of *Ec*-DHDPS have given evidence to indicate that the product of DHDPS is (R)-HTPA. [6-8] More evidence is needed to confirm the stereochemistry of HTPA produced by *Cj*-DHDPS. It is possible for either the 'R' or the 'S' isomer of HTPA to dehydrate forming DHDP. Therefore, it may be possible that *Cj*-DHDPS and *Ec*-DHDPS actually produce opposite isomers of HTPA. However, the methods used to obtain crystal structures of *Cj*-DHDPS:lac:ASA may have induced an artifactual conformation of ASA within the modified active site. Additional evidence may be obtained from NMR studies of the product produced by *Cj*-DHDPS, or to improve the crystallographic methods.

5.5 Confirmation of ASA crystal structure with an alternative dead-end complex

The structure of DHDPS:lac:ASA was dependent upon formation of a dead end complex, to prevent condensation with ASA. This was accomplished by reducing the active site K166-pyr Schiff base to form K166-lac. However, the K166-lac has a tetrahedral geometry, as opposed to the trigonal planar geometry of K166-pyr. This change may be enough to alter the preferred binding conformation of ASA.

Another method for dead-end inhibition of DHDPS was described by Karsten *et al.*[9] using β-fluoropyruvate; although, another report indicates that β-fluoropyruvate is not an inhibitor.[10] Karsten *et al.*[9] used this strategy for kinetic studies of *E. coli* DHDPS to determine binding order of substrates. At pH 8.0, β-fluoropyruvate is a competitive inhibitor with respect to pyruvate, and a noncompetitive inhibitor with respect to ASA.[9] Other fluorinated pyruvate derivatives may behave similarly such as 3,3-Difluoro-2-oxopropanoic acid, and 3,3,3-Trifluoro-2-oxopropanoic acid; but, these have not been studied. β-fluoropyruvate binds to *Ec*-DHDPS with a K_i

which is similar to the K_m of pyruvate,[9] therefore it may remain covalently bound throughout the crystallization process as seen with pyruvate.[11] Once covalently bound to the active site K166, the subsequent K166-βfp would be expected to retain a trigonal planar geometry (Scheme 5.1). Subsequent crystallization and diffraction with ASA would be able to confirm or refute the observations we have made with DHDPS:lac:ASA.

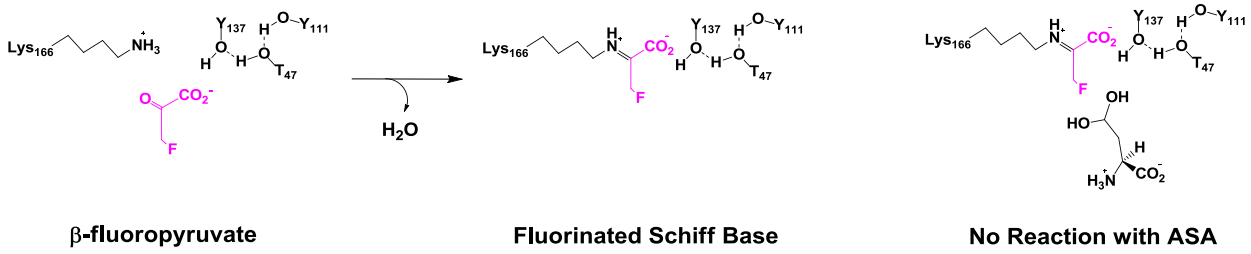

Scheme 5.1 – **Proposed irreversible inhibition of DHDPS by β-fluoropyruvate.** The trigonal plannar geometry is expected to be retained during dead-end inhibition with β-fluoropyruvate. It may be possible to crystalize DHDPS:βfp with ASA. This strategy may confirm the binding conformation of ASA in a DHDPS active site with the natural confirmation of the Schiff base.

5.6 Further development of synthetic inhibitors.

The synthetic inhibitor R,R-bislysine was designed to mimic the symmetrical binding of two L-lysine molecules. Exceptional inhibition of DHDPS by R,R-bislysine can be largely attributed to an anticipated decrease in binding entropy. In other words, R,R-bislysine binds tighter than L-lysine, but does not significantly alter the structural changes to the enzyme that contribute to inhibition. To enhance allosteric inhibition further it would be necessary for an inhibitor to either bind tighter or to target specific structural changes which have been correlated to inhibition: or both.

The bivalent inhibitor design comes with entropy advantages and will likely provide a successful skeleton for the foundation of future functionalization. Three avenues to explore include: the nature of the 2 carbon linker, the terminal amino group, and the carboxyl groups.

Design of a new spacer, instead of the 2 carbon bridge, may include double bonds or ring structures to add rigidity, or perhaps inclusion of additional hydroxyl or amine groups to provide additional interactions with the enzyme. In wt-DHDPS Y110 makes hydrogen bond to the carboxyl of L-lysine, or bislysine. However, studies of Y110F-DHDPS have demonstrated that the hydroxyl of Y110 is not mandatory for inhibition. Therefore it may be able to modify the carboxyl group to favor tighter binding or increased structural perturbation. Finally interactions between H56, H59 and the terminal amino group of the inhibitor are important for inhibition; although the underlying reason is not clear. It may be possible to modify the carbon chain or terminal group by adding bulk or modifying the ionic characteristic, each of which may result in tighter binding or increased structural perturbation.

5.7 Allosteric inhibition of L-lysine-Insensitive DHDPS.

DHDPS from gram positive bacteria, such as *S. aureus*, are inherently insensitive to L-lysine inhibition.[12-14] Although the overall structure is similar to other DHDPS certain modified residues at the tight dimer cleft prevent the binding of L-lysine and its mimics. Residues equivalent to H56, H59 and E88 in *Cj*-DHDPS are often substituted for Lys (or Arg) in DHDPS from gram positive bacteria (Figure 5.1).[12-16] Although the tertiary and secondary structures necessary for an allosteric site are intact, the increased density of positive charge prevents allosteric inhibition by L-lysine.

However, inhibition of *Cj*-Y110F-DHDPS by bislysine has demonstrated that single point mutations cannot eliminate the potential for DHDPS to be allosterically inhibited.[17] Therefore, it is likely possible to design synthetic inhibitors which will successfully bind to the latent allosteric site of gram positive DHDPS and successfully inhibit enzymatic activity. A symmetrical molecule having the same 2,5-diamino adipic acid scaffold as R,R-bislysine will serve as a good starting

point. The symmetric scaffold could then be functionalized with shorter tail and polar, non-positive functional groups.

Mutagenesis studies could be conducted on DHDPS from gram positive bacteria to introduce allosteric L-lysine inhibition as a proof of concept. Each combination of Lys/Arg in the latent allosteric site would be systematically mutated to match the equivalent residue in *Cj*-DHDPS. If allosteric inhibition can be introduced it would enforce the idea that an inspired synthetic molecule could be developed to inhibit the wild type gram positive DHDPS.

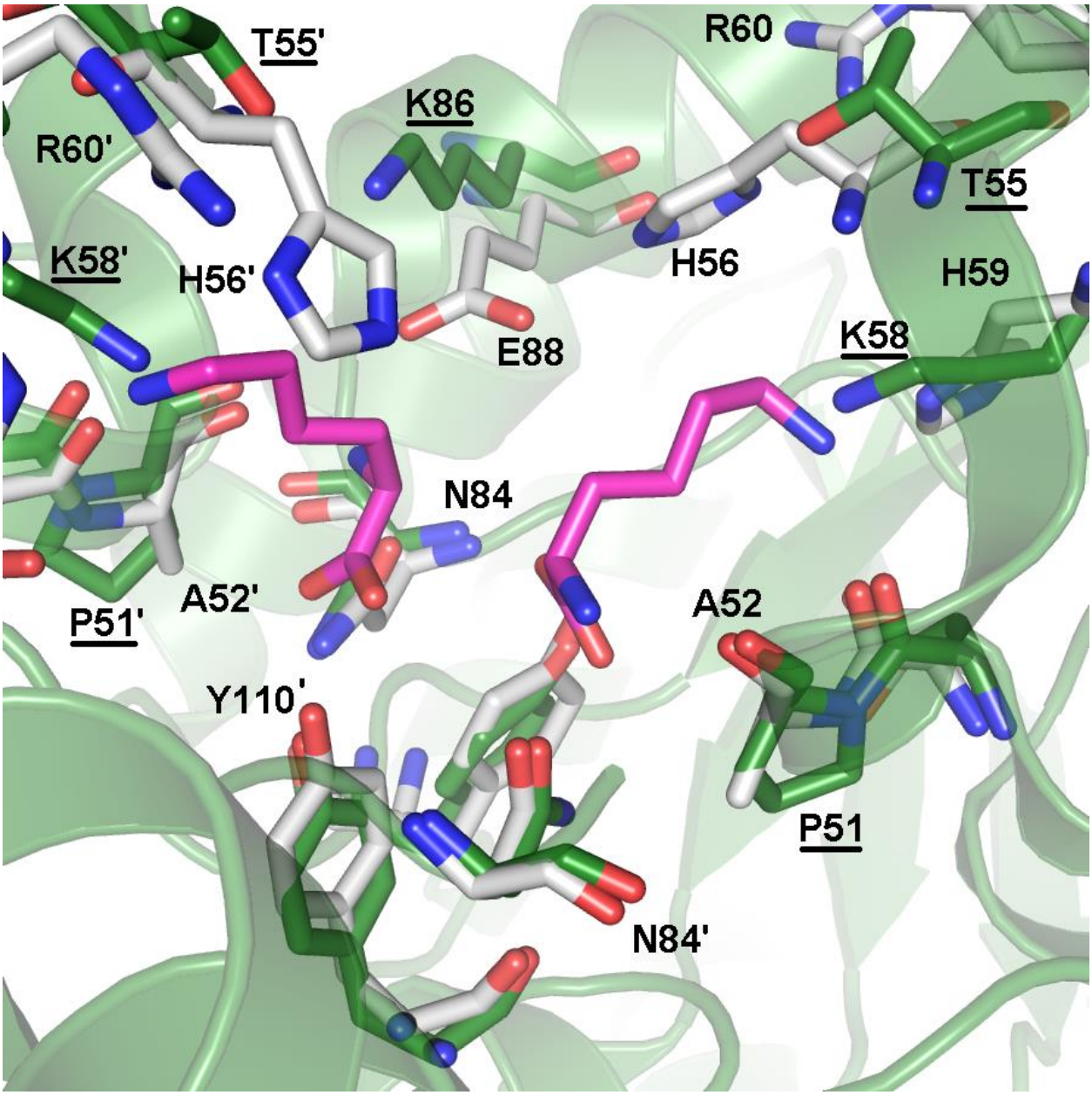

Figure 5.1 – **Super Position of *Cj*-DHDPS:pyr:lys (4M19) and *Sa*-DHDPS:pyr (3DI1).** Structural alignment depicting the differences at the allosteric site of *Cj*-DHDPS:pyr:lys (white), and *Sa*-DHDPS:pyr (green). The inhibitor L-lysine is shown in purple. Residue labels belonging to *Sa*-DHDPS are underlined.

5.6 References

[1] Griffin, M. D. W., Dobson, R. C. J., Pearce, F. G., Antonio, L., Whitten, A. E., Liew, C. K., Mackay, J. P., Trewhella, J., Jameson, G. B., Perugini, M. A., and Gerrard, J. A. (2008) Evolution of quaternary structure in a homotetrameric enzyme, *Journal of Molecular Biology 380*, 691-703.

[2] Griffin, M. D., Dobson, R. C., Gerrard, J. A., and Perugini, M. A. (2010) Exploring the dihydrodipicolinate synthase tetramer: how resilient is the dimer-dimer interface?, *Archives of Biochemistry & Biophysics 494*, 58-63.

[3] Voss, J. E., Scally, S. W., Taylor, N. L., Atkinson, S. C., Griffin, M. D. W., Hutton, C. A., Parker, M. W., Alderton, M. R., Gerrard, J. A., Dobson, R. C. J., Dogovski, C., and Perugini, M. A. (2010) Substrate-mediated stabilization of a tetrameric drug target reveals achilles heel in anthrax, *Journal of Biological Chemistry 285*, 5188-5195.

[4] Atkinson, S., Dogovski, C., Downton, M., Czabotar, P., Dobson, R. J., Gerrard, J., Wagner, J., and Perugini, M. (2013) Structural, kinetic and computational investigation of *Vitis vinifera* DHDPS reveals new insight into the mechanism of lysine-mediated allosteric inhibition, *Plant Molecular Biology 81*, 431-446.

[5] Konermann, L., Vahidi, S., and Sowole, M. A. (2014) Mass spectrometry methods for studying structure and dynamics of biological macromolecules, *Analytical Chemistry 86*, 213-232.

[6] Dobson, R. C. J., Griffin, M. D. W., Roberts, S. J., and Gerrard, J. A. (2004) Dihydrodipicolinate synthase (DHDPS) from *Escherichia coli* displays partial mixed inhibition with respect to its first substrate, pyruvate, *Biochimie 86*, 311-315.

[7] Blickling, S., Renner, C., Laber, B., Pohlenz, H. D., Holak, T. A., and Huber, R. (1997) Reaction mechanism of *Escherichia coli* dihydrodipicolinate synthase investigated by X-ray crystallography and NMR spectroscopy, *Biochemistry 36*, 24-33.

[8] Boughton, B. A., Hor, L., Gerrard, J. A., and Hutton, C. A. (2012) 1,3-Phenylene bis(ketoacid) derivatives as inhibitors of *Escherichia coli* dihydrodipicolinate synthase, *Bioorganic & Medicinal Chemistry 20*, 2419-2426.

[9] Karsten, W. E. (1997) Dihydrodipicolinate synthase from *Escherichia coli*: pH dependent changes in the kinetic mechanism and kinetic mechanism of allosteric inhibition by L-lysine, *Biochemistry 36*, 1730-1739.

[10] Laber, B., Gomisruth, F. X., Romao, M. J., and Huber, R. (1992) *Escherichia coli* dihydrodipicolinate synthase - identification of the active-site and crystallization, *Biochemical Journal 288*, 691-695.

[11] Conly, C. J. T., Skovpen, Y. V., Li, S., Palmer, D. R. J., and Sanders, D. A. R. (2014) Tyrosine 110 plays a critical role in regulating the allosteric inhibition of *Campylobacter jejuni* dihydrodipicolinate synthase by lysine, *Biochemistry 53*, 7396-7406.

[12] Burgess, B. R., Dobson, R. C. J., Dogovski, C., Jameson, G. B., Parker, M. W., and Perugini, M. A. (2008) Purification, crystallization and preliminary X-ray diffraction studies to near-atomic resolution of dihydrodipicolinate synthase from methicillin-resistant *Staphylococcus aureus*, *Acta Crystallographica F 64*, 659-661.

[13] Burgess, B. R., Dobson, R. C. J., Bailey, M. F., Atkinson, S. C., Griffin, M. D. W., Jameson, G. B., Parker, M. W., Gerrard, J. A., and Perugini, M. A. (2008) Structure and evolution of a novel dimeric enzyme from a clinically important bacterial pathogen, *Journal of Biological Chemistry 283*, 27598-27603.

[14] Girish, T. S., Sharma, E., and Gopal, B. (2008) Structural and functional characterization of *Staphylococcus aureus* dihydrodipicolinate synthase, *Federation of European Biochemical Societies Letters 582*, 2923-2930.
[15] Domigan, L. J., Scally, S. W., Fogg, M. J., Hutton, C. A., Perugini, M. A., Dobson, R. C. J., Muscroft-Taylor, A. C., Gerrard, J. A., and Devenish, S. R. A. (2009) Characterisation of dihydrodipicolinate synthase (DHDPS) from *Bacillus anthracis*, *Biochimica et Biophysica Acta - Proteins and Proteomics 1794*, 1510-1516.
[16] Rice, E. A., Bannon, G. A., Glenn, K. C., Jeong, S. S., Sturman, E. J., and Rydel, T. J. (2008) Characterization and crystal structure of lysine insensitive *Corynebacterium glutamicum* dihydrodipicolinate synthase (cDHDPS) protein, *Archives of Biochemistry and Biophysics 480*, 111-121.
[17] Skovpen, Y. (2014) *Novel inhibitors of dihydrodipicolinate synthase*, (Doctor of Philosphy). Retrieved from Department of Chemistry, University of Saskatchewan

APPENDIX A

Table A.1 – **Pertinent Data Collection Statistics of each structure presented in this thesis.**

Crystal	**apo:DHDPS (4R53)**	**wt:pyruvate (4LY8)**	**wt:pyr:lys (4M19)**	**Y110F:pyr (4MLJ)**	**Y110F:pyr:lys (4MLR)**	**Wt:pyr:thialysine**	**Wt:pyr:bislysine (4RT8)**	**Y110F:bislysine (4RT9)**	**BH-DHDPS:lac**	**BH-DHDPS:lac:ASA**
Growth conditions	0.2 M sodium acetate, 20% PEG4000, 0.1M TRIS, pH 8.5	0.25 M sodium acetate, 18% PEG4000, 0.1M TRIS, pH 8.5	0.25 M sodium acetate, 20% PEG4000, 0.1M TRIS, pH 8.5	0.2 M sodium acetate, 18% PEG4000, 0.1M TRIS, pH 8.5	0.15 M sodium acetate, 17% PEG4000, 0.1M TRIS, pH 8.5	0.2 M sodium acetate, 20% PEG4000, 0.2 M TRIS, pH 8.5	0.2 M sodium acetate, 16% P4000, 0.1 mM Tris pH 8.5	0.28 M sodium Acetate, 30% PEG 4000, 0.1 M TRIS pH 8.5	0.2 M sodium acetate, 15% PEG4000, 0.1 mM TRIS, pH 8.5	0.16 M di-ammonium Tartarate, 12% PEG3350, pH 8.5
Temperature (K)	100	100	100	100	100	100	100	100	100	100
X-ray source	CLS (08BM-01)	CLS (08ID-01)	CLS (08B1-1)	CLS (08ID-01)	CLS (08ID-01)	CLS (08ID-01)	CLS (08ID-01)	CLS (08ID-01)	CLS (08ID-01)	CLS (08B1-1)
Wavelength (Å)	0.97952	0.9796	0.9798	0.9798	0.9795	0.9795	0.9798	0.9795	0.9798	1.0332
Distance (mm)	250.00	239.993	289.995	250.00	239.936	260.289	239.019	280.123	228.127	279.38
Space group	$P2_1$	$P2_12_12_1$	$P2_1$	$P2_12_12_1$	$P2_1$	$P2_1$	$P2_12_12_1$	$P2_12_12_1$	$P2_12_12_1$	$P2_12_12_1$
Unit cell parameters (Å)	77.2, 97.6, 82.4 90, 104.47, 90	81.3, 101.4, 148.0 90, 90, 90	78.6, 97.0, 79.6 90, 111.5, 90	81.1, 97.9, 149.7 90, 90, 90	91.0, 97.6, 131.4 90, 92.1, 90	91.3, 97.35, 132.15 90, 92.1, 90	81.27, 96.95, 146.97 90, 90, 90	79.59, 96.78, 145.98 90, 90, 90	78.67, 103.36, 135.95 90, 90, 90	86.50, 110.79, 140.12 90, 90, 90
Resolution range	46-2.0 (2.07-2.0)	43.01-1.60 (1.66-1.60)	50 – 2.0 (2.05 -2.0)	41-2.10 (2.17-2.10)	43.45-2.20 (2.28-2.20)	47.52 – 1.90 (1.97 – 1.90)	48.48 – 2.20 (2.79 – 2.20)	48.39 – 2.35 (2.43 – 2.35)	48.31 – 1.93 (1.99 – 1.93)	43.45 – 2.37 (2.46 – 2.37)
Measured reflections	324248	886712	280550	251823	485813	725968	444885	392031	695113	595175
Unique reflections	77665	158522	73356	63293	116487	178323	59651	47688	83957	54596
R_{sym} (%)	17.8 (117.7)	14.0 (54.1)	8.1(51.2)	19.2 (60.8)	16.8 (78.4)	11.82 (66.40)	16.73 (78.1)	16.73 (95.2)	14.00 (83.50)	10.1 (69.6)
R_{merg} (%)	25.3 (116.0)	12.9 (44.0)	12.99(56.9)	16.8 (52.6)	14.7 (68.6)	10.27 (61.38)	15.57 (72.87)	15.67 (89.6)	13.12 (74.58)	9.4 (65.0)
Completeness (%)	99.9 (99.9)	98.3 (89.1)	97.6(80.8)	90.16 (93.15)	99.9 (100)	98.07 (92.78)	100 (100)	99.98 (99.4)	100 (100)	98.56 (96.81)
Mean I/σ (I)	7.95 (1.64)	5.8 (1.5)	17.61(3.21)	7.16 (2.18)	4.5 (1.4)	10.73 (2.55)	11.79 (3.45)	11.71 (3.53)	12.83 (3.06)	10.26 (1.82)
Matthews coef. ($Å^3$/Da)	2.15	2.24	2.07	2.18	2.14	2.16	2.13	2.07	2.03	2.47
Solvent content (%)	42.87	45.15	40.65	43.7	42.66	43.03	42.25	40.53	39.51	50.27
# Molecules in ASU	4	4	4	4	8	8	4	4	4	4

Table A.2 – **Final Refinement Statistics of each structure presented in this Thesis**

Crystal	**apo:DHDPS (4R53)**	**wt:pyruvate (4LY8)**	**wt:pyr:lys (4M19)**	**Y110F:pyr (4MLJ)**	**Y110F:pyr:lys (4MLR)**	**Wt:pyr:thialysine**	**Wt:pyr:bislysine (4RT8)**	**Y110F:bislysine (4RT9)**	**BH-DHDPS:lac**	**BH-DHDPS:lac:ASA**
Resolution range (Å)	46.03 – 2.00	43.03 – 1.70	48.51 – 1.99	48.6 – 2.1	43.45 – 2.20	47.53 – 1.90	48.49 -2.20	48.4 – 2.35	48.32 – 1.93	43.46 – 2.37
R_{work}/R_{free} (%)	17.4 / 21.3	20.9 / 25.5	15.1 / 19.2	20.19 / 24.36	21.9 / 26.8	19.26 / 23.50	15.71 / 20.28	17.06 / 22.93	14.89 / 20.03	19.63 / 24.71
# Amino acid residues	1183	1190	1185	1187	2371	2366	1186	1186	1181	1185
# Solvent atoms	579	651	533	407	202	971	401	302	561	136
# Ligand Atoms	92	272	85	37	126	149	160	108	250	36
Rmsd										
Bond lengths (Å)	0.005	0.006	0.006	0.007	0.003	0.008	0.008	0.010	0.010	0.007
Bond angles (°)	0.928	1.11	1.02	1.09	0.820	1.15	1.04	1.04	1.18	0.98
B-factors ($Å^2$)	22.40	29.10	24.10	20.20	49.90	21.5	24.6	34.40	20.60	66.30
Protein	21.70	28.00	23.80	19.80	49.80	20.90	24.1	34.20	19.40	66.40
Ligand/ion	42.30	55.10	27.40	37.80	65.60	43.20	41.1	45.80	42.60	92.60
Water	30.70	34.30	28.90	26.50	41.90	29.10	29.9	31.00	31.00	50.00
Ramachandran (%) most favoured	97.79	97.19	97.16	98	96.88	98.0	99.0	98.0	98.0	97.0
Additionally allowed (%)	2.21	2.13	2.49	2.00	2.90	2.0	1.0	1.75	2.0	2.75

Table A.3 – **Effect of ligand binding on the active site and allosteric site volumes of wild-type and Y110F DHDPS.**

	DHDPS crystal Structures									
	apo (4R53)	**wt:pyr (4LY8)**	**wt:pyr:lys (4M19)**	**wt:pyr: bislysine**	**Y110F:pyr (4MLJ)**	**Y110F:pyr:lys (4MLR)**	**Y110F: bislysine**	**wt:pyr: thialysine**	**wt:BH:lac**	**wt:BH:lac: ASA**
Active site volume [a] ($Å^3$)	36 ± 1	20 ± 1	26 ± 5	27 ± 1	22 ± 2	20 ± 1	26 ± 3**	21 ± 1	18 ± 1	60 ± 2
Allosteric site volume [a] ($Å^3$)	494 ± 14	417 ± 15	239 ± 5	214 ± 2	446 ± 41	332 ± 7	278 ± 29	267 ± 11	355 ± 1	609 ± 103

****** Estimated solvent accessible volume if pyruvate had been present in the active site.

[a] Solvent accessible volumes calculated using CASTp as described in the text, and excluding L-lysine from the model

Figure A.1 – **Sequence alignment of DHDPS from various species.**[a]

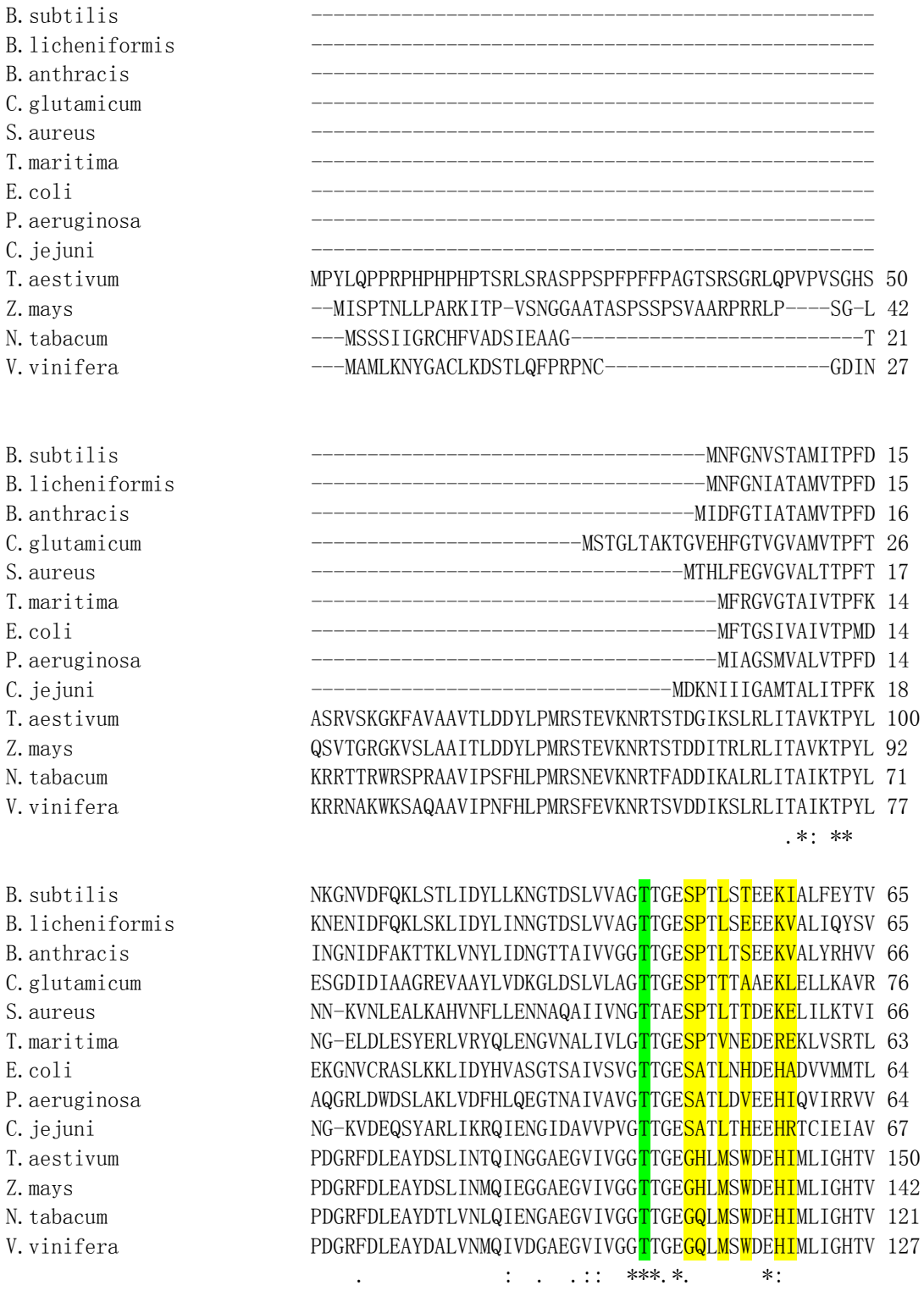

[a] Catalytic triad is shown in green, the key catalytic lysine (K166) is shown in cyan, a residue of interest at the active site (K113') is shown in pink, residues implicated at the weak dimer interface are shown in purple.

```
B.subtilis              KEVNG-RVPVIAGTGSNNTKDSIKLTKKAEEAGVDAVMLVTPYYNKPSQE 114
B.licheniformis         KEAAG-RVPIIAGTGSNNTKASIKLTKKAEEAGADAVMLVTPYYNKPSQE 114
B.anthracis             SVVDK-RVPVIAGTGSNNTHASIDLTKKATEVGVDAVMLVAPYYNKPSQE 115
C.glutamicum            EEVGD-RAKLIAGVGTNNTRTSVELAEAAASAGADGLLVVTPYYSKPSQE 125
S.aureus                DLVDK-RVPVIAGTGTNDTEKSIQASIQAKALGADAIMLITPYYNKTNQR 115
T.maritima              EIVDG-KIPVIVGAGTNSTEKTLKLVKQAEKLGANGVLVVTPYYNKPTQE 112
E.coli                  DLADG-RIPVIAGTGANATAEAISLTQRFNDSGIVGCLTVTPYYNRPSQE 113
P.aeruginosa            DQVKG-RIPVIAGTGANSTREAVALTEAAKSGGADACLLVTPYYNKPTQE 113
C.jejuni                ETCKGTKVKVLAGAGSNATHEAVGLAKFAKEHGADGILSVAPYYNKPTQQ 117
T.aestivum              NCFGA-NIKVIGNTGSNSTREAVHATEQGFAVGMHAALHVNPYYGKTSTE 199
Z.mays                  NCFGS-RIKVIGNTGSNSTREAVHATEQGFAVGMHAALHINPYYGKTSAE 191
N.tabacum               NCFGG-SIKVIGNTGSNSTREAIHATEQGFAVGMHAALHINPYYGKTSLE 170
V.vinifera              NCFGG-SIKVIGNTGSNSTREAIHATEQGFAVGMHAALHINPYYGKTSLE 176
                        .        :: ..*:* *  ::         *  . : : ***.:.. .

B.subtilis              GMYQHFKAIAAETSLPVMLYNVPGRTVASLAPETTIRLAADIPNVVAIKE 164
B.licheniformis         GMYRHFRAIAEETSLPVMLYNVPGRTAASLAPETTIRLA-EIPNIIAIKE 163
B.anthracis             GMYQHFKAIAESTPLPVMLYNVPGRSIVQISVDTVVRLS-EIENIVAIKD 164
C.glutamicum            GLLAHFGAIAAATEVPICLYDIPGRSGIPIESDTMRRLS-ELPTILAVKD 174
S.aureus                GLVKHFEAIADAVKLPVVLYNVPSRTNMTIEPETVEILS-QHPYIVALKD 164
T.maritima              GLYQHYKYISERTDLGIVVYNVPGRTGVNVLPETAARIAADLKNVVGIKE 162
E.coli                  GLYQHFKAIAEHTDLPQILYNVPSRTGCDLLPETVGRLA-KVKNIIGIKE 162
P.aeruginosa            GMYQHFRHIAEAVAIPQILYNVPGRTSCDMLPETVERLS-KVPNIIGIKE 162
C.jejuni                GLYEHYKAIAQSVDIPVLLYNVPGRTGCEISTDTIIKLFRDCENIYGVKE 167
T.aestivum              GLISHFKEVLPMG--PTIIYNVPSRTSQDIPPPVIEALS-SYSNMAGVKE 246
Z.mays                  GMISHFEAVLPMG--PTIIYNVPSRSAQDIPPEVILAIS-GYTNMAGVKE 238
N.tabacum               GLISHFESVLPMG--PTIIYNVPSRTGQDIPPRVIQTMA-KSPNLAGVKE 217
V.vinifera              GLVSHFESVLPMG--PTVIYNVPSRTGQDIPPGVIHTVA-QSANLAGVKE 223
                        *:  *:  :         :*::*.*:   :   .   :      : .:*:

B.subtilis              ASGDLEAITKIIAETPE---DFYVYSG-DDALTLPILSVGGRGVVSVASH 210
B.licheniformis         ASGDLDAITKIVAETPE---DFAVYSG-DDSLTLPALSVGARGIVSVASH 209
B.anthracis             AGGDVLTMTEIIEKTAD---DFAVYSG-DDGLTLPAMAVGAKGIVSVASH 210
C.glutamicum            AKGDLVAATSLIKET-----GLAWYSG-DDPLNLVWLALGGSGFISVIGH 218
S.aureus                ATNDFEYLEEVKKRIDTN--SFALYSG-NDDNVVEYYQRGGQGVISVIAN 211
T.maritima              ANPDIDQIDRTVSLTKQARSDFMVWSG-NDDRTFYLLCAGGDGVISVVSN 211
E.coli                  ATGNLTRVNQIKELVSD---DFVLLSG-DDASALDFMQLGGHGVISVTAN 208
P.aeruginosa            ATGDLQRAKEVIERVGK---DFLVYSG-DDATAVELMLLGGKGNISVTAN 208
C.jejuni                ASGNIDKCVDLLAHEPR----MMLISG-EDAINYPILSNGGKGVISVTSN 212
T.aestivum              CVGHERVKCYTDKG-------ISIWSGNDDECHDSRWKYGATGVISVASN 289
Z.mays                  CVGHERVKHYADKG-------ITIWSGNDDECHDSKWKHGATGVISVTSN 281
N.tabacum               CVGNDRVEQYTSDG-------VVVWSGNDDECHVSRWDYGATGVISVTSN 260
V.vinifera              CVGNDRIKQYTDNR-------IVVWSGNDDQCHDAKWDYGATGVISVTSN 266
                        .  .                 .   ** :*         *. * :** .:
```

[a] Catalytic triad is shown in green, the key catalytic lysine (K166) is shown in cyan, a residue of interest at the active site (K113') is shown in pink, residues implicated at the weak dimer interface are shown in purple.

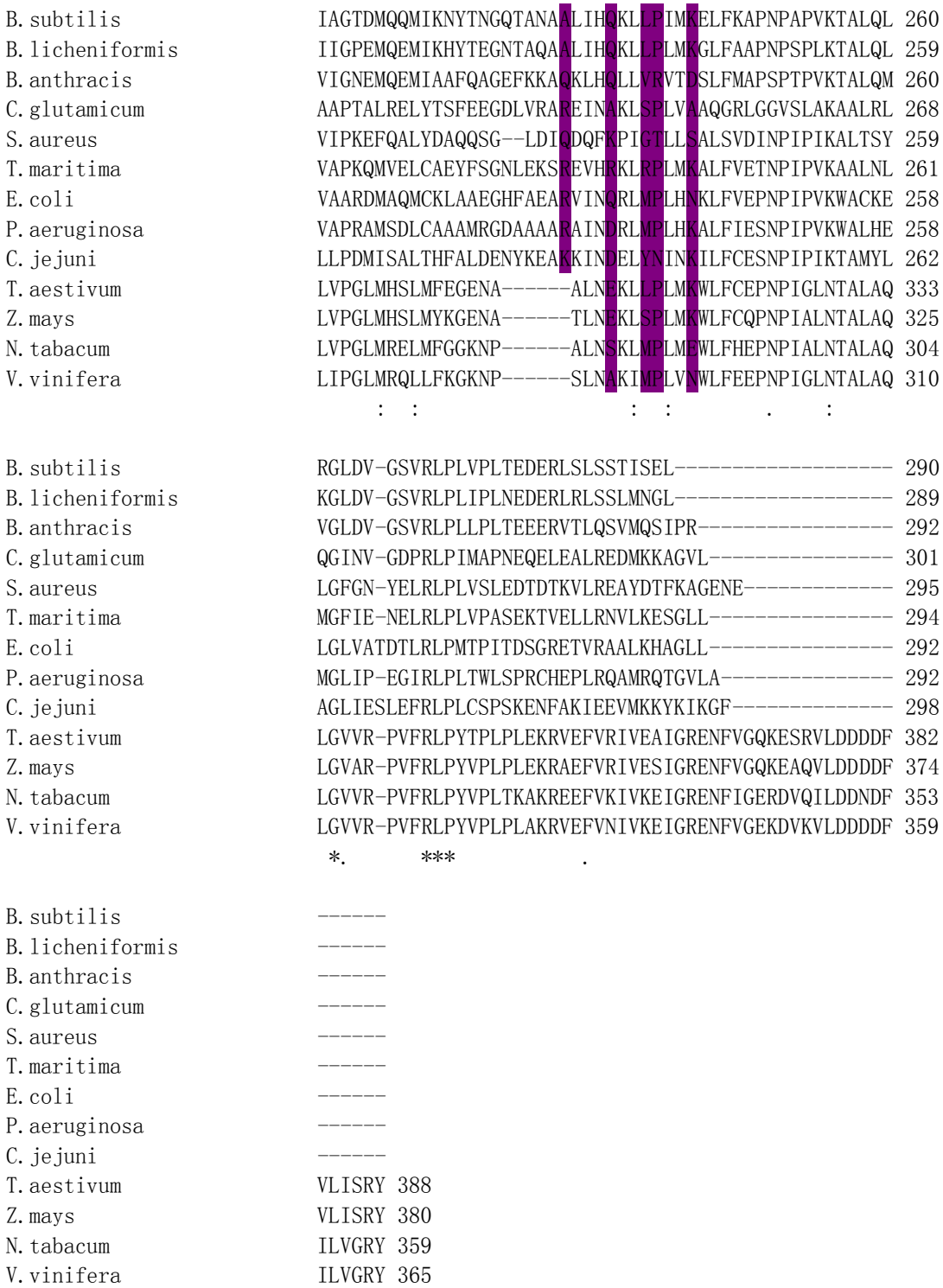

[a] Catalytic triad is shown in green, the key catalytic lysine (K166) is shown in cyan, a residue of interest at the active site (K113') is shown in pink, residues implicated at the weak dimer interface are shown in purple.

APPENDIX B

B.1 Brief Description for Uncommon Software

B.1.1 Introduction to dynamic Domains

Biomolecular function involves conformational change in response to the change of state that occurs when a biomolecule carries out its task. It is currently accepted that this change in conformation is not merely an unimportant side effect of function but is integral to it. This is certainly true for an allosteric mechanism where the binding of a ligand at one site affects binding affinities at a distant site.[1]

Many large proteins are built from domains, and interdomain motions are likely to be the slowest of all motions in proteins. Functional sites are often located at interdomain clefts, implying that these interdomain motions are of functional significance.[2] It has been suggested that domain motions, which have been described as hinge, shear, or a combination of hinge and shear motions, correspond to low energy conformational changes available to the protein at its functional temperature.[3] Although for some proteins the domain structure is obvious, others may exist in a dynamical sense and may not be easily recognizable from the structure.[4]

DynDom is a program that analyzes conformational change in proteins for dynamic domains, hinge axes, and hinge-bending regions. It is primarily used by X-ray crystallographers when they have more than one conformation of a protein for analysis of its domain motion.[5]

B.1.2 Brief Summary of the dynDom Algorithm

The DynDom program will determine dynamic domains, hinge axes, and hinge-bending residues from two protein structures, representing the conformational change. Details of the basic methodology are given in the original publication, and a brief description follows here.[6] The intent

of DynDom is to identify those regions of a protein which move as a unit in the same direction and with the same magnitude. These regions are named dynamic domains. The algorithm for identifying domains uses a combination of a group of methods for identifying conformational change, rather than those methods based purely on structural information.[4] DynDom assumes that some proteins can, in the first approximation, consist of parts that can be treated as behaving dynamically as rigid bodies which can be distinguished by their differing rotational properties in the low frequency modes.[5] These parts may or may not have any correspondence to structurally defined domains, and to distinguish them from structurally defined domains they are termed "dynamical domains". This approximation requires that the interaction between these parts be small when compared with interactions within a single part.[4]

Movement of domains is identified by generation of short main-chain segments using a sliding window. The sliding window serves to reduce the noise of local variations, and the overlapping segments smoothes the distribution of rotation points.[7] The calculation of rotation vectors of each of these segments relative to a reference structure reveals segments that rotate together, and perhaps comprise a rigid domain within the protein.[7] The demarcation between domains is based on their differing rotation relative to a reference structure. Thus, DynDom is used to analyze the conformational change between two structures in terms of a model whereby domains move. DynDom is not designed to detect or measure individual residue movements, nor will it define multiple movement vectors which are not of similar direction or magnitude.

Once the dynamical domains have been identified, the interdomain screw axis can be determined. One domain is fixed in space, and the motion of the other domain, the rotating domain, is described by a screw axis.[5] The method is such that the location of the interdomain screw axis reveals the type of motion occurring. If the interdomain screw axis is located between

the two domains near regions known to be involved in the interdomain motion, we could reasonably assume that the interdomain connections effectively create a physical hinge axis.[4] Usually a number of residues are involved in the motion of one domain relative to another. For example, this may involve the bending of an interdomain helix. Hinge axes are further classified into two extreme types; twist, and closure axes.[4] A twist axis is one located along or parallel to an imaginary line joining the center of mass for each domain, whereas a closure axis lies perpendicular to the imaginary line which joins the center of mass for each domain.[4] Any hinge axis may represent simultaneous properties of twist and closure. DynDom thus describes a hinge axis as a certain percentage where 100% is perfect closure, and 0% is a perfect twist.[4]

B.2.1 Introduction to CASTp for the definition of protein pockets and cavities

Cavities on a protein's surface as well as specific amino acid positioning within it create the physico-chemical properties needed for a protein to perform its function. Allosteric transformations in proteins are associated with changes in domain contacts and concomitantly with sizes and shapes of interfacial cavities. Furthermore, water-filled cavities play the role of modulating pK_a values of acidic and basic residues surrounding the cavities.[8]

The Computer Atlas of Surface Topography program (CASTp) identifies pockets and cavities in protein crystal structures and quantifies their size. The method of the CASTp algorithm is a computational geometry treatment of complex shapes, based on alpha shape and discrete flow theory, and a related suite of programs.[9-12] CASTp provides a full description of protein pockets and cavities including: volume, surface area, protein atoms that line the concavity, and features of pocket mouths including identification of mouth atoms as well as measurement of mouth area and circumference.[13]

Pockets are defined as empty concavities on protein surface into which solvent (probe 1.2 Å) can gain access. Shallow depressions are excluded from the calculation. The criterion of a pocket is as follows: among the infinite number of possible cross sections of a pocket, at least one is larger than the mouth opening of the pocket. A cavity (or void) is an interior empty space that is not accessible to the solvent probe. It has no mouth openings to the outside bulk solvent.

CASTp uses the models of Lee and Richards for solvent accessible surfaces (SA) and molecular surfaces (MS) of proteins.[14] The model presents a molecule as the union of many fused spherical balls in three-dimensional space where each ball represents an atom by adopting spatial location and the appropriate van der Waals radius of the atom. Thus, the van der Waals (VW) model is the union of these spherical balls.[8] The SA and the MS models are defined by the same solvent sphere rolling about the VW model. The solvent is treated as a sphere of appropriate radius and is rolled around the van der Waals surface of the protein. The center of the solvent sphere sweeps out the surface of the solvent accessible or SA model, while the front of the solvent sphere defines the molecular surface or MS model.[14, 15] This subtle distinction means the area and the volume of the two models may differ significantly.

CASTp uses an algorithm based on alpha shapes for measuring space-filling-based molecular models (such as van der Waals, solvent accessible, and molecular surface descriptions).[8] Utilizing the surfaces defined by the solvent probe, alpha shape theory is used to define the cavities and compute their volume (an introduction to alpha shape theory can be found on the web site http://alpha.ncsa.uiuc.edu/alpha). In brief, alpha shape theory provides a quantitative method to accurately describe and compute shapes at multi-levels of detail in three-dimensional space.[9, 16] It is integral to computation of molecular surface area and volume for both SA and MS.[17]

B.2.2 Availability of CASTp

CASTp web server and the associated mapping database can be freely accessed at http://cast.engr.uic.edu.

B.3 References

[1] Swain, J. F., and Gierasch, L. M. (2006) The changing landscape of protein allostery, *Current Opinion in Structural Biology 16*, 102-108.

[2] Schulz, G. E. (1991) Domain motions in proteins, *Current Opinion in Structural Biology 1*, 883-888.

[3] Gerstein, M., Lesk, A. M., and Chothia, C. (1994) Structural mechanisms for domain movements in proteins, *Biochemistry 33*, 6739-6749.

[4] Hayward, S., Kitao, A., and Berendsen, H. J. C. (1997) Model-free methods of analyzing domain motions in proteins from simulation: A comparison of normal mode analysis and molecular dynamics simulation of lysozyme, *Proteins: Structure, Function, and Bioinformatics 27*, 425-437.

[5] Hayward, S., and Lee, R. A. (2002) Improvements in the analysis of domain motions in proteins from conformational change: DynDom version 1.50, *Journal of Molecular Graphics & Modeling 21*, 181-183.

[6] Hayward, S., and Berendsen, H. J. C. (1998) Systematic analysis of domain motions in proteins from conformational change: New results on citrate synthase and T4 lysozyme, *Proteins 30*, 144-154.

[7] Poornam, G. P., Matsumoto, A., Ishida, H., and Hayward, S. (2009) A method for the analysis of domain movements in large biomolecular complexes, *Proteins 76*, 201-212.

[8] Liang, J., Edelsbrunner, H., Fu, P., Sudhakar, P. V. and Subramaniam, S. (1989) Analytical shape computation of macromolecules: II. Inaccessible cavities in proteins, *Proteins 33*, 18-29.

[9] Edelsbrunner, H., M, E. P., #252, and cke. (1994) Three-dimensional alpha shapes, *Association of Computing Machinery Transactions on Graphics 13*, 43-72.

[10] Edelsbrunner, H., Facello, M., Ping, F., and Jie, L. (1995) Measuring proteins and voids in proteins, In *System Sciences, 1995. Proceedings of the Twenty-Eighth Hawaii International Conference on*, pp 256-264 vol.255.

[11] Edelsbrunner, H., and Shah, N. R. (1996) Incremental topological flipping works for regular triangulations, *Algorithmica 15*, 223-241.

[12] Facello, M. A. (1995) Implementation of a randomized algorithm for Delaunay and regular triangulations in three dimensions, *Computer Aided Geometric Design 12*, 349-370.

[13] Liang, J., Woodward, C., and Edelsbrunner, H. (1998) Anatomy of protein pockets and cavities: Measurement of binding site geometry and implications for ligand design, *Protein Science 7*, 1884-1897.

[14] Lee, B., and Richards, F. M. (1971) The interpretation of protein structures: Estimation of static accessibility, *Journal of Molecular Biology 55*, 379-IN374.

[15] Connolly, M. (1983) Analytical molecular surface calculation, *Journal of Applied Crystallography 16*, 548-558.

[16] Edelsbrunner, H., Kirkpatrick, D. G., and Seidel, R. (1983) On the shape of a set of points in the plane, *Institute of Electrical and Electronics Engineers - Transactions on Information Theory 29*, 551-559.

[17] Liang, J., Edelsbrunner, H., Fu, P., Sudhakar, P. V. and Subramaniam, S. (1998) Analytical shape computation of macromolecules: I. molecular area and volume through alpha shape, *Proteins 33*, 1-17.